Neuronal store-operated calcium entry in neuronal function and inflammation-induced neurodegeneration

Dissertation

zur Erlangung der Würde des Doktors der Naturwissenschaften
des Fachbereichs Physik, der Fakultät für Mathematik, Informatik
und Naturwissenschaften der Universität Hamburg

vorgelegt von

Artem Shaposhnykov

aus Alchevsk (Ukraine)

Hamburg 2021

Conducted at

Institute of Neuroimmunology and Multiple Sclerosis (INIMS)

Center for Molecular Neurobiology Hamburg (ZMNH)

University Medical Center Hamburg-Eppendorf (UKE)

Date of defense: 10th September 2021

Chair: Prof. Dr. Peter Schmelcher

Supervisor and evaluator: Prof. Dr. Robert Blick

Supervisor and evaluator: Prof. Dr. Manuel A. Friese

Referee: Prof. Dr. Simon Wiegert

Referee: Dr. Gaia Pigino

Table of Contents

List of figures 8
List of tables 9
List of supplements 10
Abbreviations 11
I. Introduction 14
1. Multiple sclerosis 14
1.1. Clinic and pathology 14
1.2. Animal model of MS 15
1.3. Neurodegeneration 16
1.3.1. Pathomechanisms of neurodegeneration in MS 17
Common features of neuronal damage during MS 17
“Virtual” hypoxia 17
Glutamate excitotoxicity 19
2. Calcium homeostasis in the cell 20
2.1. Neuronal calcium regulation 20
2.1.1. Membrane ion channels 21
2.1.2. Na^+/Ca^{2+} exchanger and plasma membrane Ca^{2+} ATPase 22
2.1.3. Intracellular organelles 22
2.1.4. Non-selective ion channels, Ca^{2+} binding proteins, lysosomes 23
2.2. Neuronal calcium regulation and MS 24
3. Store-operated calcium entry 24
3.1. Calcium release-activated channels 25
3.1.1. ORAI protein family 26
3.1.2. STIM protein family 27
3.1.3. Properties of CRAC 28

3.2. Neuronal SOCE (nSOCE) 28
3.3. nSOCE under pathophysiological condition 29
3.3.1. nSOCE and MS 29
4. Aim of the project 30
II. Materials and methods 31
1. Materials 31
1.1. Laboratory animals 31
1.2. Reagents 31
1.3. Buffers and media 41
1.4. Equipment and consumables 42
1.5. Software 45
2. Methods 45
2.1. Animals 45
2.1.1. C57BL/6J 46
2.1.2. *Orai2*$^{-/-}$ 46
2.1.3. *Orai2*$^{fl/fl}$×*Eno2*^{cre} 46
2.1.4. *Orai2*$^{fl/fl}$×*ChAT*^{cre} 46
2.1.5. *Orai2*$^{fl/fl}$×*Snap25*^{cre} 46
2.1.6. *Stim1*$^{fl/fl}$*Stim2*$^{fl/fl}$×*Snap25*^{cre} 47
2.1.7. *Stim2*$^{fl/fl}$ 47
2.2. Genotyping 47
2.3. Gene expression assay 54
2.4. Experimental autoimmune encephalomyelitis (EAE) 55
2.5. Behavioral analysis 56
2.5.2. Open field 56
2.5.3. Y maze 56

2.6. Flow cytometry and fluorescence-activated cell sorting 57
2.6.1. Cells isolation 57
2.6.2. Fluorescent immunolabeling....58
2.6.3. Flow cytometry parameters 59
2.6.4. Data analysis....61
2.7. Histopathology/Immunohistochemistry 61
Tissue preparation....61
Staining 61
2.8. Primary neuronal culture 62
2.9. Cell line 62
2.10. Cell transfection 62
2.11. Primary neuron transduction 63
2.12. Live-cell calcium imaging 63
2.13. Immunocytochemistry 64
III. Results 65
1. Determination of the neuronal SOCE composition....65
1.1. Expression of SOCE genes in neural tissue and primary neuronal culture 65
1.2. The distribution of SOCE-related proteins in neurons....66
1.3. Expression of SOCE genes in neural tissue during CNS inflammation 67
2. Contribution of *Orai2* to neurodegeneration during CNS inflammation....69
2.1. Validation of *Orai2*$^{-/-}$ mice 69
2.2. Global deletion of *Orai2* leads to amelioration of EAE disease progression.....70
2.2.1. Clinical analysis of EAE....70
2.2.2. Histopathological assessment of neuronal damage during chronic EAE....71
2.2.3. Validation of CNS infiltration by immune cells....72
2.3. Tissue-specific deletion of *Orai2*....73

2.3.1. *Orai2*$^{fl/fl}$×*Eno2*^{cre} mouse line 74

2.3.2. *Orai2*$^{fl/fl}$*ChAT*^{cre} mouse line 76

2.3.3. *Orai2*$^{fl/fl}$×*Snap25*^{cre} mouse line 77

2.4. *In vitro* validation of Ca^{2+} regulation with modified SOCE 78

2.4.1. Establishment of an *in vitro* model for neuronal Ca^{2+} activity analysis 78

2.4.2. Ca^{2+} regulation in *Orai2*$^{-/-}$ neurons 79

3. The contribution of *Stim1* and *Stim2* deletions 80

3.1. Validation of the *Stim1*$^{fl/fl}$*Stim2*$^{fl/fl}$×*Snap25*^{cre} mouse line 80

3.2. The effect of neuron-specific *Stim1* and *Stim2* deletions on CNS inflammation 80

3.2.1. Clinical and histological characterization of EAE progression in *Stim1*$^{fl/fl}$*Stim2*$^{fl/fl}$×*Snap25*^{cre} mice 81

3.2.2. Validation of the immune response after EAE induction 82

CNS infiltrating immune cell composition not altered at the chronic stage of the EAE in *Stim1*$^{fl/fl}$*Stim2*$^{fl/fl}$×*Snap25*^{cre} mice 83

Overall immune system response not altered at the pre-symptomatic stage of the EAE in *Stim1*$^{fl/fl}$*Stim2*$^{fl/fl}$×*Snap25*^{cre} mice 84

CNS has reduced signs of inflammation at the pre-symptomatic stage of the EAE in *Stim1*$^{fl/fl}$*Stim2*$^{fl/fl}$×*Snap25*^{cre} mice 85

3.3. *Stim1*$^{fl/fl}$*Stim2*$^{fl/fl}$×*Snap25*^{cre} line has a distinguished phenotype 85

3.3.1. Histological validation of healthy animals with a neuron-specific *Stim1/Stim2* deletion 87

3.3.2. *Stim1*$^{fl/fl}$*Stim2*$^{fl/fl}$×*Snap25*^{cre} mouse show abnormal hyperactivity behavior 88

Open field 89

Y maze 90

Additional remarks 90

3.4. *Stim1* and *Stim2* deletion alters neuronal Ca^{2+} homeostasis *in vitro* 90

3.4.1. *Stim1* and *Stim2* deficient neurons 91

3.4.2. *Stim2*-deficient neurons 92
IV. Discussion 93
1. Composition of neuronal CRAC 93
1.1. Murine neuronal CRAC profile 93
1.2. Murine neuronal CRAC profile during EAE 94
2. *Orai2* deletion in CNS inflammation 95
2.1. Global deletion of Orai2 95
2.1.1. The effect of global deletion of *Orai2* on SOCE-related genes 95
2.1.2. Global deletion of *Orai2* ameliorates EAE 96
2.2. Neuronal *Orai2* deletion does not influence clinical outcome of the EAE 97
2.2.1. $Orai2^{fl/fl}Eno2^{cre}$ in CNS inflammation 97
2.2.2. Motor neuron-specific deletion of *Orai2* does not affect EAE progression 98
2.2.3. Pan-neuronal deletion of *Orai2* does not affect EAE progression 98
2.3. Deletion of *Orai2 in vitro* does not affect the resting Ca^{2+} level in neurons 99
2.4. Summary 99
3. *Stim1* and *Stim2* neuron-specific double deletion mouse model 100
3.1. Neuron-specific knock out of *Stim1* and *Stim2* ameliorates EAE 100
3.2. *Stim1* and *Stim2* contribute to Ca^{2+} homeostasis *in vitro* 101
3.3. Neuron-specific *Stim1* and *Stim2* deletion influences long-term survival, behavior and epileptic predisposition in mice 101
4. Outlook 103
V. Summary 105
VI. Supplement 107
VII. Bibliography 109
Acknowledgements 123
Affidavit 124

LIST OF FIGURES

Figure 1 Model of “virtual hypoxia” 18

Figure 2 Schematic illustration of the classical mechanism of SOCE activation 26

Figure 3 Gating strategy for the immune cell subsets analysis 60

Figure 4 Expression profile of SOCE related genes 65

Figure 5 Antibodies validation and ORAI2 distribution 66

Figure 6 Expression profile of SOCE-related genes during CNS inflammation 67

Figure 7 Validation of the expression of SOCE-related genes in the *Orai2*$^{-/-}$ 69

Figure 8 Clinical analysis of EAE in the *Orai2*$^{-/-}$ mouse model 70

Figure 9 Histological analysis of *Orai2*$^{-/-}$ mice during chronic EAE 71

Figure 10 Immune cells composition at the acute EAE of *Orai2*$^{-/-}$ mice 72

Figure 11 Validation of *Eno2* expression in wild-type mice and in the *Orai2*$^{fl/fl}$×*Eno2*^{cre} mouse line 73

Figure 12 Clinical analysis of the EAE in *Orai2*$^{fl/fl}$×*Eno2*^{cre} mice 74

Figure 13 Validation of SOCE-related genes in immune cells derived from *Orai2*$^{fl/fl}$×*Eno2*^{cre} mice 75

Figure 14 Clinical analysis of EAE in *Orai2*$^{fl/fl}$×*ChAT*^{cre} mice 76

Figure 15 Validation of *Orai2* deletion in *Orai2*$^{fl/fl}$×*Snap25*^{cre} mice 77

Figure 16 Clinical analysis of EAE in *Orai2*$^{fl/fl}$×*Snap25*^{cre} mice 77

Figure 17 Calcium regulation in *Orai2*$^{-/-}$ neurons 79

Figure 18 Validation of the *Stim1*$^{fl/fl}$*Stim2*$^{fl/fl}$×*Snap25*^{cre} mouse line 80

Figure 19 Characterization of the *Stim1*$^{fl/fl}$*Stim2*$^{fl/fl}$×*Snap25*^{cre} line during CNS inflammation 81

Figure 20 Immune cells composition at the chronic EAE of *Stim1*$^{fl/fl}$*Stim2*$^{fl/fl}$×*Snap25*^{cre} mice 83

Figure 21 Immune cell composition at the pre-acute EAE of *Stim1*$^{fl/fl}$*Stim2*$^{fl/fl}$×*Snap25*^{cre} mice 84

Figure 22 Histological validation of the pre-acute EAE in *Stim1*$^{fl/fl}$*Stim2*$^{fl/fl}$×*Snap25*^{cre} mice 84

Figure 23 Characterization of the *Stim1*$^{fl/fl}$*Stim2*$^{fl/fl}$×*Snap25*^{cre} mouse line 86

Figure 24 Histological characterization of the CNS of *Stim1*$^{fl/fl}$*Stim2*$^{fl/fl}$×*Snap25*^{cre} mice 87

Figure 25 Behavioral analysis of *Stim1*$^{fl/fl}$*Stim2*$^{fl/fl}$×*Snap25*^{cre} mice 89

Figure 26 Neuronal Ca^{2+} activity in *Stim1, Stim*2 deficient neurons 91

LIST OF TABLES

Table 1 List of animal strains.....31

Table 2 Primers for genotyping 31

Table 3 Reagents and chemicals for genotyping.....33

Table 4 Reagents and chemicals for gene expression assays 34

Table 5 TaqMan primers 34

Table 6 Reagents and chemicals for *in vivo* experiments.....35

Table 7 Reagents and chemicals for flow cytometry and fluorescence-activated cell sorting.....35

Table 8 Antibodies for flowcytometry and fluorescence-activated cell sorting.....36

Table 9 Reagents and chemicals for immunohistochemistry/immunocytochemistry 37

Table 10 Primary antibodies for immunohistochemistry/immunocytochemistry 38

Table 11 Secondary antibodies for immunohistochemistry/immunocytochemistry.....38

Table 12 Reagents and chemicals for *in vitro* experiments 39

Table 13 Plasmids for *in vitro* experiments.....40

Table 14 Buffers and media 41

Table 15 Equipment and devices 42

Table 16 General consumables 43

Table 17 Software.....45

Table 18 Reagents for a single genotype PCR reaction of the *Orai2*$^{-/-}$ and *Orai2*$^{fl/fl}$ lines 48

Table 19 Thermal profile for *Orai2*$^{-/-}$ and *Orai2*$^{fl/fl}$ genotype PCR.....48

Table 20 Reagents for a single genotype PCR reaction of the *Stim1*$^{-/-}$ and *Stim1*$^{fl/fl}$ lines.....49

Table 21 Thermal profile for *Stim1*$^{-/-}$ and *Stim1*$^{fl/fl}$ genotype PCR 49

Table 22 Reagents for a single genotype PCR reaction of the *Stim2*$^{-/-}$ and *Stim2*$^{fl/fl}$ lines 50

Table 23 Thermal profile for *Stim2*$^{-/-}$ and *Stim2*$^{fl/fl}$ genotype PCR 50

Table 24 Reagents for a single genotype PCR reaction of the *Eno2*^{cre} line 51

Table 25 Thermal profile for *Eno2*^{cre} genotype PCR 51

Table 26 Reagents for a single genotype PCR reaction of the *ChAT*^{cre} line.....52

Table 27 Thermal profile for *ChAT*^{cre} genotype PCR 52

Table 28 Reagents for a single genotype PCR reaction of the *Snap25*^{cre} line 53

Table 29 Thermal profile for *Snap25*^{cre} genotype PCR 53

Table 30 Antibodies for cell suspension staining 58

Table 31 Cell suspension staining protocol 59

Table 32 Markers used for immune cell types identification.....59

Table 33 Overview of the ratios of the expression of SOCE-related genes 68

Table 34 Neuronal medium comparison.....79

LIST OF SUPPLEMENTS

Supplement 1 Relative body weight change in *Orai2*$^{-/-}$ mice during EAE 107

Supplement 2 Relative body weight change in *Stim1*$^{fl/fl}$*Stim2*$^{fl/fl}$×*Snap25*^{cre} mice during EAE...107

Supplement 3 Control qPCR of the *Stim1*$^{fl/fl}$*Stim2*$^{fl/fl}$×*Snap25*^{cre} mouse line 108

Supplement 4 Absolute quantification of the immune cell infiltration at chronic EAE in *Stim1*$^{fl/fl}$*Stim2*$^{fl/fl}$×*Snap25*^{cre} mice 108

ABBREVIATIONS

AAV	Adeno-associated virus
AD	Alzheimer`s disease
AMPAR	α-amino-3-hydroxy-5-methyl-4-isoxazole propionic acid receptor
APP	Amyloid precursor protein
ASIC	Acid-sensing ion channel
ASIC1	Proton-gated acid-sensing ion channel-1
ATP	Adenosine triphosphate
BLAST	The Basic Local Alignment Search Tool
BMDCs	Bone marrow dendritic cells
Ca^{2+}	Calcium ion
cADPR	Cyclic ADP-ribose
CaM	Calmodulin
CaR	Ca^{2+} -sensing receptor
CD	Cluster of differentiation
cDNA	Complementary DNA
CFA	Complete Freund’s adjuvant
ChAT	Choline acetyltransferase
CNS	Central nervous system
CRAC	Ca^{2+} release-activated Ca^{2}
CSF	Cerebrospinal fluid
DAI	Day after immunization
DCs	Dendritic cells
DHP	1,4-dihydropyridines
DIV	Day *in vitro*
Eno2	Neuron-specific enolase 2
FBS	Fetal bovine serum
FUdR	5-fluorodeoxyuridine
GABA	γ-aminobutyric acid

GFP	Green fluorescent protein
Glu	Glutamate
HD	Huntington`s disease
IBD	Inflammatory bowel disease
InsP3R	Inositol-1,4,5-tris-phosphate receptor
LTD	Long-term depression
LTP	Long-term potentiation
MCU	Mitochondrial Ca^{2+} uniporter
mGluR	Metabotropic glutamate receptor
MOG35-55	Myelin oligodendrocyte glycoprotein 35-55
mPTP	Mitochondrial permeability transition pore
MS	Multiple sclerosis
Na^{+}/K^{+}-ATPase	Sodium-potassium adenosine triphosphatase
nAChRs	Nicotinic acetylcholine receptors
NCLX	Mitochondrial sodium-calcium exchanger
NCX	Na^{+}/Ca^{2+} exchanger
NK cells	Natural killer cells
NK T cells	Natural killer T cells
NMDAR	N-methyl-D-aspartate receptor
OCT	Optimal cutting temperature compound
P2X	ATP-gated channels
PFA	Paraformaldehyde
PMCA	Ca^{2+} ATPase
PPMS	Primary progressive Multiple sclerosis
ROC	Receptor-operated calcium channel
ROI	Region of interest
ROS	Reactive oxygen species
RRMS	Relapsing-remitting Multiple sclerosis
RT	Room temperature

RyR	Ryanodine receptor
SARAF	SOCE-associated regulatory factor
SCID	Severe combined immune deficiency
SERCA	Sarco-/endoplasmic reticulum Ca^{2+}-ATPase
Snap25	Synaptosome Associated Protein 25
SOAR	STIM-ORAI-activating region
SOC	Store-operated calcium channel
SPMS	Secondary progressive Multiple sclerosis
STIM	Stromal interaction molecule
TPC	Two-pore channel
TPC2	Two-pore channel 2
TRP	Transient receptor potential channel
TRPM4	Transient receptor potential melastatin 4
UKE	University Medical Center Hamburg-Eppendorf
VOC	Voltage-operated calcium channel
ZMNH	Center for Molecular Neurobiology Hamburg

I. Introduction

1. Multiple sclerosis

1.1. Clinic and pathology

Multiple sclerosis (MS) is one of the most common diseases of the central nervous system (CNS) in young adults. The average disease onset is about 20 to 40 years and it affects more women than men. It causes various neurological deficits (e.g. cognitive dysfunction and sensory or motor problems) with significant impairment in the quality of life.[1] There are three clinically distinguishable disease courses of MS: relapsing-remitting (RRMS), secondary progressive (SPMS) and primary progressive MS (PPMS). The most common disease course which covers 80-85% of all MS cases, is RRMS.[2] RRMS is characterized as a sequence of neurological symptoms lasting for days or weeks (relapse) and a complete clinical recovery in between (remission). After several years, continuous progression of disability independent of relapses can occur and neurological deficits become permanent. At this stage, RRMS converts to SPMS. In some cases permanent neurological deficits already appear at the onset of the disease, the disease course is then called PPMS.

Although research about MS increases rapidly, the exact cause of MS is still unclear. Genetic or environmental factors, previous infections, smoking, and vitamin D deficiency were shown to have an impact on the development of MS, but none of them can be described as the unique trigger.[3–5] Nevertheless, MS pathophysiology at different stages of the disease is well described. MS is characterized as a multifocal demyelinating disease of the CNS. Disruption of the myelin sheath[a] is a key pathological feature observed during all forms of MS. Myelin plays a critical role in neuronal signal transmission by providing the saltatory conduction[b] in the axon.[6] Since the action potential propagation follows an all-or-none rule[7], even local myelin damage leads to the disruption of the signal transmission between neurons. During MS demyelinated regions (lesions) of various sizes and localization are formed in the CNS. The heterogeneity of the localization of lesions correlates with the variety of the clinical manifestations.[8,9] Beside demyelination, lesions characterized by neuronal loss and axonal damage. However, recent studies showed that axonal

[a] Myelin is the lipid substance forming a sheath (the myelin sheath) around the axons of certain nerve fibers; it is an electrical insulator that serves to speed the conduction of nerve impulses in these nerve fibers, which are called myelinated. [178]

[b] Saltatory conductance - a form of fast nerve impulse conduction where the impulse may jump between nodes normally insulated from each other.[179]

and neuronal loss can be observed even outside of the lesions in MS brain, at least in the late phase of MS.[10,11]

Another hallmark of MS is inflammation. The link between MS lesion formation and inflammation was under debate during the last century.[12] Growing evidence regarding the significant impact of the immune system on MS pathophysiology accumulated with the improvement of tools and the understanding of biological processes. A strong correlation, especially during RRMS, was shown between MS lesion formation and immune cell infiltration (including Cluster of differentiation 4^+ ($CD4^+$) and $CD8^+$ T cells, B cells, and macrophages) into the CNS.[13] Based on the analysis of the infiltration of the immune cells into CNS, MS is considered to be an autoimmune disorder caused by autoreactive lymphocytes. However, an exact antigen for the initial activation of the immune system was not yet found. Furthermore, it is still unclear whether immune system dysregulation leads to CNS damage (outside-in model) or the inflammation is the result of CNS-intrinsic events (inside-out model).[14] Despite unknown triggers for the immune system reaction, prevention of the infiltration of the immune cells into the CNS has been the focus of MS treatment development. Current MS therapy includes a variety of immunomodulatory drugs targeting different properties of the immune system to prevent immune cell infiltration to the CNS. Nevertheless, the currently available therapy may reduce the frequency of the relapses, but fails to prevent progression of neurological deficits in SPMS or PPMS.[15]

1.2. Animal model of MS

In medical practice, MS diagnosis given based on the detection of neurological manifestations and physiological changes in the CNS. Nevertheless, slow disease progression and extremely limited access to the affected tissue limit possibilities for fundamental research in humans. Fundamental research requires a detailed analysis of the CNS during the different stages of the disease under controlled conditions, which can be performed only in a model of the disease. A model that efficiently mimics the development of the clinical and the pathophysiological picture of the disease observed in patients is one of the key limitations in fundamental research of different human diseases. Luckily, in the beginning of the last century, during an experimental treatment against the rabies virus, a clinical picture resembling MS symptoms could be observed. Injections of dried spinal cords of animals infected with the virus were injected directly to human rabies patients in order to prevent their death. Apart from some success as an anti-rabies treatment, some of the patients showed signs of partial or complete paralysis a few months after the treatment. Later on, the link between the injected compound of the CNS and the development of

paralysis was shown in monkeys.[16] The induced disease was named experimental autoimmune encephalomyelitis (EAE).

EAE is the most commonly used model for MS research. After the immunization, the main hallmarks of MS pathology can be observed, including CNS inflammation, demyelination, and axonal loss. Contracting processes, such as remyelination, can be observed during the EAE course as well. Furthermore, most of the currently available MS therapeutics were developed by using the EAE model.[17] The main difference between EAE and MS is that external immunization is needed for the development of EAE while MS develops either spontaneously or by an unknown trigger. Usually, EAE is induced by injection of a CNS-specific antigen supplemented with an adjuvant to activate the immune system. After immunization, the EAE course may differ between various species, genetic backgrounds, and the chosen antigens. In the C57BL/6 mouse line, for example, EAE develops as a monophasic increase of clinical deficits with a peak of disease around two weeks after the induction (acute phase) followed by an incomplete recovery with remaining neurological deficits at the chronic stage.[18]

1.3. Neurodegeneration

Different aspects of MS-related pathology were observed in the EAE animal model, which led to development of treatment possibilities. Furthermore, the animal model allows to investigate pathological changes in neurons on the cellular level in MS-like conditions, which is extremely difficult or sometimes impossible in humans due to limited access to the CNS. Understanding of the mechanisms of neuronal damage is extremely valuable since the accumulation of neurological manifestations caused by the ongoing neuronal loss (neurodegeneration) in the brain and the spinal cord are crucial for MS patients. Based on animal and human studies, on a cellular level, neuronal loss is believed to be promoted by the process of myelin damage. As mentioned above, focal demyelination prevents action potential propagation by a complete blockage of the conduction in the affected areas.[19] The CNS responds to the focal demyelination by the activation of various mechanisms in order to restore axon functionality such as redistribution of ion channels in the axolemma or activation of remyelination processes.[20,21] Even though it can particularly or even completely restore the neuronal signal propagation, such an adaptation may cause long-lasting effects on the axon and leads to irreversible damage.

In the context of MS, rapid demyelination induced by local active inflammation with further restoring axonal conduction can explain the phenomenon of relapses during the RRMS form. However, rapid demyelination does not cause an immediate irreversible damage to the neurons, while it makes neurons more vulnerable to the damage caused by long-lasting inflammatory

processes. Understanding and preventing neuronal damage is the greatest challenge for treatment strategies for MS and other neurological diseases. Many theories and hypotheses about the nature of neurodegeneration during MS exist, but many aspects remain unknown and require further investigation.

1.3.1. Pathomechanisms of neurodegeneration in MS

In contrast to the relatively well described immune processes in MS, the mechanisms of neuronal and axonal damage are highly debatable. Pathological findings led to many hypotheses for the mechanism of neuronal and axonal damage in MS[21]. However, until now none of these suggested scenarios is accepted as the crucial mechanism for neurodegeneration in MS.[22,23]. The current opinion is that despite similarities in the resulting pathological outcome, the process of neurodegeneration is composed of a heterogeneous combination of neuronal responses.

Common features of neuronal damage during MS

Despite the lack of a general concept for the development of neurodegeneration during MS, some of the CNS-related pathological observations form the pool of conditions accompanying neurodegeneration in MS. Activation of microglia and astrocytes, meningeal inflammation, neuronal hypoxia, mitochondrial damage and energy failure, increased reactive oxygen species (ROS), age-related iron accumulation, and Wallerian degeneration are all contributing to the neuronal damage associated with MS development.[24]

"Virtual" hypoxia

One hypothesis for ongoing axonal degeneration during MS is called "virtual hypoxia". It is based on similarities between mechanisms of neuronal damage which occur during acute oxygen deprivation and chronic demyelination.

Neuronal damage due to hypoxia can be observed in ischemia. The concept of white matter degeneration under limited access to oxygen and glucose was proposed by P.K. Stys.[25,26] One consequence is a decreased concentration of adenosine triphosphate (ATP)[c], which then leads dysfunction of the ATP-dependent sodium-potassium adenosine triphosphatase (Na^+/K^+-ATPase) and subsequently a rapid membrane depolarization. As a result, axons are not able to propagate action potential which leads to failure of neuronal communication. This state can be reversed if the excess oxygen will be restored in a short time frame (10-15min *in vitro*). Yet, in the case of prolonged hypoxia, irreversible damage occurs in a time-dependent manner.[25,27] Over

[c] ATP: the main "energy carrier" molecule in cells that relies on oxygen for its effective synthesis.

time, the lack of ATP leads to Na^+ accumulation in the axolemma and the operation of Na^+/Ca^{2+} exchanger (NCX) in a reverse mode. Under normal conditions, NCX plays a critical role in the removal of Ca^{2+} from the cytoplasm. During one activity cycle of the NCX a single Ca^{2+} is exported from the cell in exchange for three Na^+ using the energy of the electrochemical gradient of Na^+.[28] NCX activity in the reverse mode is leading to Ca^{2+} accumulation in the axolemma, thus promoting further pathophysiological changes (e.g. reduction in ATP production followed by Ca^{2+} overload in the mitochondria) and cell death.

During MS, demyelinated axons do not have a rapid shortage of the energy supply, but rather a slow rise in the energy demand. To restore conductance, demyelinated axons require redistribution of ion channels, which are involved in action potential propagation and are usually concentrated in the node of Ranvier in myelinated axons.[29] By this, the speed of propagation of the action potential decreases (in comparison to saltatory conductance) and the process of

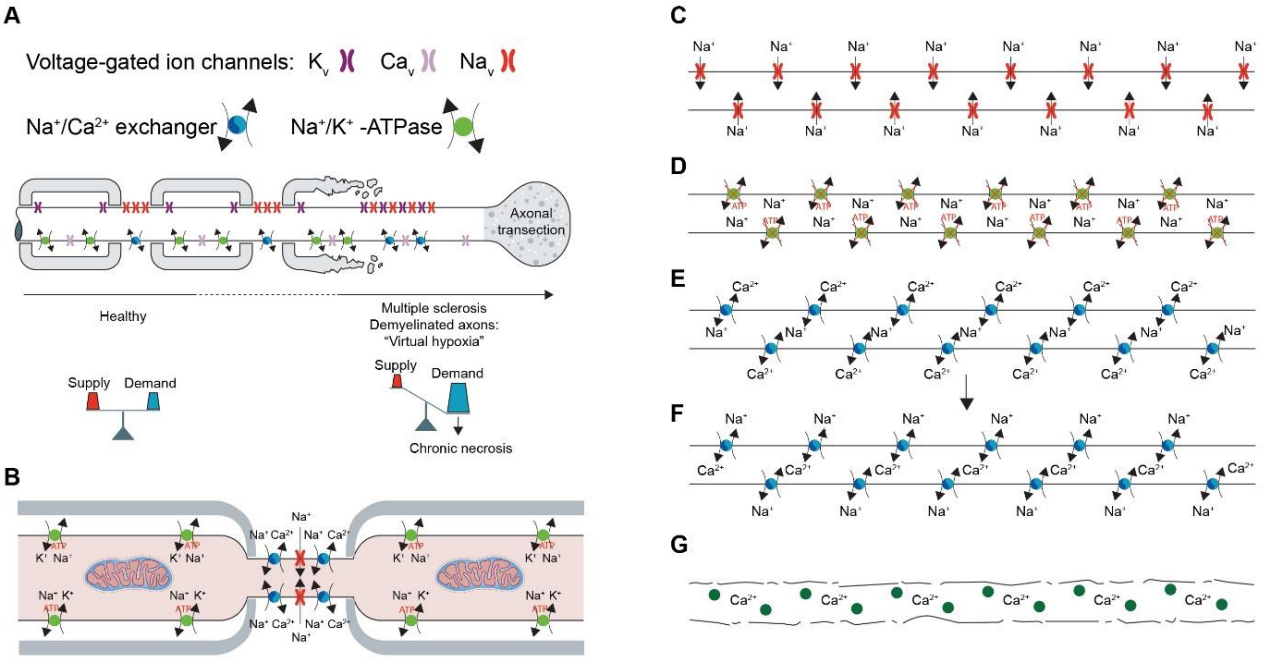

Figure 1 Model of "virtual hypoxia"

(**A**) Illustration of the proposed idea for axonal degeneration during MS. In contrast to healthy axons, with balanced energy production and demand during electrical activity, the disturbed architecture of chronically demyelinated fibers leads to inefficient conduction, with greater translocation of ions per action potential. This in turn imposes a higher metabolic load, leading to a state of increased energy demand. (**B**) Ions and ion channel distribution in the myelinated axon. (**C-G**) Critical steps of the virtual hypoxia model: (**C**) Redistribution of Na^+ ion channels to maintain conductivity of the affected axonal region; (**D**) Insufficient activity of the Na^+ clearance by Na^+/K^+ ATPase; (**E-F**) the NCX switches to the reverse operation mode; (**G**) Ca^{2+} overload leads to axonal damage. Figure adapted from.[21]

neuronal communication becomes less energy efficient. Insufficient ATP amount contributes to hypoxic-like condition, including Ca^{2+} overload and damage to the mitochondria.[30] In addition, upregulation of other channels that contribute to Na^{+} or Ca^{2+} influx, namely proton-gated acid-sensing ion channel-1 (ASIC1)[d] or transient receptor potential melastatin 4 (TRPM4)[e], was shown to be present in demyelinated axons in the MS animal model (EAE) and MS lesions.[31,32]

Glutamate excitotoxicity

Another hypothesis is based on an over activation of neuronal receptors by neurotransmitters. Neurotransmitters, such as, glutamate (Glu), are chemical molecules that are responsible for neuronal communication in the synaptic connections. Glu is the major excitatory neurotransmitter in the CNS. The release of Glu induces a cascade of responses leading to the generation of the action potential. The intracellular concentration of Glu in neurons is kept relatively high (order of magnitude of mM), whereas the extracellular concentration of Glu is very low (only a few µM) even in the cerebrospinal fluid (CFS).[33] The low extracellular concentration of Glu combined with high sensitivity of the neurons to Glu concentration changes is important to provide a good signal-to-noise ratio for synaptic communication. On the other hand, disturbance of extracellular Glu could be toxic for neurons. The toxic effect of elevated extracellular Glu level was shown first in the middle of the last century. Focal brain damage was observed after the subcutaneous administration of monosodium glutamate in mice and rhesus monkey.[34,35] Elevated Glu levels in the CSF were also detected in many CNS disorders including MS.[36] Furthermore, the involvement of Glu in neuronal damage has been shown for hypoxic neuronal death.[37] Evidence for glutamate-mediated neurodegeneration was found in Alzheimer`s disease (AD), Huntington`s disease (HD) and others neurological diseases.[38]

The underlying mechanism of Glu-mediated neurodegeneration is complex. Glu is known to stimulate a pool of receptors in neurons such as the N-methyl-D-aspartate receptor (NMDAR), α-amino-3-hydroxy-5-methyl-4-isoxazole propionic acid receptor (AMPAR), kainic acid receptors, and the metabotropic glutamate receptor family (mGluRs). Despite extensive research on excitotoxicity of Glu, the exact pathway leading to neuronal death was not explained so far.[39] One of the major problems is the heterogeneity of the neuronal damage after Glu receptor overactivation. For instance, cortical neurons *in vitro* show apoptotic and necrotic features after exposure to NMDA in a time- and concentration-dependent manner.[40] *In vivo*, the diversity of

[d] ASIC1 – pH-sensitive sodium channel, which can mediate glutamate-independent Ca^{2+} influx into neurons upon acidosis.[31]
[e] TRPM4 - Ca^{2+} activated non-selective cation channel.[32,180]

glutamate-mediated neuronal damage is more pronounced since different types of neurons have their own Glu receptor composition, as well as morphological and functional features. Nevertheless, a common pathway of Glu-mediated excitotoxicity in all neurons involves cytosolic Ca^{2+} overload. Prevention of this overload is the key component in the prevention of neuronal cell death during Glu-mediated excitotoxicity.[41,42]

2. Calcium homeostasis in the cell

Calcium ions (Ca^{2+}) are the most universal messenger of biological processes within the cell. Ca^{2+} metabolism and signalling are vital for the existence of the organism on the cellular level. Ca^{2+} mediates a wide range of intracellular processes, including gene expression, energy metabolism, immune cell activation, action potential propagation and muscle contraction. Usually, Ca^{2+} acts as a diffusible second messenger which is released in response to the interaction of the first messenger with the cell receptors. However, Ca^{2+} may also act directly, for example via G protein-coupled extracellular Ca^{2+}-sensing receptor (CaR).[43,44] Furthermore, Ca^{2+} signaling mechanism in eukaryotic cells can be self-regulated.[45] But the most noteworthy property of Ca^{2+} is its pleiotropic function. Despite its critical role in the maintenance of vital cell functions, Ca^{2+} mediates cellular stress or toxic cell death when Ca^{2+} homeostasis is disturbed.[46] As a diffusible second messenger, Ca^{2+} plays a role by variation of its intracellular concentration with a high spatial and temporal resolution. This is achieved by the activity of the range of ion channels, pumps, exchangers, Ca^{2+}-binding proteins, and intracellular Ca^{2+} stores.[47–49] For an efficient signaling at the resting state, the intracellular Ca^{2+} level is kept at an extremely low (nM) concentration in contrast to the extracellular level, which is usually around a few mM.[50] As a trade-off, disturbances of Ca^{2+} homeostasis and uncontrolled rise of intracellular Ca^{2+} levels not only disrupt Ca^{2+} depending signaling pathways but also cause a toxic effect leading to cell death.[51,52]

2.1. Neuronal calcium regulation

As neurons are postmitotic and excitable cells, precise control of neuronal Ca^{2+} level is crucial for the whole organism. A variety of intracellular neuron-specific processes are fundamentally dependent on Ca^{2+}, e.g. synaptic transmission, learning and memory formation, long-term potentiation (LTP) or long-term depression (LTD).[53–56] To maintain these and other Ca^{2+}-dependent functions, neurons have a complex and diverse toolkit controlling Ca^{2+} homeostasis by enabling to store, buffer and move Ca^{2+} across membranes.[57] A few key elements of neuronal Ca^{2+} regulation are described in the following sections.

2.1.1. Membrane ion channels

Historically, membrane Ca^{2+} channels are divided into three groups: the voltage-operated Ca^{2+} channels (VOCs), the receptor-operated Ca^{2+} channels (ROCs) and the store-operated Ca^{2+} channels (SOCs).

VOCs form the best-characterized family of neuronal Ca^{2+} channels. They transduce the changes of the membrane potential into the Ca^{2+} transients. Structurally VOCs are composed of five distinct subunits: α1, α2, β, γ, and δ. The α1 subunit forms the pore while the others play a modulatory function as part of the biophysical property of the channel.[58] VOCs can be split into three subfamilies, namely Cav1, Cav2, and Cav3, based on the structure of the α1 subunit. In accordance with their biophysical properties, VOCs are associated with one of the six classes L-, N-, P-, Q-, R-, and T-types. Each class has distinct Ca^{2+} current characteristics, activation/deactivation profile, and pharmacological features. For example, L-, N- and P/Q-types are high voltage-activated while R- and T-types are intermediate or low voltage-activated channels, respectively.[59,60] L-type channels can be blocked by 1,4-dihydropyridines (DHPs) while N- or P/Q-types are sensitive to omega-conotoxin GVIA (ω-CTx-GVIA) or Omega-agatoxins (ω-Agatoxin) and T-type has no selective blocker identified so far. VOCs are essential for various neuronal functions including regulation of neuronal Ca^{2+} transients in cell bodies and dendrites, enzymatic activity, and transcription (L-type), neurotransmitter release, dendritic Ca^{2+} transients (N-, P/Q-, R- types) and regulation of repetitive firing (T-type). Dysregulation of VOCs was shown to contribute to various disorders including autism spectrum disorders, stationary night blindness, and absence seizures.[60]

ROC channels are activated by binding to a ligand, for example to neurotransmitters or ATP. ROCs can be classified into three families: ionotropic glutamate receptors, cys-loop receptors, and ATP-gated channels. Ionotropic glutamate receptors are critical for interneuron communication and glutamate-mediated excitotoxicity (see section III.1.2.1 Glutamate excitotoxicity). Members of the cys-loop receptors family can be activated by various ligands, including γ-aminobutyric acid (GABA), glycine, acetylcholine, serotonin, and Zn^{2+}. However, most of them are not specific to Ca^{2+}. Nevertheless, activation of Ca^{2+} permeable nicotinic acetylcholine receptors (nAChRs) can not only induce direct Ca^{2+} influx but also activate VOCs or lead to the release of Ca^{2+} from intracellular stores.[61] ATP-gated channels (P2X) can be opened by binding to extracellular ATP. P2X channels modulate various neuronal functions including neurotransmitter release probability[62] and membrane conductance[63]. Although it was demonstrated that P2X channels mostly have a modulatory function, under resting membrane

potential they conduct more Ca^{2+} than other ROC channels.[64] Interestingly, P2X7 deficient mice have a suppressed development of EAE, though the specific cause was not identified yet.[65]

The function of SOCs in neurons is uncertain. It is the newest described type of Ca^{2+} channels with the most controversial role for neuronal function during healthy and pathological conditions. The activity of SOC channels requires an interplay between intracellular organelles and at least two protein complexes. This poses an additional challenge for SOC channels analysis in cells which are excitable, e.g. neurons (more details I.3).

2.1.2. Na^+/Ca^{2+} exchanger and plasma membrane Ca^{2+} ATPase

VOC, ROC, and SOC channels are regulating the influx of Ca^{2+} into the cell. The open channels do not require external energy source for Ca^{2+} conductance, only a concentration gradient across the cell membrane. While extrusion of Ca^{2+} from the cytoplasm is an energy-demanding process. Two systems on the cell membrane regulate cytoplasmic Ca^{2+} clearance: plasma membrane Ca^{2+} ATPase (PMCA) and NCX. PMCA and NCX have opposite properties in respect to the Ca^{2+} and the capacity for Ca^{2+} transport. PMCA has a high affinity for Ca^{2+} and a low capacity for the Ca^{2+} transport, thus maintaining cytosolic Ca^{2+} level close to the basal level. NCX efficiency increases with the rise in cytosolic Ca^{2+} concentration and it plays a critical role in counteracting large Ca^{2+} transients.[66]

PMCA isoforms are ubiquitously expressed in all mammalian cell types. However, some of the isoforms for example PMCA2 and PMCA3 are more abundant in excitable cells, which may reflect their contribution to specific Ca^{2+} signaling pathways.[67,68] Reduction of PMCA activity was shown to affect Ca^{2+} clearance and to contribute to the neuronal loss in various conditions including aging[69], AD[70], and CNS neuroinflammation[71,72].

NCX expression is detectable in most cell types. NCX has an electrogenic nature and it does not require energy molecules for its function. As mentioned above NCX significantly contributes to Ca^{2+} clearance after the large Ca^{2+} transients which is a common effect of neuronal activity, and thus prevents Ca^{2+} overload.[73] On the other hand, NCX is a fully reversible exchanger and it can induce Ca^{2+} influx into the cytosol. These properties of the NCX lay in core of some theories of the neuronal damage, e.g. “virtual hypoxia” model of MS-related axonal loss as was illustrated above.

2.1.3. Intracellular organelles

The endoplasmic reticulum (ER) and the mitochondria are essential players of Ca^{2+} regulation in all cell types, including neurons. They function as a buffering system by regulation of excess Ca^{2+}

during Ca^{2+} transients and as an intracellular storage of Ca^{2+} which can be mobilized internally without extracellular stimuli.

ER-mediated Ca^{2+} regulation is carried out by ryanodine receptors (RyRs), inositol-1,4,5-tris-phosphate receptors (InsP3Rs), and sarco/endoplasmic reticulum Ca^{2+}-ATPase (SERCA). RyRs and InsP3Rs are responsible for the release of Ca^{2+} from the ER. InsP3Rs requires binding to the ligand InsP3 for activation. However, cytosolic Ca^{2+} has a great impact on the biophysical property of the channel/receptor in a biphasic manner.[74] Moderate rise in cytosolic Ca^{2+} level enhances the sensitivity of the receptor to InsP3 and potentiates the channel, while high Ca^{2+} concentration inhibits InsP3R mediated Ca^{2+} influx. The major trigger for RyRs activation is cytoplasmic Ca^{2+}. A small and local rise in cytosolic Ca^{2+} may initiate a local influx via RyRs which can trigger the surrounding receptors. This phenomenon is known as Ca^{2+}-induced Ca^{2+} release (CICR).[75] Nevertheless, a wide range of molecules may modulate the activity of the RyRs including ryanodine and cyclic ADP-ribose (cADPR).[76,77] Re-uptake of Ca^{2+} to the ER is achieved via SECRA activity. Together with NCX and PMCA, SERCA plays a key role in re-establishing resting cytosolic Ca^{2+} values after the Ca^{2+} transients. The pump is ubiquitously distributed in tissues and has no distinctive characteristics in neurons.[78]

Mitochondria are another important mediator of Ca^{2+} homeostasis. It helps to shape the spatial and temporal resolution of Ca^{2+} signals produced by the plasma membrane and by ER Ca^{2+} channels. Mitochondria have an electrophoretic Ca^{2+} channel called mitochondrial Ca^{2+} uniporter (MCU), thus it does not require ATP for Ca^{2+} transport. The activity of the MCU depends on the local Ca^{2+} concentration and the mitochondrial membrane potential. Nevertheless, MCU has a low affinity to Ca^{2+} and for its effective function, the local Ca^{2+} concentration has to reach the µM order of magnitude.[79] By this, mitochondria build an emergency Ca^{2+} buffering system and participate in Ca^{2+} microdomain formation by absorbing excess Ca^{2+} and preventing Ca^{2+}-depended inactivation of the ion channels.[80–82] Ca^{2+} uptake by the mitochondria is not only part of the cytosolic Ca^{2+} homeostasis, but it is also influences canonical mitochondrial function as a major energy source of the cell. The rise in mitochondrial Ca^{2+} level can enhance ATP synthesis and it is used as a signal for the increase in energy demand of the cell.[83] Ca^{2+} efflux from the mitochondria is mediated by the mitochondrial sodium-calcium exchanger (NCLX) or by the transient opening of the mitochondrial permeability transition pore (mPTP).[84,85]

2.1.4. Non-selective ion channels, Ca^{2+} binding proteins, lysosomes

In addition to the above-described mechanisms, there are many cellular mechanisms for the modulation of Ca^{2+} influx/efflux, as well as channels with low Ca^{2+} selectivity in neurons.

Nonselective ion channels such as a few members of two-pore channels (TPCs), transient receptor potential channels (TRP channels), or acid-sensing ion channels (ASICs) can conduct Ca^{2+} current. Under “routine” neuronal activity conditions the contribution of these nonselective ion channels to the total Ca^{2+} level is neglectable in comparison to Ca^{2+} selective channels. Nevertheless, they essentially contribute to Ca^{2+} homeostasis under specific conditions while they cover a wider range of stimuli for the induction of their activity.

Ca^{2+}-binding proteins are important players for the temporal and spatial modulation of Ca^{2+} signals. Functionally they can be separated into two groups: Ca^{2+} buffer proteins and Ca^{2+} sensor proteins. However, this separation is not precise since Ca^{2+} sensors require Ca^{2+} binding and this provides a buffering function. Calmodulin (CaM) is an example for a Ca^{2+}-binding protein with a dual function. CaM is involved in the wide range of Ca^{2+} signaling cascades, including synaptic plasticity via CaM-regulated proteins[84,86], endocytosis[87] , or direct regulation of the VOC channels activity.[88] On the other hand, CaM constitutes up to 0.5% of the total protein fraction in neurons[89] and has significant Ca^{2+} buffering capacity. It was shown *in silico* that CaM is involved in short-term synaptic plasticity by direct buffering of Ca^{2+} within the presynaptic bouton.[90]

2.2. Neuronal calcium regulation and MS

The special role of Ca^{2+} signaling in routine neuronal activity demonstrates the importance of Ca^{2+} contribution to neuronal diseases. Dysregulated Ca^{2+} pathways and their involvement in neurodegeneration were shown to be present during AD, HD, hypoxia, stroke, and other neuron-related pathologies [57]. In the context of MS pathophysiology, a recent study shows the effect of Ca^{2+} influx from the extracellular space on axonal degeneration in the animal model of MS.[91] Furthermore, prevention of Ca^{2+} influx, for example by targeting Ca^{2+} permeable ion channels, or enhancing the ability of neurons to buffer additional Ca^{2+} by an increase in mitochondrial Ca^{2+} buffering capacity, is beneficial for neuronal survival during EAE.[30,31] Nevertheless, the complexity of Ca^{2+} signaling and its critical part in cellular functions require further research in order to identify potential targets for the maintenance of neuronal Ca^{2+} homeostasis under tolerated physiological conditions and the prevention of neuronal death during MS.

3. Store-operated calcium entry

Store-operated calcium entry (SOCE) is the process of Ca^{2+} influx into intracellular space in response to ER Ca^{2+} depletion. This process is mediated by store-operated channels. The biophysical property, mechanism of activation, and variability of the store-operated channels distinguishes them from other Ca^{2+} channels. Apart from their critical contribution for ER Ca^{2+} pool refilling[92], store-operated channels can also generate Ca^{2+} influx. The latter can be sustained from

minutes to hours and is essential for a wide range of biological processes, including gene transcription, secretion, and modulation of enzymatic activity. SOCE is not voltage-dependent and it can function upon negative membrane potentials, unlike most depolarization-sensitive channels (e.g. VOGs).[93] It also does not require a special ligand for its activation. The classical mechanism of SOCE activation can be initiated as a result of InsP3R- or RyR-dependent ER Ca^{2+} depletion, as well as insufficient SERCA activity.[93,94] At the same time, SOCE can be modulated by e.g. mitochondria[95,96], CaM[97], TPC[98] or TRPC[99] channels.

3.1. Calcium release-activated channels

ORAI and stromal interaction molecule (STIM) protein families are forming the Ca^{2+} release-activated Ca^{2+} (CRAC) channels, which are the key components of the SOCE. There are three main isoforms of ORAI (ORAI1, ORAI2, and ORAI3) and two isoforms of STIM (STIM1 and STIM2) known in mammalians. ORAI forms the channel pore and STIM activates the CRAC channel. The first proposed mechanism of function was given by James&Putney in 1986.[100] Nevertheless, only after the discovery of the STIM[101] and ORAI[102] proteins 20 years later, the function and molecular mechanism were elucidated for many cell types.

The classical mechanism of CRAC channel activation is linked to the depletion of the ER Ca^{2+} pool, independent of the origin of the depletion. It can be described in three main steps. (**Figure 2**) Under resting state, ORAI and STIM are homogeneously distributed among the cell and the ER membrane, respectively. Ca^{2+} release from the ER leads to conformational changes in STIM structure and results in STIMs oligomerization. Next, the ER membrane translocates in close proximity to the cell membrane, which is important for the binding of the STIM oligomers to ORAI on the cell membrane. STIM-ORAI coupling mediates the highly specific influx of Ca^{2+} into the cytosol, in a process named SOCE. The basic process of CRAC channel deactivation is independent of intracellular Ca^{2+} levels, thus only linked to ER Ca^{2+} concentration. Only when the Ca^{2+} level in the ER reaches a resting physiological level, STIM is able to bind to the ER Ca^{2+}. STIM undergoes reverse conformational changes and SOCE is thereby deactivated. Nevertheless, another mechanism for SOCE deactivation requires a high level of Ca^{2+} near the CRAC channel and is described as a Ca^{2+}-dependent inactivation. Moreover, for some conditions, Ca^{2+}-independent activation/deactivation mechanisms of SOCE were shown, e.g. oxidative stress or transient temperature increase that induces conformational changes in the STIM, and thus SOCE activation.[103]

Altogether, SOCE has a special place in the mechanisms of Ca^{2+} regulation. CRAC channels lead to a highly selective Ca^{2+} influx, which may last for hours and by this activate processes that

require prolonged rise of Ca^{2+} levels in the cytoplasm. Some of these processes are vital for the organisms, e.g. enhancing energy metabolism, T cell activation and gene expression activation.

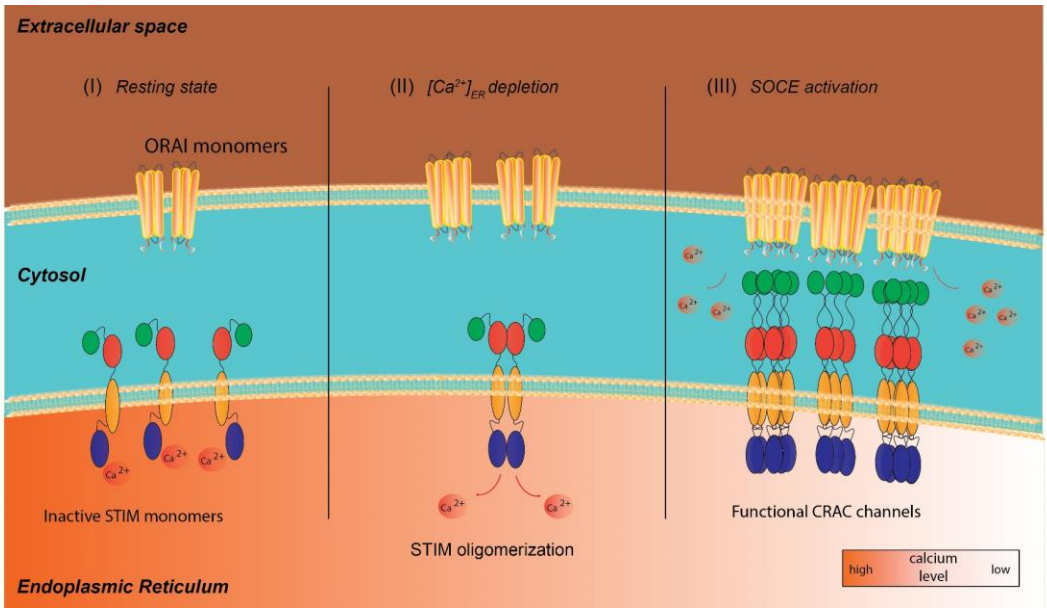

Figure 2 Schematic illustration of the classical mechanism of SOCE activation

(I) Resting state: STIM is blocked by Ca^{2+} in the ER; ORAI is distributed in the cell membrane; SOCE is not present. (II) $[Ca^{2+}]_{ER}$ depletion: Reduction of $[Ca^{2+}]_{ER}$ activates STIM oligomers formation. (III) SOCE activation: STIM oligomers induce Ca^{2+} selective pore formation by the ORAI proteins.

3.1.1. ORAI protein family

Historically, *Orai* genes and corresponding proteins were identified by genetic analysis of a patient with severe combined immune deficiency (SCID) and with an impaired SOCE in T cells. A mutation was found in the region which contained the protein-encoding gene *FLJ14466*. Expression of the wild-type variant of *FLJ14466* reconstitutes ER-depletion mediated Ca^{2+} influx in SCID T cells. Proteins encoded by *FLJ14466* and its homologs *C7orf19* and *MGC13024* were named ORAI1, ORAI2, and ORAI3 respectively in honor of the gate keepers of heaven from the Greek mythology.[102]

Members of the ORAI family are highly conserved among species on the DNA level and have 70% to 90% query cover on the protein level between each other according to The Basic Local Alignment Search Tool (BLAST[104]).[105] The *Orai* family is ubiquitously expressed on the mRNA level, however the expression level can vary tremendously among different cell types.[106] In addition, to the variation between expression profiles, experiments with dOrai (the only Orai protein in the Drosophila melanogaster) and the mammalian ORAIs show that the active pore of the CRAC requires an ORAI-ORAI interaction to form a hexametric structure.[107,108] Furthermore,

the biophysical properties of the mammalian SOCE depend on the ORAI1/ORAI2/ORAI3 ratio.[109,110]

3.1.2. STIM protein family

The identification of STIM as critical components of SOCE activity was made a year before the discovery of ORAI. 170 Ca^{2+} signaling-related genes were used in a screening experiment using the Drosophila Schneider 2 cell line in order to identify the protein involved in the SOCE pathway. Cells lacking *dStim* (the only member of the *Stim* family in the Drosophila melanogaster) had a significant reduction in intracellular Ca^{2+} increase following the depletion of the ER Ca^{2+} pool. The results were further confirmed by the selective knockdown of the human homolog STIM1 in Jurkat T cells.[111] Later on, many scientific publications further confirmed the essential role of STIM proteins to SOCE activity.

In mammals, the STIM family consists of the two main members STIM1 and STIM2. As ORAI proteins, STIM proteins are very conserved among species. They share a similar amino acid sequence and a domain structure.[112,113]

STIM proteins are mainly localized in the ER membrane, but they were detected in the cytosol or in acidic organelle membranes as well.[114,115] Moreover, they are ubiquitously present in mammalian organisms with variation in the STIM1/STIM2 expression ratio. Both STIMs have a canonical EF-hand[f] Ca^{2+}- binding motif facing the ER lumen, which allows them to react to the decrease in ER Ca^{2+} levels. Isolated EF-hand from STIM1 or STIM2 has a similar affinity to Ca^{2+} which is in the range of the ER Ca^{2+} level at the resting state of the cell (Kd = 0.2-0.6 mM).[116,117] Nevertheless, the full-length STIM1 and STIM2 proteins show a significant difference in their Ca^{2+} binding properties, leading to different demands in ER Ca^{2+} levels for their activation. STIM2 is two-fold more sensitive to the ER Ca^{2+} in comparison to STIM1, and is particularly active even without ER depletion.[118] On the other hand, STIM2 has a slower activation kinetic and a lower affinity to the ORAI proteins in comparison to STIM1.[119] At resting state STIM proteins are distributed in the ER surface and appear in the form of dimers.[120] ER Ca^{2+} release triggers the oligomerization of the STIMs and ER membrane translocation in close proximity to the cell surface.[101] Dimer structure, oligomerization, and binding to the ORAI protein depend on the complex structure and conformational state of the STIM-ORAI-activating region (SOAR) of the

[f] EF-hand is a helix-loop-helix structural motif topologically like the spread thumb and forefinger of the human hand, in which the Ca2 + ions can be fixed. [181]

STIM protein.[120–122] Both STIMs can activate the CRAC, however the properties of the active channel depend on STIM1 to STIM2 and STIM to ORAI ratios.[123,124]

3.1.3. Properties of CRAC

Multiple factors can influence the properties of CRAC channels and SOCE, including channel composition, Ca^{2+} homeostasis or other ion channels. Mechanistic experiments using HEK293 cells with a stable expression of STIM1 and an overexpression of a single ORAI (ORAI1/ORAI2/ORAI3) showed a drastic difference in the biophysical properties of the CRAC channel. For example, the activation time differs from 21 seconds for the channel formed by STIM1-ORAI2 to 63 seconds for the channel formed by STIM1-ORAI3, Ca^{2+} dependent fast and slow deactivation of the channel varied from the “not present” to “strongly dependent”, and the reaction to pharmacological compounds (e.g. 2ABP) changed from complete blockage to potentiation of the channel. In addition, it was shown that ORAI forms a heterogenic channel, but how the different members of ORAI influence the final properties of the pore is not described.[125] On the other hand, in addition to the different biophysical properties of STIM1 and STIM2 combined with diverse expression profiles between different cell types, STIM can be modulated by other proteins and thus change SOCE. For example, two-pore channel 2 (TPC2) or transmembrane protein 66 (or SOCE-associated regulatory factor, SARAF) were shown to contribute to CRAC channel activity modulation.[98,126] Physiological conditions influence SOCE as well (e.g. alkaline stimuli).[127] These and other findings show that the properties of CRAC channels and SOCE can have a different outcome in the different cell types and metabolic conditions.

3.2. Neuronal SOCE (nSOCE)

SOCE has a tight link to ER Ca^{2+} depletion with the key function of the intracellular Ca^{2+} store refilling. Therefore, it is the main Ca^{2+} source in non-excitable cells, in which ER Ca^{2+} depletion is usually followed by a specific stimulation. The picture is more complex in excitable cells, like neurons, in which the ER Ca^{2+} pool is used regularly in an activity-dependent manner. In addition, during the excitation, a variety of activity-dependent Ca^{2+} channels (e.g. VGCC) trigger the significant rise in intracellular Ca^{2+} level, which can be used for the intracellular Ca^{2+} store refilling. It was assumed that SOCE is not present in neurons because if it exists, it should be permanently activated and produce additional Ca^{2+} influx, which is not necessary and even harmful.[128] Therefore, it was surprising, that *Stim* genes were found to be expressed in murine and human brain samples.[129,130] Similar to *Stim*, all members of the *Orai* family were detected in mouse and human neural tissues.[130] The existence of nSOCE was confirmed by many studies in which the application of pharmacological inhibitors of SOCE (confirmed in non-excitable cells) or genetic

ablation of the essential CRAC channels components reduced or abolished SOCE influx in neurons. For example, nSOCE influx, which is induced by the inhibition of the SERCA was blocked by the known SOCE inhibitors ML-9 or 2-APB.[124,131] Significant reduction of nSOCE influx was also observed in primary cortical neuronal culture from a mouse with a global deletion of *Stim2*. Nevertheless, a global deletion of *Stim2* led to spontaneous death of the animals around 8 weeks from birth in the same study.[129] Additional studies showed a significant impact of nSOCE on critical neuronal function including synaptic formation and plasticity[132] or AMPA receptor trafficking in spines.[133]

3.3. nSOCE under pathophysiological condition

Apart from studies to decipher its physiological function, nSOCE was shown to contribute to the pathophysiology of several diseases of the CNS including AD, HD, epilepsy, and others. Nevertheless, these studies showed controversial results. For example, reduced neuronal expression of *Stim2* promotes neuronal loss in the mouse model of familial AD by contributing to the long-term stability of the mushroom spines.[134] On the other hand experiments with the HD mouse model showed that enhanced activity of nSOCE led to synaptic loss and that inhibition of SOCE can be used as a potential neuroprotective strategy.[135] Moreover, experiments demonstrated that deletion of *Stim2* results in a protective phenotype in the mouse model of transient focal cerebral ischemia.[129] Furthermore, upregulation of *Stim1* and *Stim2* expression levels were detected in brain samples from the pilocarpine-induced chronic epilepsy mouse model, and high protein levels of STIM1 and STIM2 were observed in a hippocampal specimen from a patient with medial temporal lobe epilepsy.[130] These and other studies indicated that “optimal” activity of nSOCE is essential for the long-term survival and functionality of neurons, however it is unclear if an increase or a decrease of nSOCE could contribute to neuroprotection.

3.3.1. nSOCE and MS

There are no data directly linking nSOCE and neurodegeneration during MS or EAE. Nevertheless, many pathological processes observed in neurons during MS such as mitochondrial dysfunction, Ca^{2+} overload, pH changes in the axolemma and ER “stress” can modulate or directly regulate SOCE in different cell types. The absence of a unique neurodegenerative pathway and the idea that neuronal death resembles between various CNS diseases, makes nSOCE an attractive target for investigation in the context of MS-related neurodegeneration.

4. Aim of the project

Neurodegeneration is a crucial pathological process leading to the clinical disability in MS. Until now, no specific neuroprotective treatment is available to prevent it. During MS, inflammation and chronic demyelination affect essential intracellular processes in neurons, including protein and energy metabolism or action potential propagation. Ca^{2+} plays a fundamental role in the regulation of intracellular processes, while dysregulation of Ca^{2+} homeostasis can lead to drastic cellular responses, including cell death. The SOCE pathway is essential for various cell types and links the intracellular Ca^{2+} stores and the extracellular Ca^{2+} pool. However, the knowledge about the role of SOCE in neuronal Ca^{2+} homeostasis is limited and controversial, especially during the different neuropathological conditions. Therefore, the overarching aim of this dissertation is to investigate the contribution of nSOCE to neuronal Ca^{2+} homeostasis and inflammatory neurodegeneration in order to validate their neuroprotective potential. The project comprises the following three Aims:

Aim 1 Profiling of nSOCE-related gene expression in neurons and in neuronal tissue.

Aim 2 Validation of the contribution of nSOCE components to neurodegeneration during CNS inflammation.

Aim 3 Characterization of Ca^{2+} activity in the neuronal network with nSOCE modification.

II. Materials and methods

1. Materials

1.1. Laboratory animals

Table 1 List of animal strains

Mouse strain name	*Used abbreviations*	*Source of the mouse strain*
C57BL/6	wild-type	The Jackson Laboratory; stock number: 000664
Orai2 global knock out	*Orai2*$^{-/-}$	Prof. Dr. Freichel Laboratory (Heidelberg University, Heidelberg)
Orai2$^{flox/flox}$	*Orai2*$^{fl/fl}$	Prof. Dr. Freichel Laboratory (Heidelberg University, Heidelberg)
Stim1$^{flox/flox}$ *Stim2*$^{flox/flox}$	*Stim1*$^{fl/fl}$*Stim2*$^{fl/fl}$	Prof. Dr. Freichel Laboratory (Heidelberg University, Heidelberg)
Stim2$^{flox/flox}$	*Stim2*$^{fl/fl}$	Prof. Dr. Freichel Laboratory (Heidelberg University, Heidelberg)
FVB.Cg-Tg(Eno2-cre)39Jme/J	*Eno2*^{cre}	The Jackson Laboratory; stock number: 006297
B6;129S6-Chat(tm2(cre)Lowl)/J	*ChAT*^{cre}	The Jackson Laboratory stock number: 006410
B6;129S-Snap25(tm2.1(cre)Hze)/J	*Snap25*^{cre}	The Jackson Laboratory stock number: 023525

1.2. Reagents

Table 2 Primers for genotyping

Primer	*Source*	*Sequence*
B-Actin_frw	Biomers	AGAGGGAAATCGTGCGTGAC
B-Actin_rev	Biomers	CAATAGTGATGACCTGGCCGT
Chat^{cre} frw	Biomers	GCAAAGAGACCTCATCTGTGGA
Chat^{cre} Mut frw	Biomers	CAAAAGCGCTCTGAAGTTCCT

Chat^{cre} rev	Biomers	CAGGGTTAGTAGGGGCTGAC
Cre_frw	Biomers	TAACATTCTCCCACCGCTAGTACG
Cre_rev	Biomers	AAACGTTGATGCCGGTGAACGTGC
Orai2_control_rev	Biomers	GCTCCACCCACACTAAGTCT
Orai2_frw	Biomers	TCCCTGACAGGAAGAGTCAGTG
Orai2_rev	Biomers	AATGAAGAGCTGGGGCATGG
Snap25^{cre} frw	Biomers	AACGTGCAACAAAGATGCTG
Snap25^{cre} Mut_rev	Biomers	CTGCAAAGGGTCGCTACAG
Snap25^{cre} rev	Biomers	AATGGGGGTGACTGACTCTG
Stim1_frw	Biomers	GATGGTCTCACGGTCTCTAG
Stim1_ko_frw	Biomers	TACAAACGTCGTTGCT
Stim1_rev	Biomers	GGCTCTGCTGACCTGGAAC
Stim2_frw	Biomers	GCTACGAATAAACATAGTCACC
Stim2_ko_frw	Biomers	AAACCCTGACAGCTTC
Stim2_rev	Biomers	GGTTTCTCTGTGTAATAGCCC

Table 3 Reagents and chemicals for genotyping

Name	*Company*
dNTPs Mix (10mM)	Thermo Fisher Scientific
DreamTaq™ Hot Start Green DNA Polymerase, 5 U/µl	Thermo Fisher Scientific
DreaTaq™ Hot Start Green PCR Master Mix (10x)	Thermo Fisher Scientific
Ethylenediaminetetraacetic acid (EDTA), 0.5 M	Sigma–Aldrich
GeneRuler DNA Ladder Mix	Thermo Fisher Scientific
Nuclease-Free H_2O	Thermo Fisher Scientific
Primers	Biomers
QuickExtract™ DNA Extraction Solution	Lucigen
ROTI®-Safe GelStain	Carl Roth
Tris ultrapure	Applichem
UltraPure™ Agarose	Invitrogen
Acetic Acid	Merck

Table 4 Reagents and chemicals for gene expression assays

Name	*Company*
RNeasy® Mini Kit	Qiagen
β-mercaptoethanol	Sigma-Aldrich
QIAshredder™ homogenizer	Qiagen
Ethanol, absolute, ≥99.8%	Sigma-Aldrich
RNase-Free DNase	Qiagen
RevertAid First Strand cDNA Synthesis Kit	Thermo Fisher Scientific
TaqMan™ Gene Expression Master Mix, 2x	Applied Biosystems
RNase-free water	Thermo Fisher Scientific
TaqMan™ Primers	Thermo Fisher Scientific

Table 5 TaqMan primers

Gene name	*Company*	*Primer ID*
Eno2	Thermo Fisher Scientific	Mm00469062_m1
Orai1	Thermo Fisher Scientific	Mm00774349_m1
Orai2	Thermo Fisher Scientific	Mm01207170_m1
Orai3	Thermo Fisher Scientific	Mm01612888_m1
Stim1	Thermo Fisher Scientific	Mm01158413_m1
Stim2	Thermo Fisher Scientific	Mm01223103_m1
Tbp	Thermo Fisher Scientific	Mm01277042_m1

Table 6 Reagents and chemicals for *in vivo* experiments

Name	*Company*
DietGel® Recovery	Clear H2O
Freud's adjuvant	Difco laboratories
Ketanest® S 25mg/ml (Ketamine)	Pfizer Pharma
Mouse/rat MOG_{35-55} peptide	Peptides & elephants
Mycobacterium tuberculosis	Difco laboratories
Nekrolyt® Salbe	CP-Pharma
O_2/CO_2 gas mixture (20%/80%)	SOL
Phosphate-buffered saline (PBS, 1X)	Pan-Biotech
Pertussis toxin (*Bordetella pertussis*)	Calbiochem
Rompun® 2% (Xylazine)	Bayer

Table 7 Reagents and chemicals for flow cytometry and fluorescence-activated cell sorting

Name	*Company*
BD Cytofix	BD Biosciences
BD FACS Clean Solution	BD Biosciences
BD FACS Flow (20 l)	BD Biosciences
BD FACS Rinse Solution	BD Biosciences
Brilliant Stain Buffer	BD Biosciences
ddH_2O	Generated in house
Fetal calf serum (FCS)	Biochrome (Merck)
Fixable Aqua Dead Cell Stain Kit	Invitrogen
PBS (1X)	Pan-Biotech
Percoll (1.13 g/ml)	GE Healthcare
Potassium bicarbonate ($KHCO_3$)	Sigma-Aldrich
Amoniumchloride (NH_4Cl)	Sigma-Aldrich

Na_2EDTA	Thermo Fisher Scientific
Bovine serum albumin (BSA)	Merck
Sodium azide (NaN_3)	Carl Roth
Collagenase A	Roche
DNase I	Merck
RPMI 1640 medium	Pan-Biotech

Table 8 Antibodies for flowcytometry and fluorescence-activated cell sorting

Antibody	*Company*	*Lot number*	*Dye*
CD11b	BD Biosciences	B247470	PE-TxRed
CD11c	BD Biosciences	B222652	Pe-Cy7
CD19	BD Biosciences	B260592	BV650
CD317	BD Biosciences	B246759	APC
CD3e	BD Biosciences	B274312	FITC
CD45	BD Biosciences	B274307	Alexa700
CD8	BD Biosciences	B273618	BV786
F4/80	BD Biosciences	B262036	BV421
Ly6G	BD Biosciences	B264760	APC-Cy7
MHC II	BD Biosciences	B248049	BV711
NK1.1	BD Biosciences	E01931-1633	PE

Table 9 Reagents and chemicals for immunohistochemistry/immunocytochemistry

Name	*Company*
D(+)-Saccharose	Sigma–Aldrich
High Precision Microscope Cover Glasses	Marienfeld
Normal Donkey Serum (NDS)	Merck
PAP pen 2 mm tip width (Liquid Blocker)	Sigma–Aldrich
Paraformaldehyde (PFA)	Sigma–Aldrich
PBS (1X)	Pan-Biotech
ROTI®Mount FluorCare	Carl Roth
ROTI®Mount FluorCare DAPI	Carl Roth
Superfrost Plus™ Adhesion Microscope Slides	Thermo Fisher Scientific
Tissue-Tek® O.C.T.™	Sakura
Triton-X® 100	Carl Roth

Table 10 Primary antibodies for immunohistochemistry/immunocytochemistry

Name	*Host organism*	*Clone*	*Source*	*Dilution*	*PRID*
Anti-STIM1	rabbit	polyclonal	Alomone Labs	1:200	AB_2039893
Anti-STIM2	rabbit	polyclonal	Alomone Labs	1:200	AB_2040218
Anti-ORAI2	rabbit	polyclonal	Alomone Labs	1:200	AB_2040046
Anti-ORAI2S	rabbit	polyclonal	Professor Dr. Flockerzi lab.	1:150	Not published
Anti-ORAI2L	rabbit	polyclonal	Professor Dr. Flockerzi lab.	1:150	Not published
Anti-NeuN	chicken	polyclonal	Millipore	1:250	AB_11205760
Anti-MAP2	chicken	polyclonal	Abcam	1:2000	AB_2138153
Anti-ChAT	goat	polyclonal	Millipore	1:300	AB_90650
Anti-IBA1	rabbit	polyclonal	WAKO	1:100	AB_839504
Anti-APP	mouse	22C11	Millipore	1:3000	AB_94882
Anti-CD3	rabbit	SP7	Abcam	1:100	AB_443425
Anti-GFP	chicken	polyclonal	Abcam	1:200	AB_300798

Table 11 Secondary antibodies for immunohistochemistry/immunocytochemistry

Name	*Host organism*	*Target Antigen*	*Company*	*Dilution*	*PRID*
Alexa Fluor® 488 α-chicken	Donkey	IgY (H+L)	Jackson Labs	1:500	AB_2340375
Alexa Fluor® 647 α-rabbit	Donkey	IgG (H+L)	Abcam	1:500	AB_2752244
Alexa Fluor® 488 a-goat	Donkey	IgG (H+L)	Abcam	1:500	AB_2687506

Table 12 Reagents and chemicals for *in vitro* experiments

Name	*Company*
(+)-Bicuculline	Sigma-Aldrich
5-Fluor-2′-Desoxyuridin (FUdR)	Sigma–Aldrich
B-27Plus™ Supplement (50X), serum free	Thermo Fisher Scientific
B-27™ Supplement (50X), serum free	Thermo Fisher Scientific
BrainPhys™	StemCell
DMEM-F12	Gibco
DMSO	Sigma–Aldrich
Dulbecco's Modified Eagle Medium (DMEM)	Thermo Fisher Scientific
FCS	Carl Roth
GlutamMAX™ Supplement	Thermo Fisher Scientific
HBSS, no calcium, no magnesium	Gibco
Hibernate™-E Medium	Thermo Fisher Scientific
Ionomycin	Alomone
MACS™ neuronal	Mieltonyc
NeurobasalPlus™ Medium	Thermo Fisher Scientific
Neurobasal™ Medium	Thermo Fisher Scientific
NeuroCult™	StemCell
Opti-MEM™	Gibco
PBS (1X)	Pan-Biotech
Penicillin-Streptomycin (10.000 U ml^{-1})	Invitrogen
PNGM™ Primary Neuron Growth Medium BulletKit™	Lonsa
Poly-D-Lysine hydrobromide	Sigma–Aldrich

Trypanblue solution	Sigma-Aldrich
Trypsin-EDTA (0.05%), phenol red	Gibco
Uridine	Sigma–Aldrich
Roswell Park Memorial Institute (RPMI) 1640 Medium	Gibco

Table 13 Plasmids for *in vitro* experiments

Insertion	*Source*	*Use*
GCaM6f	Addgene, ID 100837	AAV7 vector production
mCherry	Addgene, ID 20299	AAV7 vector production
Cre	Addgene, ID 105537	AAV7 vector production
Orai2S-IRES-GFP	Generated by Dr. Ulrich Wissenbach[136]	Cells transfection
Orai2L-IRES-GFP	Generated by Dr. Ulrich Wissenbach[136]	Cells transfection

1.3. Buffers and media

Table 14 Buffers and media

Name	*Ingredients*	*Amount*
FUdR 20mM[137]	DMSO	solvent
	Uridine	1 µM
	5-Fluor-2′-Desoxyuridin	0.1 µM
CNS digestion solution	RPMI 1640	solvent
	Collagenase A	1 mg ml^{-1}
	DNase I	0.1 mg ml^{-1}
Cell growth medium	500 ml DMEM, high glucose, GlutaMAX™ Supplement	solvent
	FCS	10% v/v
	Penicillin-Streptomycin	100 U ml^{-1}
FACS buffer	PBS	solvent
	BSA	0.5% w/v
	NaN_3	2 mM
Tris-acetate-EDTA (TAE), 50X	ddH_2O	solvent
	Acetic Acid	5.7% v/v
	EDTA	0.05 M
	Tris	2 M
Erylysis buffer	ddH_2O	solvent
	$KHCO_3$	10 mM
	NH_4Cl	0.15 M
	Na_2-EDTA	0.1 mM

1.4. Equipment and consumables

Table 15 Equipment and devices

Name	*Company*
ABI Prism 7900 HT Fast Real-Time PCR	Applied biosystems
BD FACS Aria III cell sorter	BD Biosciences
BD FACS LSR II analyser	BD Biosciences
Bench Top Microcentrifuge	Eppendorf
Binocular Stereo Microscope	Leica
Biometra Low Voltage Power Supply	Analytik Jena
Biometra Thermocycler	Analytik Jena
Centrifuge	Heraeus
Chemical fume hood	Kugel medical
Computer	HP
Epifluorescence Microscope Eclipse	Nikon
Eppendorf® Thermomixer Compact	Eppendorf
FlexCycler2	Analytik Jena
Freezer (-20 °C)	Liebherr
Freezer (-80 °C)	Sanyo
Fridge (4 °C)	Liebherr
Fume hood	Belec Vario Lab
Gel documentary device	INTAS Science Imaging
Hot bead Sterilizer	FST Fine Scientific Tools
HT 7900 real-time PCR instrument	Thermo Fisher Scientific
INC153 incubator	Memmert
Light Microscope	Olympus
LSM700 confocal laser scanning microscope	Zeiss

Microme HM 560 Cyrostat	Thermo Fisher Scientific
Neubauer cell count chamber	Marienfeld
Picus® Electronical Pipettes	Picus® Electronical Pipettes
Pipettes	Gilson, Satorius
QuantStudio™ 6 Flex Real-Time PCR Instrument	Thermo Fisher Scientific
SevenCompact pH-meter	Mettler-Toledo
SevenCompact pH-meter	Mettler-Toledo
Sterile hood	Thermo Fisher Scientific
Surgical instruments	FST Fine Scientific Tools
Water bath with shaker	GFL
NanoDrop™ 1000 Spectrophotometer	Thermo Fisher Scientific

Table 16 General consumables

Name	*Company*
µ-Dish 35 mm Quad	Ibidi
Cell Culture Dishes	Thermo Fisher Scientific
Cell scrapers, 16 cm handle length	Sarstedt
CELLSTAR EASYstrainer (40 µm)	Greiner
Disposable hemocytometer	NanoEntek
Eppendorf tubes (0.2, 0.5, 1.5, 2.5 ml)	Sarstedt
FACS tubes (5 ml)	Sarstedt
Falcon tubes (15 and 50 ml)	Greiner

Glass Bottom Dish 35 mm	Ibidi
Liquid reservoir for multichannel pipettes	Integra
Multiwell plates (96-well, 24-well, 6-well)	Greiner
Nonstick, RNase-free Microfuge Tubes	Applied biosystems
Parafilm N	Carl Roth
Pasteur pipette 230 mm (glass)	Heinz Herenz Medizinbedarf
PCR plate sealing tape	Sarstedt
Pipette tips	Sarstedt
RNase Zap™	Invitrogen
Serological pipettes (2ml, 5ml, 10ml and 25ml)	Greiner, Sarstedt
StarGuard® Comfort gloves	Starlab
Syringes and needles	BD Biosciences

1.5. Software

Table 17 Software

Name	*Company*
ImageJ (Fiji)	Open source (https://imagej.nih.gov/ij/index.html)
Qupath	Open source (https://qupath.github.io)
ZEN black	Zeiss
FlowJo v10	BD Biosciences
Prism v9.0.0	Graph Pad Software
Word	Microsoft
Exel	Microsoft
Tierbase	4D-Software
RQ Manager v1.2.1	Applied Biosystem
SDS v2.4	Applied Biosystem
QuantStudio	Applied Biosystem
FACSDiva™	BD Biosciences
Adobe Photoshop	Adobe Inc.
Adobe Illustrator	Adobe Inc.
Anaconda (Python)	Open source version (https://www.anaconda.com/)

2. Methods

2.1. Animals

All mice (**Table 1**) were kept under specific pathogen-free conditions in the central animal facility of the university medical center Hamburg-Eppendorf, Hamburg, Germany. To avoid potential toxicity of the CRE protein, animals heterozygous for *cre* and homozygous for *LoxP* insertion sites were used in all experiments with tissue-specific genetically modified mouse lines. All genetically modified mice have a C57BL/6J genetic background. The animals were housed in a facility with 55–65% humidity at 24 ± 2 °C with a 12-hour light/dark cycle and had free access to food and water. Sex- and age-matched adult animals (8–20 weeks of age) were used in all experiments.

All experiments were approved by the local ethics committee (Behörde für Soziales, Familie, Gesundheit und Verbraucherschutz in Hamburg), Tierversuchsantrag Nr. G13-022, Nr. 17-122 and ORG 713.

2.1.1. C57BL/6J

C57BL/6J mice were received from The Jackson Laboratory, USA. This mouse strain was used as the genetic background strain for all genetically modified mice.

2.1.2. *Orai2*$^{-/-}$

The *Orai2*$^{-/-}$ mouse line was created at the laboratory of Professor Dr. Marc Freichel (Heidelberg University)[138] and was imported directly. Animals were back crossed with the C57BL/6J line after 10 consecutive breeding cycles to avoid spontaneous mutation accumulation. C57BL/6J animals were used as a control (wild-type) mouse line.

2.1.3. *Orai2*$^{fl/fl}$×*Eno2*^{cre}

The *Orai2*$^{fl/fl}$×*Eno2*^{cre} mouse line was obtained by crossing the FVB.Cg-Tg(Eno2-cre)39Jme/J (*Eno2*^{cre}) and the *Orai2*$^{fl/fl}$ mouse lines. The *Eno2*^{cre} strain was purchased from The Jackson Laboratory, USA. The *Orai2*$^{fl/fl}$ line was created at the Freichel laboratory (Heidelberg University) and was imported directly.[138] Animals were back crossed with the C57BL/6J line after 10 consecutive breeding cycles to avoid spontaneous mutation accumulation. *Orai2*$^{fl/fl}$ littermate animals were used as a control mouse line.

2.1.4. *Orai2*$^{fl/fl}$×*ChAT*^{cre}

The *Orai2*$^{fl/fl}$×*ChAT*^{cre} mouse line was obtained by crossing the B6;129S6-Chat(tm2(cre)Lowl)/J (*ChAT*^{cre}) and the *Orai2*$^{fl/fl}$ mouse lines. The *ChAT*^{cre} line was purchased from The Jackson Laboratory, USA. The animals were back crossed with the C57BL/6J line after 10 consecutive breeding cycles to avoid spontaneous mutation accumulation. *Orai2*$^{fl/fl}$ animals were used as a control mouse line.

2.1.5. *Orai2*$^{fl/fl}$×*Snap25*^{cre}

The *Orai2*$^{fl/fl}$×*Snap25*^{cre} mouse line was obtained by crossing the B6;129S-Snap25(tm2.1(cre)Hze)/J (*Snap25*^{cre}) and the *Orai2*$^{fl/fl}$ mouse lines. The *Snap25*^{cre} line was purchased from The Jackson Laboratory, USA. The animals were back crossed with the C57BL/6J line after 10 consecutive breeding cycles to avoid spontaneous mutation accumulation. *Orai2*$^{fl/fl}$ animals were used as a control mouse line.

2.1.6. *Stim1*$^{fl/fl}$*Stim2*$^{fl/fl}$×*Snap25*^{cre}

The *Stim1*$^{fl/fl}$*Stim2*$^{fl/fl}$×*Snap25*^{cre} mouse line was obtained by crossing the *Snap25*^{cre} and the *Stim1*$^{fl/fl}$*Stim2*$^{fl/fl}$ mouse lines. The *Stim1*$^{fl/fl}$*Stim2*$^{fl/fl}$ mouse line was created by *M. Oh-hora* and colleagues[139] and was received from the group of Professor Dr. Marc Freichel (Heidelberg University).The animals were back crossed with the C57BL/6J line after 10 consecutive breeding cycles to avoid spontaneous mutation accumulation. *Stim1*$^{fl/fl}$*Stim2*$^{fl/fl}$ animals were used as a control mouse line.

2.1.7. *Stim2*$^{fl/fl}$

The *Stim2*$^{fl/fl}$ mouse line was obtained by back crossing the *Stim1*$^{fl/fl}$*Stim2*$^{fl/fl}$ mouse line to the C57BL/6J background strain. The animals were used for primary neuronal culture preparation. The animals were back crossed with the C57BL/6J line after 10 consecutive breeding cycles to avoid spontaneous mutation accumulation.

2.2. Genotyping

Samples. For the general mouse line genotyping, tail biopsies taken from newborn genetically modified mice were used. After the completion of the experiments, additional control genotyping was performed with ear biopsies taken at the end of the experiment. For genotyping of primary neuronal cultures, a non-neuronal tissue sample from each embryo was taken and analyzed prior to cell suspension preparation. Genetic mutations were controlled on a DNA level by polymerase chain reaction (PCR).

Experimental procedure. DNA ´extraction was performed using the QuickExtract reagent, which was applied for 6 min at 65 °C, 500 rpm, followed by a heat inactivation for 2 min at 98 °C, 350 rpm. The obtained DNA was used as a template with the corresponding genotyping PCR primers (**Table 2**) or stored at -20°C. Reaction compositions and amplification programs were adjusted for each genotype (**Table 18**-**Table 29**). The PCR product was analyzed using an agarose gel containing RotiSafe Gel Stain with an agarose concentration adjusted to the expected product size. Pictures of the respective gels were taken with a gel documentary device and were analyzed with ImageJ.

Table 18 Reagents for a single genotype PCR reaction of the *Orai2*$^{-/-}$ and *Orai2*$^{fl/fl}$ lines

Reagent	*Company*	*Amount (µL)*
ddH_2O	Thermo Fisher Scientific	16.83
Dream Taq Green HS Taq Buffer 10x	Thermo Fisher Scientific	2.5
dNTPs (10mM)	Thermo Fisher Scientific	0.5
Orai_frw (10µM)	Biomers	1.5
Orai_rev (10µM)	Biomers	1
Orai_control_rev (10µM)	Biomers	0.5
DreamTaq Polymerase	Thermo Fisher Scientific	0.17
Template		2

Table 19 Thermal profile for *Orai2*$^{-/-}$ and *Orai2*$^{fl/fl}$ genotype PCR

Temperature	95 ºC	95 ºC	66 ºC	72 ºC	72 ºC	15ºC
Time	10 min	30 sec	1 min	30 sec	10 min	hold
Repeats		40 cycles				

Table 20 Reagents for a single genotype PCR reaction of the *Stim1*$^{-/-}$ and *Stim1*$^{fl/fl}$ lines

Reagent	*Company*	*Amount (µL)*
ddH_2O	Thermo Fisher Scientific	16.7
Dream Taq Green Buffer 10x	Thermo Fisher Scientific	2.5
dNTPs (10mM)	Thermo Fisher Scientific	0.5
Stim1_frw (10µM)	Biomers	1.5
Stim1_ko_frw (10µM)	Biomers	1.5
Stim1_rev (10µM)	Biomers	1.5
DreamTaq Polymerase	Thermo Fisher Scientific	0.3
Template		2

Table 21 Thermal profile for *Stim1*$^{-/-}$ and *Stim1*$^{fl/fl}$ genotype PCR

Temperature	94 ºC	94 ºC	66 ºC	72 ºC	94 ºC	60 ºC	72 ºC	72 ºC	4 ºC
Time	1.5 min	30 sec	30 sec	30 sec	30 sec	30 sec	30 sec	5 min	hold
Repeats		10 cycles with -0.5 ºC per cycle			25 cycles				

Table 22 Reagents for a single genotype PCR reaction of the *Stim2*$^{-/-}$ and *Stim2*$^{fl/fl}$ lines

Reagent	*Company*	*Amount (µL)*
ddH_2O	Thermo Fisher Scientific	16.7
Dream Taq Green Buffer 10x	Thermo Fisher Scientific	2.5
dNTPs (10mM)	Thermo Fisher Scientific	0.5
Stim2_frw (10µM)	Biomers	1.5
Stim2_ko_frw (10µM)	Biomers	1.5
Stim2_rev (10µM)	Biomers	3
DreamTaq Polymerase	Thermo Fisher Scientific	0.3
Template		2

Table 23 Thermal profile for *Stim2*$^{-/-}$ and *Stim2*$^{fl/fl}$ genotype PCR

Temperature	94 ºC	94 ºC	66 ºC	72 ºC	94 ºC	60 ºC	72 ºC	72 ºC	4 ºC
Time	1.5 min	30 sec	30 sec	30 sec	30 sec	30 sec	30 sec	5 min	hold
Repeats		10 cycles with -0.5 ºC per cycle			25 cycles				

Table 24 Reagents for a single genotype PCR reaction of the *Eno2*^{cre} line

Reagent	*Company*	*Amount (µL)*
ddH_2O	Thermo Fisher Scientific	16.03
Dream Taq Green HS Taq Buffer 10x	Thermo Fisher Scientific	2.5
dNTPs (10mM)	Thermo Fisher Scientific	0.5
Cre_frw (10µM)	Biomers	1
Cre_rev (10µM)	Biomers	1
B-Actin_frw (10µM)	Biomers	0.9
B-Actin rev (10µM)	Biomers	0.9
DreamTaq Polymerase	Thermo Fisher Scientific	0.17
Template		2

Table 25 Thermal profile for *Eno2*^{cre} genotype PCR

Temperature	94 ºC	94 ºC	58 ºC	72 ºC	72 ºC	15 ºC
Time	2 min	30 sec	30 sec	30 sec	5 min	hold
Repeats		35 cycles				

Table 26 Reagents for a single genotype PCR reaction of the *ChAT*^{cre} line

Reagent	*Company*	*Amount (µL)*
ddH_2O	Thermo Fisher Scientific	17
Dream Taq Green HS Taq Buffer 10x	Thermo Fisher Scientific	2.5
dNTPs (10mM)	Thermo Fisher Scientific	0.5
ChatCre WT frw (10µM)	Biomers	0.8
ChatCre Mut frw (10µM)	Biomers	1
ChatCre rev (10µM)	Biomers	1
DreamTaq Polymerase	Thermo Fisher Scientific	0.2
Template		2

Table 27 Thermal profile for *ChAT*^{cre} genotype PCR

Temperature	94 ºC	94 ºC	66 ºC	72 ºC	94 ºC	60 ºC	72 ºC	72 ºC	4 ºC
Time	1.5 min	30 sec	30 sec	30 sec	30 sec	30 sec	30 sec	5 min	hold
Repeats		10 cycles with -0.5 ºC per cycle			30 cycles				

Table 28 Reagents for a single genotype PCR reaction of the *Snap25*^{cre} line

Reagent	*Company*	*Amount (µL)*
ddH_2O	Thermo Fisher Scientific	16.83
Dream Taq Green HS Taq Buffer 10x	Thermo Fisher Scientific	2.5
dNTPs (10mM)	Thermo Fisher Scientific	0.5
Snap25cre_frw (10µM)	Biomers	1
Snap25cre_WT_rev (10µM)	Biomers	1
Snap25cre_Mut_rev (10µM)	Biomers	1
DreamTaq Polymerase	Thermo Fisher Scientific	0.17
Template		2

Table 29 Thermal profile for *Snap25*^{cre} genotype PCR

Temperature	95 ºC	95 ºC	66 ºC	72 ºC	95 ºC	54 ºC	72 ºC	72 ºC	15 ºC
Time	10 min	30 sec	30 sec	30 sec	30 sec	30 sec	30 sec	5 min	hold
Repeats		12 cycles			17 cycles				

2.3. Gene expression assay

RNA isolation. Total RNA isolation was performed using the RNAeasy mini kit according to the manufacturer's instruction. Briefly, frozen tissue samples or cell pellets were resuspended in the lysis buffer supplemented with β-mercaptoethanol and were disrupted using QIAshredder columns. Then an equal volume of 70% (v/v) ethanol was added and mixed until a homogeneous solution was obtained. The solution was transferred into a RNAeasy mini spin column and was centrifuged (> 15000 g, RT, 20 sec). Afterwards, the columns were washed with 700 µl buffer RW1 (centrifugation at > 15000 g, RT, 20 sec), 500 µl buffer RPE (centrifugation at > 15000 g, RT, 20 sec), 500 µl buffer RPE (centrifugation at > 15000 g, RT, 2 min) and finally were centrifuged (full speed, RT, 1 min). The RNA was eluted into a fresh 1.5 ml tube by the addition of 45 µl RNase-free water (centrifugation at full speed, RT, 1 min). The purified RNA was quantified using the NanoDrop and stored at –80 °C until further use.

Additionally, DNA digestion was performed after the first washing step using RNase-free DNase according to manufacturer`s instruction.

cDNA synthesis. Synthesis of complementary DNA (cDNA) was performed according to manufacturer's instruction using the RevertAid First Strand cDNA synthesis kit. 11 µl of thawed RNA were mixed with 1 µl random hexamer primer and were incubated at 65 °C for 5 min for denaturation. Then, reaction buffer, RiboLock RNase inhibitor, 10 mM dNTP Mix and RevertAid reverse transcriptase were added and mixed by pipetting. Reverse transcription was performed at 42 °C for 60 min followed by inactivation at 70 °C for 5 min. cDNA was stored at -20 °C.

Quantitative real-time Polymerase Chain Reaction (qPCR). Gene expression was analyzed by qPCR, which was performed using the HT 7900 RT-PCR (or QuantStudio 6 Flex) instrument with commercial TaqMan probes (**Table 5**). All samples were run in triplicates according to manufacturer's recommendation. A single reaction contained 0.5 µl of 20×TaqMan probe, 5µl of 2×TaqMan gene expression master mix, 2.5µl RNase-free water and 2 µl cDNA template. The reaction was performed with the following thermal profile: 50 °C for 2 min, 95 °C for 10 min, 40 cycles: 95 °C for 15 sec and 60 °C for 1 min. DNA-free water control and the housekeeping gene *tata box binding protein* (*Tbp*) as endogenous control were used for all experiments.

Data analysis. Expression profile of the investigated genes were determined as ΔΔCT relative to *Tbp* expression. All data are presented as $2^{-\Delta\Delta C}$. Data analyses were performed with SDS 2.4, RQ Manager or QuantStudio software with an automatic baseline identification.

2.4. Experimental autoimmune encephalomyelitis (EAE)

The active immunization protocol was used for EAE induction. All experiments were performed genotype-blinded upon the data analysis. All animals were sex and age matched (8-12 weeks of age at the day of the immunization). All experiments were approved by the local ethics committee: (TVA Nr. G13-022; TVA Nr. 17-122)

Immunization. Animals were anesthetized with 1%-2% isoflurane in oxygen (v/v) and subcutaneously immunized with 1:1 emulsion containing 200 µg of myelin oligodendrocyte glycoprotein 35-55 (MOG35–55) peptide diluted in 1X PBS (2 mg ml^{-1}) and an equal volume of complete Freund's adjuvant (CFA supplemented with 2 mg ml^{-1} *M. tuberculosis*). At the day of immunization and 48 hours later 100µl of the pertussis toxin (PTX) diluted in 1X PBS (2 µg ml^{-1}) were injected intraperitoneal.

Scoring and housing condition. Animals were observed, weighted, and scored at the day of immunization, at day 2after immunization and daily from day 6 after immunization. Clinical disability was assessed by the following system: 0, no clinical deficits; 1, tail weakness; 2, hind limb paresis; 3, partial hind limb paralysis; 3.5, full hind limbs paralysis; 4, full hind limbs paralysis and forelimb paresis; 5, premorbid or dead. Animals reaching a clinical score ≥ 4 or having ≤ 75% of the body weight at the day of immunization were sacrificed according to the regulations of the Animal welfare act. Animals were supplied with food and water *ad libitum.* Additional high-water content food and rough cage surface cover were provided at the first day of observed neurological deficits. Skin irritations and inflamed injection areas were treated with Nekrolyt ointment.

Data analysis. Absolute and relative body weight changes, clinical score, onset, and maximum clinical score were analyzed at the end of the experiment. Animals without symptoms, with maximum clinical score ≤ 1, with disease onset ≥ day 15 post immunization, and animals that were eliminated during the experiment were excluded from the analysis. Additional histological assessment was performed with a set of representative animals, if significant difference was observed in the clinical assessment. Data visualization and statistics were performed by GraphPad Prism (v 9.0.0).

2.5. Behavioral analysis

Behavioral experiments were performed in collaboration with the behavioral unit of the UKE, together with Dr. rer. nat. Fabio Morellini. The experiments were approved by the local ethics committee (TVA Nr. 17-122). Litter-matched and gender-matched animals were used for the experiment. A maximum of two paired animals from the same litter were used for the cohort formation. Four weeks prior to the experiment and during the experiment, the animals were housed in a reversed 12-hour light/dark cycle and had a free access to food and water. During the adaptation time each animal was handled at least twice a week by the person performing the experiment. Experiments were performed genotype-blinded upon data analysis.

2.5.2. Open field

Animals were placed in the center of a square and clean empty box. The position of an animal was recorded for 20 minutes, and the parameters of the recorded traces (total distance, and proximity to the walls of the box) were analyzed. Four animals were analyzed simultaneously in identical boxes under controlled light condition (maximum 26 lux).

2.5.3. Y maze

Animals were placed in the center of a clean Y-maze. All arms were identical and open. Each animal was observed for 15 minute or for 27 arm visits. The number of alternations (visits to the novel arm) were recorded.

2.6. Flow cytometry and fluorescence-activated cell sorting

2.6.1. Cells isolation

Splenocytes. For the isolation of splenocytes, mice were anesthetized with the O_2/CO_2 gas mixture and subsequently killed with 100% CO_2. The spleen was harvested with sterile instruments and placed into ice-cold PBS. Cell suspensions were prepared by homogenizing spleens from all animals simultaneously using a 40-µm cell strainer and ice-cold PBS. To remove the PBS, cell suspensions were spun down by centrifugation (300 g, 10 min, 4 °C) and then resuspended in 1 ml FACS buffer. To remove the red blood cells, 5 ml ice-cold Erylysis buffer were added to the cell suspension and were incubated for 5 min on ice. Lysis was stopped by the addition of 40 ml FACS buffer. Afterwards, the cells were spun down by centrifugation (300 g, 10 min, 4 °C) and resuspended in 5 ml PBS.

To reduce the number of animals used in the experiments, histological analysis was combined with immune cells analysis. In this case spleen isolation was performed prior to PFA perfusion.

Blood. Whole blood was taken prior to spleen isolation by inferior vena cava punction with EDTA-coated syringe and was placed into EDTA-coated tubes. 50 µL of blood from each animal was used for the experiments. The samples were stored in EDTA-coated tubes on the rotation plate for 3 hours at RT.

CNS infiltrating immune cells. For the isolation of CNS infiltrating immune cells, animals were sacrificed as described at "**Splenocytes**". Immediately after the animals were perfused intracardially with 10 ml of ice-cold PBS, brains and spinal cords were isolated, placed into ice-cold PBS and mechanistically disrupted. After the collection of all samples, brains and spinal cords were incubated in digestion buffer for 1 hour at 37 °C. Tissues were homogenized by triturating through a 40 µm cell strainer and washed with 50 ml PBS. The obtained cell suspensions were spun down, washed with 50mL PBS and then spun down again by centrifugation (300 g, 10 min, 4 °C). Immediately afterwards, the cells were resuspended in 4 ml 30% Percoll solution (in RPMI medium). 2 ml 78% Percoll solution (in RPMI medium) was added underneath. Samples were centrifuged (2500 rpm, 30 min, 4 °C) and the interphase, which contained the immune cells, was collected. The obtained cell suspension was washed with ice cold PBS and centrifuged again (300g, 10 min, 4 °C). Finally, the cells were resuspended in ice-cold PBS for further live/dead staining.

2.6.2. Fluorescent immunolabeling

Staining was performed immediately after cell suspension preparation. Live/dead staining was performed separately from the other stainings. All antibodies were applied simultaneously as a mixture with an adjusted final concentration. Fluorochrome, antigen and final dilutions are presented in (**Table 30**). The staining protocol is presented in (**Table 31**). After the final washing step, the samples were fixed with fixation buffer, which was applied for 30 min at 4 °C and washed with FACS buffer (300 g, 10 min, 4 °C). Cells were resuspended in FACS buffer and stored at 4 °C upon measurements. All measurements were performed within 24 hours after the fixation of the samples. Prior to the measurement, counting beads were added to each sample according to the manufactory recommendation for quantitative measurements.

Table 30 Antibodies for cell suspension staining

Antigen	*Fluorochrome*	*Final Dilution*
CD11b	PerCP/Cy5.5	1:100
CD11c	PE-Cy7	1:300
CD19	BV650	1:100
CD317	APC	1:100
CD3e	FITC	1:100
CD45	Alexa700	1:100
CD8	BV786	1:100
F4/80	BV421	1:100
Fc block	--	1:100
Live/Dead	AmCyan	1:1000
Ly6G	APC-Cy7	1:200
MHCII	BV711	1:100
NK1.1	PE	1:300

Table 31 Cell suspension staining protocol

Live/dead staining

Solvent	*Incubation parameters*	*Washing parameters*
PBS	30min at 4 °C	PBS, 300g, 10 min, 4 °C

Antibodies staining

Solvent	*Incubation parameters*	*Washing parameters*
FACS buffer	30 min at 4 °C	FACS buffer, 300g, 10 min, 4 °C

2.6.3. Flow cytometry parameters

Markers used for the identification of specific immune cell subsets are presented bellow (**Table 32**). For the flow cytometry analysis of the blood samples and for the fluorescent-activated cell sorting, only antibodies required for the identification of the analysed cell types were used for staining. Gating strategy was not changed.

Table 32 Markers used for immune cell types identification

Cell type	*Markers*
Neutrophils	L/D; $CD45^{+}$; Ly6G+
Microglia	L/D; $CD45low^{+}$; $Ly6G^{-}$; $CD11b^{+}$
Macrophages	L/D; $CD45hi^{+}$; $Ly6G^{-}$; $CD11b^{+}$; $F4/80^{+}$
cDCs	L/D; $CD45hi^{+}$; $Ly6G^{-}$; CD11b+; $F4/80^{-}$; MHC II^{+}; $CD11c^{+}$
NK cells	L/D; $CD45hi^{+}$; $Ly6G^{-}$; $CD11b^{-}$ $NK1.1^{+}$; $CD3^{-}$
NK T cells	L/D; $CD45hi^{+}$; $Ly6G^{-}$; $CD11b^{-}$ $NK1.1^{+}$; $CD3^{+}$
B cells	L/D; $CD45hi^{+}$; $Ly6G^{-}$; $CD11b^{-}$ $NK1.1^{-}$; $CD19^{+}$
CD4 T cells	L/D; $CD45hi^{+}$; $Ly6G^{-}$; $CD11b^{-}$ $NK1.1^{-}$; $CD19^{-}$; $CD3^{+}$; $CD8a^{-}$
CD8 T cells	L/D; $CD45hi^{+}$; Ly6G-; $CD11b^{-}$ $NK1.1^{-}$; $CD19^{-}$; $CD3^{+}$; $CD8a^{+}$
pDCs	L/D; $CD45hi^{+}$; Ly6G-; $CD11b^{-}$ $NK1.1^{-}$; $CD19^{-}$; $CD317^{+}$
lymDCs	L/D; $CD45hi^{+}$; $Ly6G^{-}$; $CD11b^{-}$ $NK1.1^{-}$; $CD19^{-}$; $CD317^{-}$; MHC II^{+}; $CD11c^{+}$

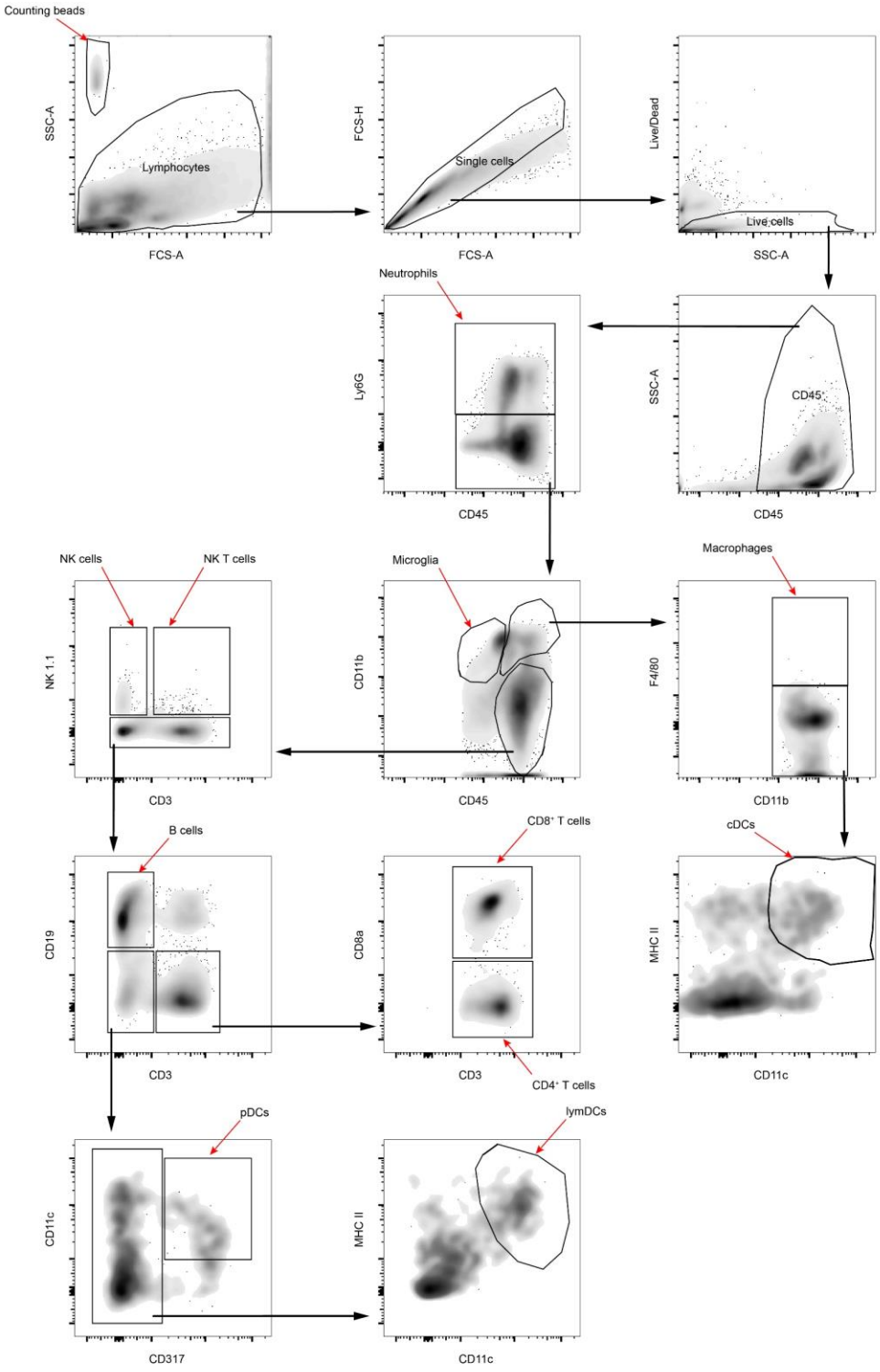

Figure 3 Gating strategy for the immune cell subsets analysis

Lymphocytes and counting beads were identified by size and granularity (FCS-A and SSC-A). Single cells were separated by high and area of the forward scatter (FCS-H and FCS-A). Live cells were further separated and analyzed. Immune cell subsets were defined according to **Table 32** in the way represented on the scheme. In case of the reduced number of required subsets (for blood samples, or FACS analysis), unused markers were excluded from the panel.

2.6.4. Data analysis

Schematic representation of the gating strategy for the flow cytometry data analysis is shown in **Figure 3**. All data were analysed with the FlowJo software, by manual gating of the originally generated data according to the gating strategy. Absolute quantifications and relative to CD45 representations of the cell subtypes were collected and analyzed. All comparisons, visual representations, and statistics were performed with GraphPad Prism (v 9.0.0) software.

2.7. Histopathology/Immunohistochemistry

Tissue preparation. Mice were anaesthetized intraperitoneally with 100 µl of anesthetic solution per 10 g of body weight. For histopathology and immunohistochemistry mice were perfused with 4% w/v paraformaldehyde (PFA) solution. Spinal cord and brain were dissected, fixed for 45 min with 4% PFA and then transferred to 30% w/v sucrose solution at 4 °C for dehydration and stored until the tissue sunk. Dehydrated tissues were embedded in optimal cutting temperature compound (OCT) and stored at -80 °C. Midcervical spinal cord sections or whole brain sections were cut at 12 µm thickness using a microtome-cryostat. Sections were then stored at –80 °C prior to staining.

Alternatively, brain and spinal cord samples were post fixed with 4% PFA for at least 24 hours than embedded into paraffin, cut and stained at the UKE mouse pathology facility.

Staining. Prior to staining samples were washed three times with 1X PBS at RT for at least 5 minutes per wash. Permeabilization of the samples was performed with TritonX-100 dissolved in PBS (0.5%, v/v). Permeabilization solution was applied for 45 minutes to the tissue sections. Donkey serum dissolved in PBS (10%, v/v) was used as blocking solution. Permeabilization and blocking reagents were combined in one solution and applied simultaneously. Primary antibodies were diluted in 1X PBS and applied overnight at 4 °C. Secondary antibodies with corresponding target sites and fluorophore were applied for 3 h at RT. All secondary antibodies were generated in donkey.

Imaging. All images were generated with ZEISS LSM700 confocal microscope using 20x, 40x or 63x objectives.

Analysis. Depending on the target of the analysis, ImageJ, QuPath or ZEN Black software were used for the quantification or preparation of representative images.

2.8. Primary neuronal culture

Tissue preparation. All experiments were done using 16.5 days old embryos (E16.5). The pregnant mouse was anesthetized with O_2/CO_2 mixture and decapitated afterwards. Immediately after, the abdomen was rinsed with 70% ethanol and dissected to reveal the body cavity. The uterine horns were cut and placed in a new cell culture dish containing 1X HBSS. The uterus was dissected and embryos were removed from the embryo sacs. The embryos were decapitated and the brains were removed and placed in the fresh 1X HBSS media. If prolonged storage was required, they were stored in 1X Hibernate medium.

If required, genotype control was performed with the non-neuronal tissue collected during the brain dissection.

Cell suspension. Embryonic cortical tissue was isolated under a binocular and collected in a 15 ml polypropylene tube in ice cold 1X HBSS media. For the dissociation, collected samples were placed in 1mL 0.05% Trypsin/EDTA solution and incubated for 6 minutes at 37°C. After the incubation, 5 ml of DMEM/F12 medium supplemented with 10% (v/v) fetal bovine serum (FSC) were added to quench trypsinization. Then media was replaced by 1mL of neuronal medium. Mechanistic dissociation was performed by manual pipetting with a 1000 µl pipette (~15 times) followed by manual pipetting with a Pasteur pipette (~10 times). The obtained cell suspension was filtered through a 40 µm strainer and counted with a hemocytometer in a 1:1 trypan blue solution (0.4% v/v). Cell suspension volume was adjusted to the required cell concentration.

Seeding and growth condition. Neurons were seeded on glass surface coated with Poly-D Lysine. 45 minutes after the seeding, the medium was replace by the required amount of neuronal growth medium and incubated at 37°C, 5% CO_2 . To obtain pure neuronal culture 20µM 5-fluorodeoxyuridine (FUdR) was added 48-72 hours after seeding.

2.9. Cell line

The HEK293 cell line was purchased from the CLS Cell Lines Service. Cells were seeded at a density of $1x10^4$ cells/cm^2 and cultured at 37°C, 5% CO_2 in DMEM medium containing 10% (v/v) FCS and 1% (v/v) penicillin-streptomycin mixture. For maintenance, cells were reseeded every four days. The cell line was used for up to 10 passages.

2.10. Cell transfection

HEK293 cells with a confluency of 70% were transfected by corresponding plasmids using Lipofectamine 2000 according to the manufacturer`s protocol (Thermo Fisher Scientific Protocol Pub. No. MAN0007824 Rev.1.0). Primary neuronal cultures were transfected at day 7 after the

seeding (day *in vitro* 7, DIV7). Immunocytochemistry protocol was performed 48 hours after the transfection of the HEK293 cells or at DIV12-DIV14 for the cultured primary neurons.

2.11. Primary neuron transduction

Adeno-associated virus vector serotype 7 (AAV7) containing a sequence for GCaMP6f, Cre, or mCherry-Cre-reporter protein production, was used for the transduction. Plasmids for vectors production were purchased from Addgene repository and used without modifications (**Table 13**). All AAVs were produced at the UKE vector facility. Primary neuronal cultures were transduced at DIV7-DIV10 by direct addition of the vectors into the culture. Multiple vectors, if required, were added simultaneously. Cultures were analyzed at DIV14-DIV21. Effective multiplicity of infection (MOI) was determined for each batch of the vectors by trial transduction. MOI for all experiments and all vectors were in range of 10×10^3-50×10^3 AAV capsids per cell.

2.12. Live-cell calcium imaging

Live-cell Ca^{2+} imaging was performed with primary neuronal culture transduced with AAV viruses. Imaging was performed using ZEISS LSM700 confocal microscope in the time lapse mode. The cultures were placed in the P-Set 2000 imaging chamber with the controlled CO_2 condition (5%). Active compounds were added during the experiment by direct pipetting to chamber. All live-cell imaging data sets were generated with 478ms temporal resolution, 20x magnification, and maximum size of the pin hole of the confocal microscope. At the end of each experiment ionomycin at a final concentration of 4µM was added to obtain the maximum fluorescent intensity for signal normalization.

Data analysis. Segmentation of the time lapse series was performed manually using ImageJ. Every segmented region of interest (ROI) contains the signal from a single neuronal soma. Signal intensity series of each ROI were stored in the .cvs format. Normalization and analysis were performed using custom-made script written in Python 3.6. The analyzed parameters were adjusted in the script according to the requirements of the experiments. Basic script and definitions of the parameters were previously published.[30] Amplitude (A), mean signal intensity (Mean) and numbers of Ca^{2+} transients = firing rate (N), were defined as followed:

$$N_i = n \ \ if \ (F(n) \geq F(a), where \ a \in [n-\delta \ldots n+\delta]) \ and \left(F(n) > \frac{1+\gamma}{2\theta+1} \sum_{j=n-\theta}^{n+\theta} F(j) \right)$$

Firing rate (N_i) : N: Ca^{2+} transient count; F: normalized signal intensity; i and n: indexes for defined frame (n) and cell (i); parameters δ, θ and γ were set as 3,7 and 0.6 for all analyzed cultures by

manual assessment (5 % of randomly depicted traces were compared) of effective pick detection > 80%

$$A_i = \frac{1}{k_i}\sum_{j=1}^{k_i} Fp_{ij}$$

Amplitude (A_i): amplitude for the i^{th} cell with detected k spikes; Fp_i – amplitude of individual spike of i^{th} cell

$$Mean_{[a,b]} = \frac{1}{b-a}\sum_{j=a}^{b} F(j)$$

$Mean_{[a,b]}$: mean of recorded signal from frame a till frame b, F(j) – signal extracted from j^{th} frame; parameters a and b were determined for each experiment individually for each experiment with a constant analyzed interval; last frame was recorded before ionomycin addition.

2.13. Immunocytochemistry

Primary neurons or HEK cells were fixed with 4% PFA for 15 minutes at RT, then washed with 1X PBS twice for 10 minutes. Samples were stored in 1x PBS at 4°C prior to staining. Staining was performed within a week after the fixation of the samples. Permeabilization of the samples were performed with TritonX-100 dissolved in PBS (0.5%, v/v), which was applied for 15 minutes at RT. Donkey serum dissolved in PBS (10%, v/v) was used as a blocking solution. To prevent unspecific binding, samples were incubated in the blocking solution for 30 min at RT immediately after permeabilization. Primary antibodies diluted in 1X PBS were applied for 4 hours at 4 °C. Secondary antibodies with corresponding target sites and fluorophore were applied for 1 hour at RT. All secondary antibodies were generated in donkey. After the staining samples were mounted on a glass microscopic slid using ROTI®Mount FluorCare medium with or without 4′,6-diamidino-2-phenylindole (DAPI) supplement. Images were taken at least 48 hours after the staining, but within a month from staining. All images were generated with ZEISS LSM700 confocal microscope with 20x, 40x or 63x objective.

III. Results

1. Determination of the neuronal SOCE composition

To narrow down the potential targets for investigation regarding the contribution of SOCE to neuronal Ca^{2+} regulation and neurodegeneration, genetic expression of critical SOCE-related genes was done in neural tissue in healthy and EAE wild-type mice and primary neuronal culture.

1.1. Expression of SOCE genes in neural tissue and primary neuronal culture

The expression of *Orai* and *Stim* gene families was analyzed in the hippocampus, cortex, cerebellum, and spinal cord of healthy C57BL/6 (wild type) mice. *Orai2*, *Stim1*, and *Stim2* genes were detected as highly expressed in all neural tissue samples. (**Figure 4 A-D**). The highest expression of *Orai2* was detected in samples from the hippocampus (**Figure 4 C**), followed by the spinal cord (**Figure 4 A**) and the cortex (**Figure 4 B**). The expression profile of *Orai2* reflects the neuronal density in the analyzed neural tissue to some extent. Thus, it can be assumed, that *Orai2* is the predominantly expressed *Orai* in neuronal cells. Further expression analyses were performed on primary neuronal culture prepared from cortical neurons. Starting from 14 days of growth (day *in vitro* 14, DIV14), cortical neuronal cultures showed an expression profile which is comparable to the one of neural tissue. (**Figure 4 E-H**).

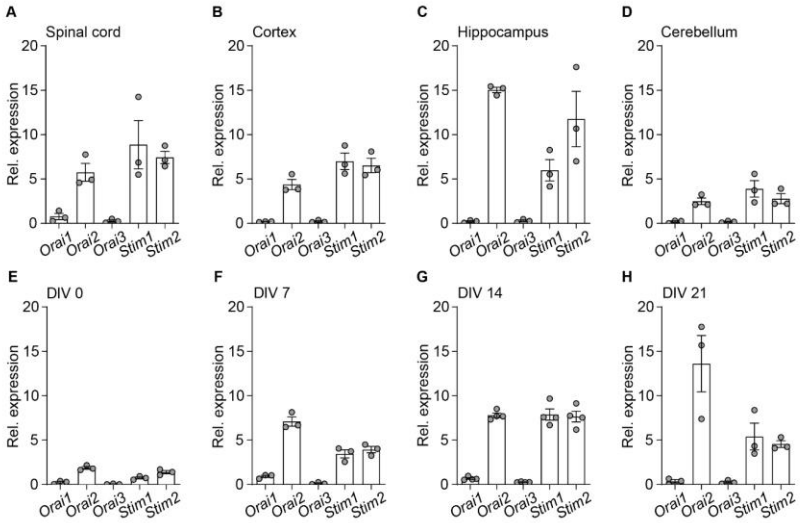

Figure 4 Expression profile of SOCE related genes

Relative qPCR mRNA expression of *Orai1*, *Orai2*, *Orai3*, *Stim1*, and *Stim2* in murine spinal cord (**A**), cortex (**B**), hippocampus (**C**), cerebellum (**D**) and in primary neuronal culture samples at DIV 0, 7, 14, and 21 (**E-H**). Healthy C57BL/6 female mice, 8-10 weeks of age (n=3), and C57BL/6 E16.5 neurons (n=3) were used for all experiments. Data presented as a fold change compared with *Tbp* expression, and plotted as mean +/- s.e.m.

1.2. The distribution of SOCE-related proteins in neurons

For the characterization of protein distribution, immunofluorescence labeling was performed on neural tissue samples and cultured primary neurons from wild-type mice. Unfortunately, commercially available antibodies against ORAI2 and STIM2 showed no or unspecific signal. In collaboration with the laboratory of Professor Dr. Veit Flockerzi from the Saarland University, antibodies against the ORAI2 protein were generated. Two antibody types directed against the C- and N- terminus of the ORAI2 protein were produced by the Flockerzi group. Antibodies against the N- terminus were designed to target only a splice variant with an extended amino acid sequence (ORAI2 large) while the C- terminus targeting antibodies can bind to the small and the large variants of the ORAI2 protein (ORAI2S and ORAI2L respectively).[136] Validation of the antibodies was performed using the HEK293 cell line and plasmids with insertion of either ORAI2S or ORAI2L and green fluorescent protein (GFP) transcripts with independent expression. Both antibodies were suitable for the detection of the overexpressed ORAI2 protein in HEK293 cells (**Figure 5 A, B**). However, an attempt to validate the antibodies using spinal cord tissue samples with a global *Orai2* deletion, demonstrated that only the C-terminus anti-ORAI2 antibodies showed no fluorescent signal in *Orai2*-deleted tissue, as expected (**Figure 5 C**). For this reason, in the next experiments, only these antibodies were used to detect ORAI2.

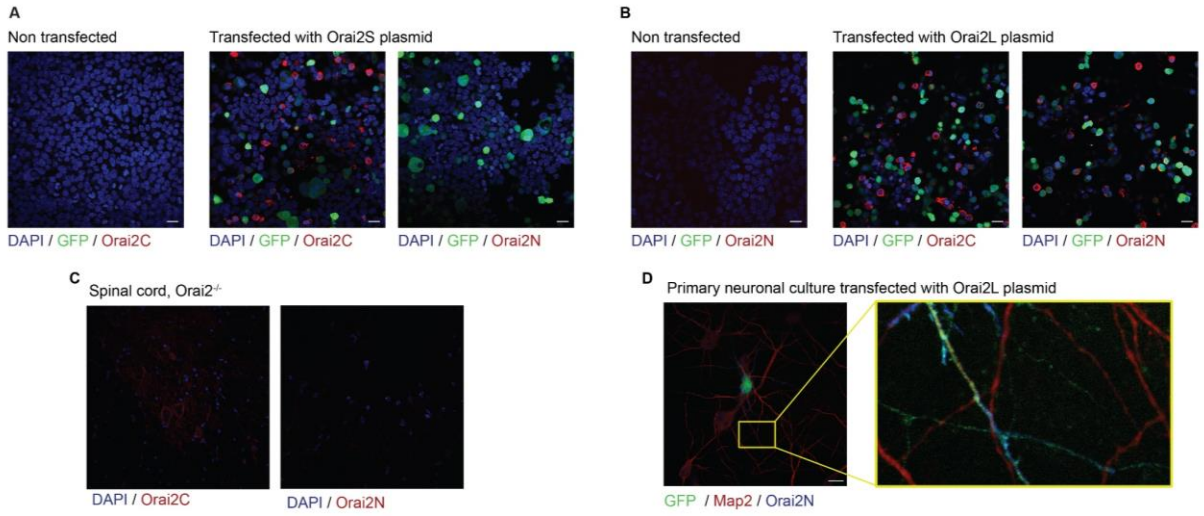

Figure 5 Antibodies validation and ORAI2 distribution

(**A**-**B**) Representative confocal images of HEK293 cells transfected with an Orai2S-GFP or an Orai2L-GFP plasmid and stained with antibodies against C- or N- terminus of ORAI2 (Orai2C, Orai2N) and DAPI. Successful transfection was confirmed by green GFP detection, scale bar 20µM. (**C**) Representative confocal images of spinal cord sections from Orai2$^{-/-}$ mice stained with antibodies against C- or N- terminus of ORAI2 (Orai2C, Orai2N) and DAPI. (**D**) Representative confocal images of wild-type primary neuronal culture transfected with an Orai2L-GFP plasmid and stained with antibodies against N- terminus of ORAI2 (Orai2N) and DAPI. Successful transfection was confirmed by GFP detection. Scale bar 20µM

Despite the specificity of the ORAI2 antibodies, validation of the distribution of the ORAI2 protein in neural tissue could not be performed due to the high fluorescent signal from the overall tissue. Tissue samples with cell-specific deletion of *Orai2* could not be analyzed either because of the high background signal. Moreover, wild-type primary neuronal culture could not be stained with the same antibodies with a sufficient signal-to-noise ratio, thus the obtained signals were indistinguishable from the background. Nevertheless, primary neurons transfected with the *Orai2* plasmids could be specifically stained against ORAI2. The result of this experiment shows that overexpressed ORAI2 protein is localized primarily to the cell membrane (**Figure 5 D**). Furthermore, based on the morphology of the neurons, overexpressed ORAI2 protein could be observed in dendritic spines and axons (**Figure 5 D**).

1.3. Expression of SOCE genes in neural tissue during CNS inflammation

In order to validate nSOCE composition during different stages of neuroinflammatory processes, cortex, hippocampus and spinal cord samples from wild-type mice during different stages of EAE, and the corresponding healthy controls were used for gene expression analysis using qPCR (**Figure 6 A-C**). A significant reduction in *Stim1* expression and a trend of downregulation of the *Orai2* and *Stim2* genes was observed at acute EAE in cortical tissue with recovery in chronic EAE

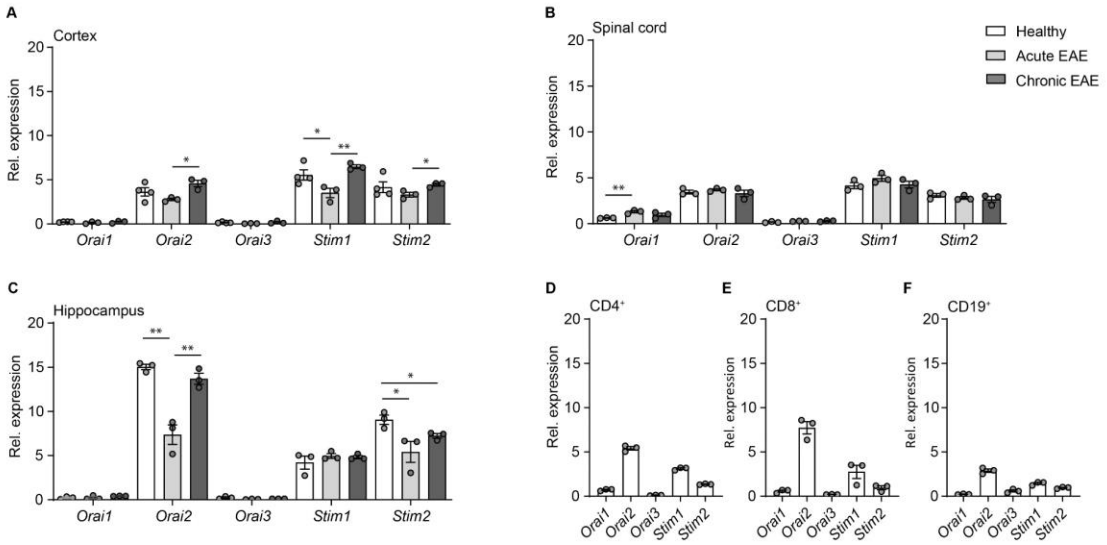

Figure 6 Expression profile of SOCE-related genes during CNS inflammation

Relative qPCR mRNA expression of *Orai1*, *Orai2*, *Orai3*, *Stim1*, and *Stim2* in cortex (**A**), spinal cord (**B**), hippocampus (**C**), $CD4^+$ and $CD8^+$ T cells (**D**, **E**), B cells (**F**). Neural tissue samples were isolated from wild-type mice at acute and chronic EAE as well as healthy controls. Immune cells were isolated from the spleen of the healthy wild-type animals by fluorescence-activated cell sorting. Three biological replicates (n=3) were performed in all experiments except for the healthy control cortical tissue samples (n=4). Data presented as a fold change to *Tbp* expression, and plotted as mean +/- s.e.m. Statistical analysis was performed by unpaired, two-tailed Student's t-test, * $p < 0.05$; ** $p < 0.01$

(**Figure 6 A**). In the hippocampus *Orai2* and *Stim2* transcripts show a significant reduction with no complete recovery in the expression of *Stim2* at the chronic stage of EAE (**Figure 6 C**). The expression levels of *Orai2, Stim1* and *Stim2* were not affected in the spinal cord (**Figure 6 B**). In addition, expression of *Orai1, Orai2, Orai3, Stim1* and *Stim2* genes was analyzed in T cell subsets ($CD4^+$ and $CD8^+$ T cells) and B cells (CD19) from wild-type healthy mice (**Figure 6 D-F**). Surprisingly, the mRNA expression pattern of the *Orai* gene family in the immune cells was very similar to that of neural tissue. Nevertheless, the ratio of *Orai2* to *Orai1* was lower for the immune cells in comparison to the mature primary neuronal culture or the hippocampus. The expected relative abundance of *Stim1* over *Stim2* expression was observed for all analyzed immune cell subtypes (**Table 33**).

Table 33 Overview of the ratios of the expression of SOCE-related genes

	Orai2/Orai1	*Orai2/Orai3*	*Stim2/Stim1*
Cortex	22.6	19.0	0.93
Spinal cord	7.3	21.0	0.83
Hippocampus	69.1	52.6	1.96
Cerebellum	12.6	13.7	0.71
Primary neurons (DIV14)	11.5	28.3	0.97
Primary neurons (DIV21)	38.7	51.0	0.84
$CD4^+$ T cells	14.8	29.8	0.35
$CD8^+$ T cells	15.9	32.2	0.28
B cells	7.6	3.3	0.51

2. Contribution of *Orai2* to neurodegeneration during CNS inflammation

The analysis of SOCE gene expression profile showed a clear dominance of *Orai2* expression in neuronal tissue and a significant change in *Orai2* expression in the CNS during EAE. These observations indicated that *Orai2* can potentially be an important player in neuronal Ca^{2+} homeostasis during CNS inflammation. Furthermore, *Orai2* inhibition was reported to be irrelevant for various cell types, including immune cells, with mild or no effect on the activity of the SOCE. This suggests that *Orai2* is a good candidate for neuron-specific pharmacological treatment that could be applied to prevent neuronal damage during CNS inflammation.

2.1. Validation of *Orai2*$^{-/-}$ mice

Next, mice with a genetic deletion of the gene of interest were used in an *in vivo* model to investigate the contribution of that specific protein. A mouse line with a global deletion of the *Orai2* gene was generated at the laboratory of Professor Dr. Marc Freichel (Heidelberg University).[138] qPCR analysis of SOCE-related genes revealed that the mRNA level of *Orai2* was not detectable in hippocampal and spinal cord samples from knock out animals (**Figure 7**); *Orai3* gene expression was significantly reduced in the spinal cord, though the level of expression was near to the detection limit; other SOCE-related genes were unaffected.

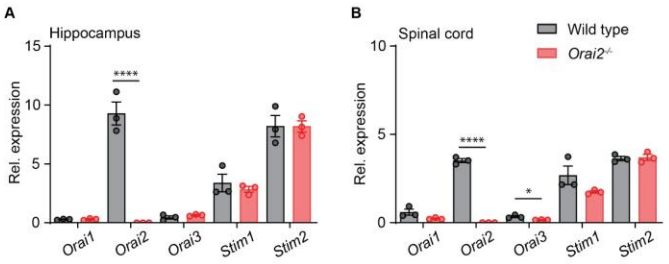

Figure 7 Validation of the expression of SOCE-related genes in the *Orai2*$^{-/-}$

qPCR mRNA expression of *Orai1*, *Orai2*, *Orai3*, *Stim1*, and *Stim2* genes in the hippocampus (**A**) and the spinal cord (**B**) of *Orai2*$^{-/-}$ and wild-type mice. Healthy animals, 8-10 weeks of age (n=3), were used for this experiment. Data presented as a fold change to *Tbp* expression, and plotted as mean +/- s.e.m.. Statistical analysis was performed by unpaired, two-tailed Student's t-test. * p< 0.05; **** p <0.0001

2.2. Global deletion of *Orai2* leads to amelioration of EAE disease progression.

Validation of the expression profile of SOCE-related genes in *Orai2*$^{-/-}$ mice showed no impact of *Orai2* deficiency on the expression level of other SOCE genes on the mRNA level. Thus, a mouse model with *Orai2* deficiency would be suitable to investigate the contribution of *Orai2* to inflammatory neurodegeneration. The outcome of CNS inflammation was analyzed in *Orai2*$^{-/-}$ and the corresponding wild-type mouse line by using MOG-induced EAE model.

2.2.1. Clinical analysis of EAE

A daily assessment of neurological disability during EAE disease course is presented in **Figure 8 A**. A clear difference between the two genotypes with respect to the clinical score can be observed. Yet, no significant variation in the body weight of animals on the day of immunization nor on the disease onset was visible (**Figure 8 C, D**). In addition to the significant difference in the area under the curve (AUC), there was a trend to a milder maximum disease score (p = 0.0501) in the *Orai2*$^{-/-}$ animals in comparison to wild-type animals. (**Figure 8 B, E**) Relative body weight change during EAE disease course, which represents general inflammation, was not different between the cohorts (**Supplement 1**).

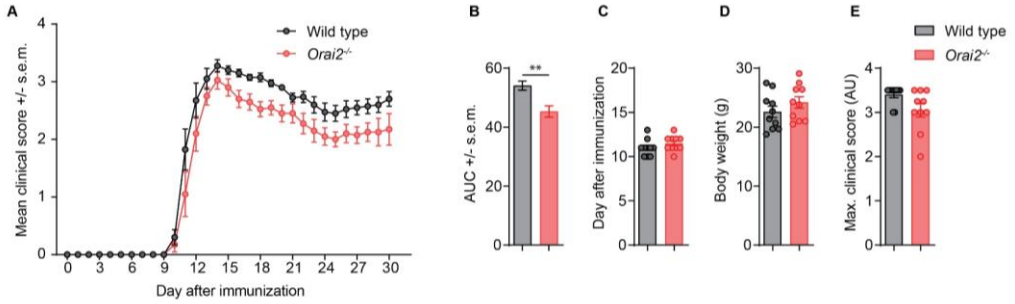

Figure 8 Clinical analysis of EAE in the *Orai2*$^{-/-}$ mouse model

(**A-B**) Mean clinical scores of *Orai2*$^{-/-}$ (n = 10) and wild-type (n = 10) mice undergoing EAE and AUC comparison. (**C**) Comparison of day of the disease onset. (**D**) Comparison of body weight at the day of immunization. (**E**) Comparison of maximum clinical score. Data plotted as mean +/- s.e.m; Statistical analysis was performed by unpaired, two-tailed Student's t-test. ** p< 0.01

2.2.2. Histopathological assessment of neuronal damage during chronic EAE

For further validation of neuronal survival, five gender-matched animals from each genotype on day 30 after immunization were utilized for histological analysis. Animals were chosen to represent a score variation with a mean value corresponding to the mean value of the whole cohort on day 30 after immunization. There was no clear difference in the total amount of remaining neurons between the two genotypes (**Figure 9 A**). Nevertheless, significant reductions in the immune cell count ($CD3^+$) and activated microglia ($Iba1^+$) were observed in spinal cord sections of animals with a genetic deletion of *Orai2* (**Figure 9 C, D**). In addition, a remarkable but

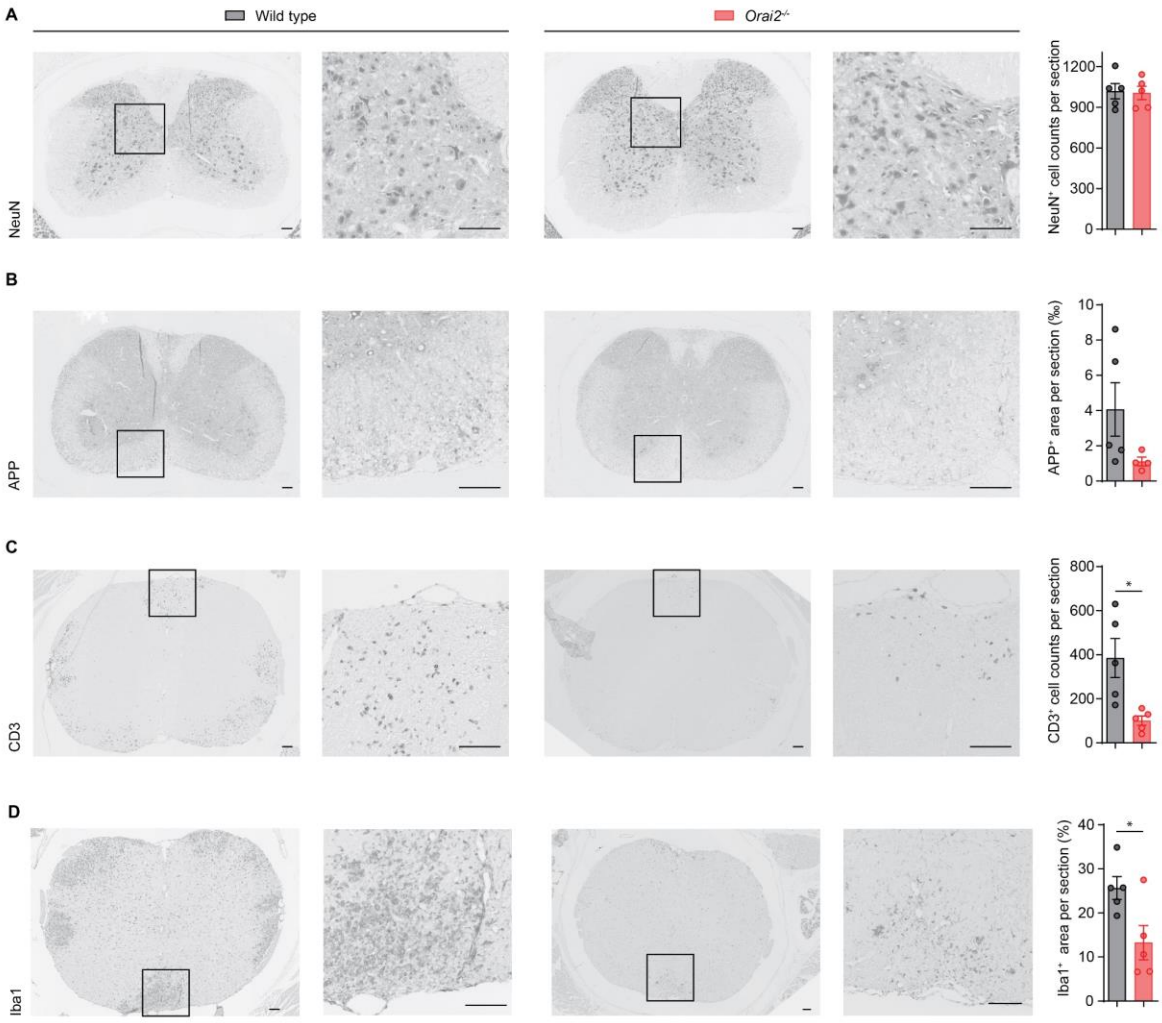

Figure 9 Histological analysis of *Orai2*$^{-/-}$ mice during chronic EAE

(**A**-**D**) Representative images and quantification of neurons ($NeuN^+$), damaged axons (APP^+), immune cells ($CD3^+$), and microglia ($Iba1^+$) in the cervical spinal cord on day 30 after the immunization in wild-type (n=5) and *Orai2*$^{-/-}$ (n=5) mice. Every data point is an average of 2-3 spinal cord sections. Data plotted as mean +/- s.e.m. Statistical analysis was performed by unpaired, two-tailed Student's t-test, * $p< 0.05$.

not significant reduction in amyloid precursor protein (APP)-positive axons was observed in stainings from *Orai2*$^{-/-}$ animals. (**Figure 9 B**), indicating a decreased number of damaged axons.

2.2.3. Validation of CNS infiltration by immune cells

Since, a significant decrease in CD3^{+} cell infiltration into the CNS was observed during the chronic phase of the EAE, further characterization of immune cell infiltration into the CNS at the acute phase was performed by flow cytometry analysis (**Figure 10**). There was no difference in the main

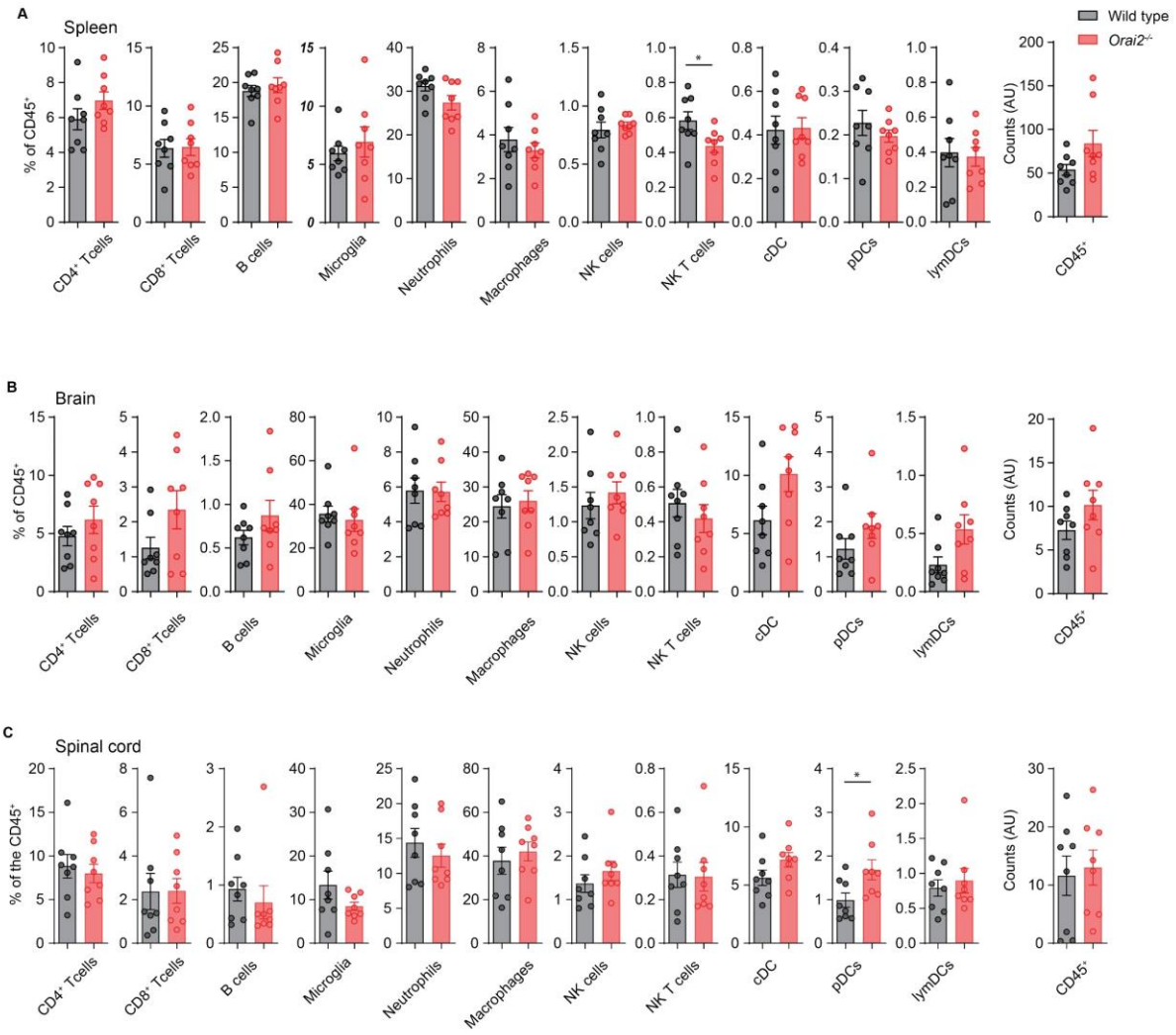

Figure 10 Immune cells composition at the acute EAE of *Orai2*$^{-/-}$ mice

(**A**-**C**) The relative proportion of CD4^{+} T cells, CD8^{+} T cells, B cells, microglia, neutrophils, macrophages, Natural killer cells (NK cells), Natural killer T cells (NK T cells), conventional dendritic cells (cDC), plasmacytoid dendritic cells (pDC) and lymphoid dendritic cells (lymDC) among CD45 positive cells and the absolute counts of CD45 positive cells for the spleen, brain and spinal cord harvested from *Orai2*$^{-/-}$ (n=8) and wild-type (n=8) mice at the acute stage of EAE. Data plotted as mean +/- s.e.m. Statistical analysis was performed by unpaired, two-tailed Student's t-test. * p< 0.05.

subsets of the immune cells, e.g. T or B cells. Nevertheless, significant changes were observed in the percentage of the dendritic cells among CD45^{+} cells in spinal cord samples (**Figure 10 C**) and natural killer (NK) T cells in the spleen (**Figure 10 A**). This should be taken into account in order to properly conclude what is the origin of the observed protective phenotype.

2.3. Tissue-specific deletion of *Orai2*

Since the histological data demonstrated that immune cell infiltration is significantly reduced during the chronic stage of EAE, the next step was the validation of the neuronal origin of the phenotype observed in the *Orai2*$^{-/-}$ mouse, meaning analysis of a neuron-specific deletion of the *Orai2* gene. To do so, the Cre-LoxP recombination system was used to generate tissue-specific knock out animals.[140] A mouse line with expression of LoxP insertion sites in a close proximity to the essential encoding region the *Orai2* gene was generated at laboratory of Professor Dr. Marc Freichel at Heidelberg University. Tissue-specific Cre recombinase enzyme production was achieved by an insertion of the *cre* encoding sequence together or directly after the promoter of the gene that has the tissue-specific expression pattern. Generation of the specific and efficient neuronal deletion of the *Orai2* gene was a critical tool for the proper interpretation of the

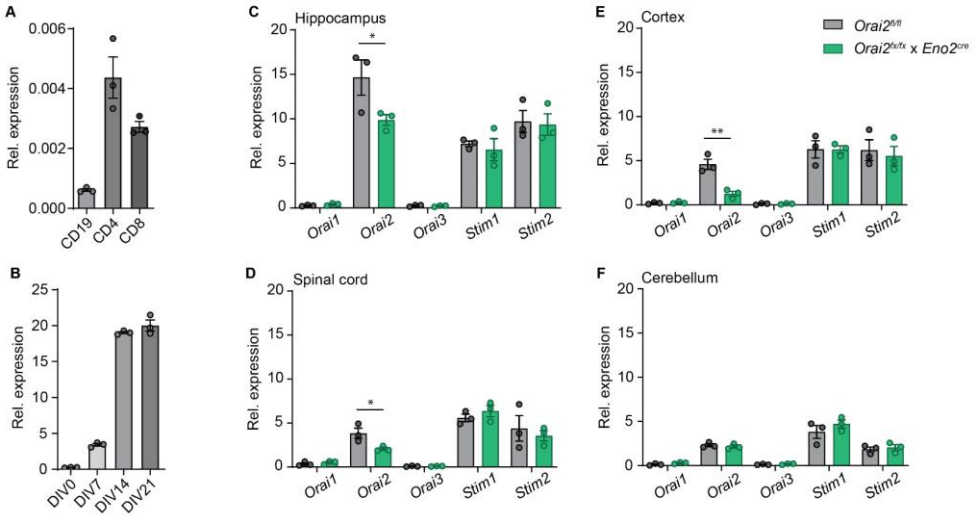

Figure 11 Validation of *Eno2* expression in wild-type mice and in the *Orai2*$^{fl/fl}$×*Eno2*^{cre} mouse line

(**A**) qPCR mRNA expression of *Eno2* in T cells (CD4^{+} and CD8^{+}) and B cells (CD19^{+}) isolated from the spleen of healthy *Orai2*$^{fl/fl}$ mice (n=3) by fluorescence-activated cell sorting (**B**) qPCR mRNA expression of *Eno2* in primary neurons cultured for 0, 7, 14, and 21 days. (**C**-**F**) qPCR mRNA expression of *Orai1*, *Orai2*, *Orai3*, *Stim1*, and *Stim2* genes in the hippocampus, spinal cord, cortex and cerebellum of *Orai2*$^{fl/fl}$×*Eno2*^{cre} and *Orai2*$^{fl/fl}$ mice. Healthy animals, 8-10 weeks of age (n=3), were used for the experiment. Data presented as a fold change to *Tbp* expression, and plotted as mean +/- s.e.m.. Statistical analysis was performed by unpaired, two-tailed Student's t-test. * p< 0.05; ** p <0.01

observations, mainly because the EAE mouse model relies on a complex interaction between the immune system and the CNS.

2.3.1. *Orai2*$^{fl/fl}$×*Eno2*^{cre} mouse line

Neuron-specific enolase 2 (*Eno2)* is a widely used as a promoter to obtain a mouse line with a neuron-specific cre expression. The mouse line *Eno2*^{cre} is a transgenic line[g] with a pan neuronal expression of the *cre-recombinase* following *Eno2* expression pattern. First, *Eno2* expression was validated in primary neuronal culture and immune cells from healthy wild-type mice (**Figure 11 A, B**). The mRNA expression level was on the border of the detection limit for the main immune cell subsets, suggesting a potentially specific expression. The generated mouse line *Orai2*$^{fl/fl}$*Eno2*^{cre} shows a significant reduction in *Orai2* mRNA level in the hippocampus, cortex and spinal cord of the *cre* positive animals in comparison to the *Orai2*$^{fl/fl}$ mice (**Figure 11 C-F**). Genes that encode other CRAC components (*Orai1, Orai3, Stim1* and *Stim2*) were not altered.

Based on the negligible level of *Eno2* expression in immune cells and a significant reduction of *Orai2* in neural tissue in *Orai2*$^{fl/fl}$*Eno2*^{cre} mice, an EAE experiment was performed with gender- and age-matched cohort of animals. Clinical score, disease onset, body weight and maximum score did not differ between genotypes (**Figure 12 A-E**).

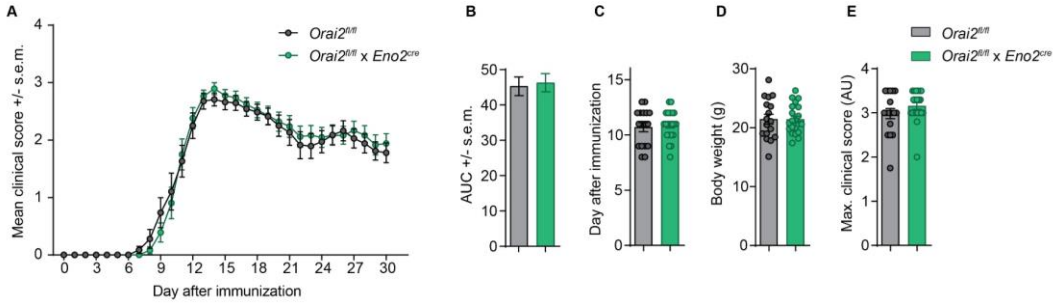

Figure 12 Clinical analysis of the EAE in *Orai2*$^{fl/fl}$×*Eno2*^{cre} mice

(**A-B**) Mean clinical scores of *Orai2*$^{fl/fl}$×*Eno2*^{cre} (n = 17) and *Orai2*$^{fl/fl}$ (n = 22) mice undergoing EAE, and comparison of the AUC. (**C**) Comparison of day of the disease onset. (**D**) Comparison of body weight at the day of immunization. (**E**) Comparison of maximum clinical score at the day of the disease onset. Data plotted as mean +/- s.e.m.. Presented data were pooled from two independent experiments. Statistical analysis was performed by unpaired, two-tailed Student's t-test.

[g] *Eno2*^{cre} mouse line is a transgenic line, in which *cre* encoding sequence is randomly integrated into the mouse genome together with promoter region of rat *Eno2.*

Additional validation of the *Orai2*$^{fl/fl}$*Eno2*^{cre} mouse line was performed in order to assess *Orai2* deletion from unspecific tissues. CD4^{+} T, CD8^{+} T and B immune cells from *Orai2*$^{fl/fl}$*Eno2*^{cre} animals were analyzed on the mRNA level in comparison to *Orai2*$^{fl/fl}$. A significant reduction in *Orai2* mRNA level was observed for all investigated immune cell types (**Figure 13**). The obtained data suggest that the *Eno2* promoter expression is not specific enough to address the question regarding the neuronal origin of *Orai2*-mediated protection within the EAE model.

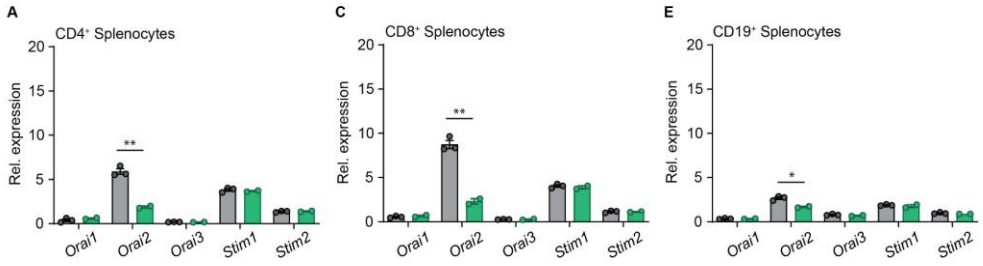

Figure 13 Validation of SOCE-related genes in immune cells derived from *Orai2*$^{fl/fl}$×*Eno2*^{cre} mice

(**A**-**C**) qPCR mRNA expression of *Orai1*, *Orai2*, *Orai3*, *Stim1*, and *Stim2* genes in T cells (CD4^{+}, CD8^{+}), and B cells (CD19^{+}) from *Orai2*$^{fl/fl}$×*Eno2*^{cre} (n=2) and *Orai2*$^{fl/fl}$ (n=3) mice. Spleens isolated from healthy animals were used for the experiment. Data presented as a fold change to *Tbp* expression, and plotted as mean +/- s.e.m.. Statistical analysis was performed by unpaired, two-tailed Student's t-test. *p< 0.05; ** p <0.01.

2.3.2. *Orai2*$^{fl/fl}$*ChAT*^{cre} mouse line

To overcome the deletion of *Orai2* in the immune system, the promoter of the *choline acetyltransferase (ChAT)* gene was used as a driver for the expression of *cre*. The mouse line *ChAT*^{cre} in a knock-in line[h] which has been reported to have a highly specific cre expression in the relatively small ChAT positive neuronal population, which covers mainly motor neurons in the spinal cord. Nevertheless, spinal cord motor neurons are an essential neuronal population for the clinical outcome of EAE disease progression in the C57BL/6 mouse line. An EAE experiment was performed with gender and age-matched animals. No differences could be observed in the clinical EAE score (**Figure 14 A,B**), the day of disease onset (**Figure 14 C**) and the maximum disease score (**Figure 14 E**) of *Orai2*$^{fl/fl}$*ChAT*^{cre} animals in comparison to the *Orai2*$^{fl/fl}$ animals. An insufficient amount of targeted neuronal population may explain this observation.

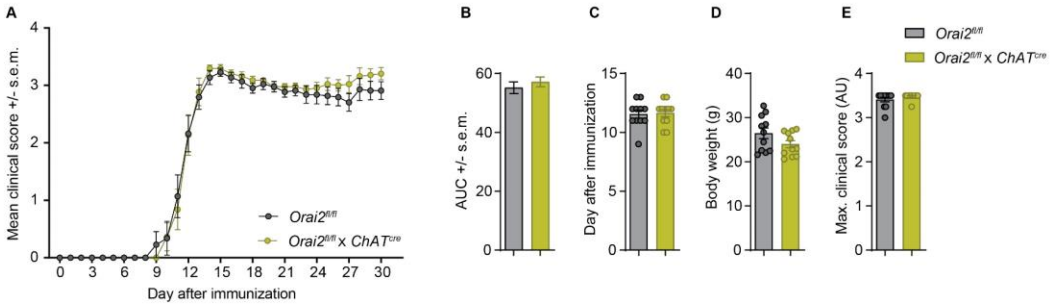

Figure 14 Clinical analysis of EAE in *Orai2*$^{fl/fl}$×*ChAT*^{cre} mice

(**A-B**) Mean clinical scores of *Orai2*$^{fl/fl}$×*ChAT*^{cre} (n = 11) and *Orai2*$^{fl/fl}$ (n = 11) mice undergoing EAE and comparison of the AUC. (**C**) Comparison of day of the disease onset. (**D**) Comparison of body weight at the day of immunization. (**E**) Comparison of maximum clinical score at the day of the disease onset. Data plotted as mean +/- s.e.m. Statistical analysis was performed by unpaired, two-tailed Student's t-test.

[h] *ChAT*^{cre} mouse line is knock-in line where *cre* sequence encoding located directly after the *ChAT* promoter region.

2.3.3. *Orai2*$^{fl/fl}$×*Snap25*^{cre} mouse line

Mouse line with *cre* insertion in the promoter region of *Synaptosomal-associated protein 25* (*Snap25)* was used for the generation of a animals with a neuron-specific *Orai2* knock out. To do so, *Snap25*^{cre} mouse line[i] was crossed with *Orai2*$^{fl/fl}$. The *Orai2*$^{fl/fl}$×*Snap25*^{cre} animals showed a specific and efficient DNA recombination in different neuronal tissues and an absence of

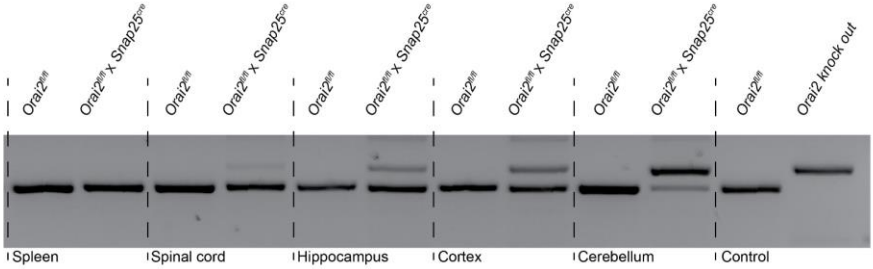

Figure 15 Validation of *Orai2* deletion in *Orai2*$^{fl/fl}$×*Snap25*^{cre} mice

Representative image of the detection of DNA recombination by cre in neuronal tissues of *Orai2*$^{fl/fl}$×*Snap25*^{cre} and *Orai2*$^{fl/fl}$ control animals. Experiment was performed with tree pairs of animals. Amplification was performed according to the protocol used for the genotype of the *Orai2*$^{fl/fl}$×*Snap25*^{cre} mouse line.

recombination in the spleen (**Figure 15)**. An EAE experiment was performed with a gender and age-matched cohort of animals according to the standard procedure. Analysis of the data demonstrated no visible differences between the genotypes with respect to the clinical score, the onset of disease, and the maximum clinical score (**Figure 16**).

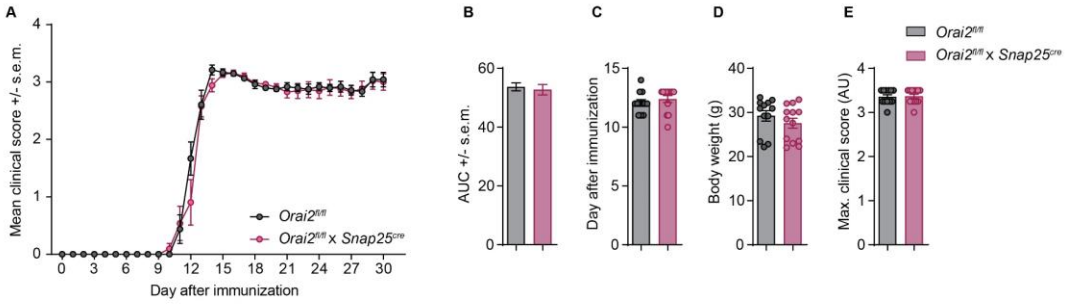

Figure 16 Clinical analysis of EAE in *Orai2*$^{fl/fl}$×*Snap25*^{cre} mice

(**A-B**) Mean clinical scores of *Orai2*$^{fl/fl}$×*Snap25*^{cre} (n = 11) and *Orai2*$^{fl/fl}$ (n = 11) mice undergoing EAE and comparison of the AUC. (**C**) Comparison of day of the disease onset. (**D**) Comparison of body weight at the day of immunization. (**E**) Comparison of maximum clinical score at the day of the disease onset. Data plotted as mean +/- s.e.m. Statistical analysis was performed by unpaired, two-tailed Student's t-test.

[i] *Snap25*^{cre} line is knock-in line where *cre* sequence insertion located directly after the *Snap25* promoter region.

2.4. *In vitro* validation of Ca^{2+} regulation with modified SOCE

After having explored the function of *Orai2 in vivo*, it was not clear whether this holds true also on the cellular level. To test that, optimal culturing condition and analyzed parameters need to be defined. Neuronal activity is the key function of neurons and is required for complex neuron-neuron interaction and intraneuronal pathway activity. Mimicking neuronal activity *in vitro* is not a trivial task, since an artificial 2D environment do not fulfill all the requirements of neurons. In addition, neuronal activity usually decreases neuronal survival *in vitro*. Survival of neurons in culture was a major factor for the optimization of the growth conditions. Neurobasal medium with B27 supplement is the most widely used serum-free medium for neuronal culture, but its composition is optimized for survival and compromises neuronal activity.[141] Spontaneous Ca^{2+} transients can be observed *in vivo* or in brain slice cultures. The problem is insufficient control of the conditions since the surrounding glial cells produce a wide range of active compounds supporting neurons in their function. SOCE highly depends on intracellular Ca^{2+} regulation especially, ER Ca^{2+} levels, which is highly dynamic in neurons and changes upon neuronal activity. Thus, for the analysis of SOCE, a neuronal culture with regular Ca^{2+} transients and long-time survival properties is required.

2.4.1. Establishment of an *in vitro* model for neuronal Ca^{2+} activity analysis

Viability and network formation of neurons *in vitro* highly depend on the seeding density in all culturing conditions.[141] However, technical limitations arise regarding imaging and data processing due to the ability to isolate a of the single neuronal soma in the mature culture without a significant overlap with the neuronal network formed by dendrites and axons of the surrounding cells. Optimal neuronal density was set at 100-120×10^3 cells per cm^2 for primary embryonic cortical neurons. Under this condition, a single cell body could be isolated manually, and Ca^{2+} transients could be tracked.

Activity and survival of primary neurons, cultured in commercially available media, were tested at DIV14. Neuronal activity was compared among the different media by validation of the Ca^{2+} transient under the resting state. Based on the survival and Ca^{2+} activity parameters of tested cultures (**Table 34**), Neurobasal Plus and PNGM media were chosen to be used in all the *in vitro* experiments presented in this dissertation.

Table 34 Neuronal medium comparison

Commercial name	14 days survival	Ca^{2+} activity
Neurobasal	good	poor
Neurobasal Plus	good	good
BrainPhys	poor	ND[j]
NeuroCult	moderate	poor
NeuroCult (DIV0-2) – BrainPhys (DIV3-14)	moderate	high
MACS neuronal	poor	ND
PNGM	good	good

2.4.2. Ca^{2+} regulation in *Orai2*$^{-/-}$ neurons

Primary neurons form the *Orai2*$^{-/-}$ mouse line were compared with cultured wild-type neurons. The cultures were maintained under the same conditions and their preparation was performed using 1:1 matching. The analysis of 4 biologically and technically independent cultures revealed that *Orai2* deletion does not affect the mean Ca^{2+} level in neurons (**Figure 17 B**) and the amplitude of the spontaneous Ca^{2+} transients (**Figure 17 C**). Thus, the current data is in line with the *in vivo* experiments, which showed mild or no effect of neuron-specific *Orai2* deletion on neuronal survival during CNS inflammation.

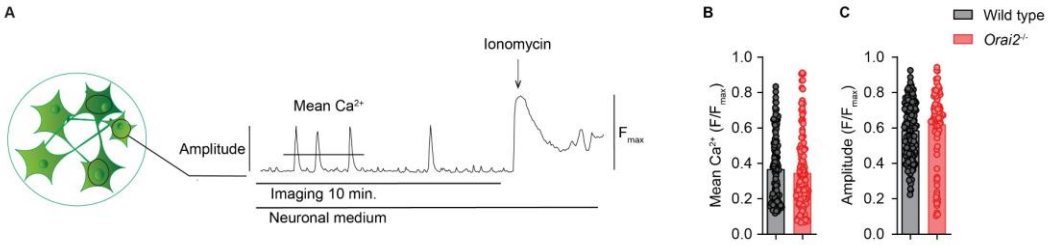

Figure 17 Calcium regulation in *Orai2*$^{-/-}$ neurons

(**A**) Experimental approach for analysis of Ca^{2+} signaling. GCamp6f fluorescence was recorded in spontaneously active cortical primary neuronal culture (DIV15) prior to ionomycin application used for signal normalization**.** Adapted from[30]. (**B,C**) Quantification of mean cytosolic Ca^{2+} signal intensity (B) and average Ca^{2+} transient amplitude (C) of GCaMP6f-transduced cortical primary neuronal culture of wild-type (n = 178 cells from 4 different mice; DIV14-DIV19) and *Orai2*$^{-/-}$ (n = 94 cells from 4 different mice; DIV14-DIV19). Bars show mean values ± s.e.m. Statistical analysis was performed by unpaired, two-tailed Student's t-test.

[j] Not defined

3. The contribution of *Stim1* and *Stim2* deletions

The functionality of the CRAC channel entirely depends on STIM1 and STIM2. The deletion of *Orai2* has no evident influence on the clinical outcome of the EAE and on neuronal Ca^{2+} regulation. Therefore, for the analysis of the role of SOCE in CNS during pathophysiological condition, a mouse line with the double deletion of *Stim1* and *Stim2* genes was generated. Genetic ablation of *Stim1* and *Stim2* should lead to an inability of CRAC channel formation and thus the inability of SOCE activation. A global deletion of the *Stim1* or *Stim2* genes is lethal[142,143], therefore only a tissue-specific deletion can be used for *in vivo* experiments. Based on the previous data (III.2.3 Tissue-specific deletion of Orai2), a mouse line with neuronal-specific *Stim1* and *Stim2* deletions was generated by crossing the $Snap25^{cre}$ line with the $Stim1^{fl/fl}Stim2^{fl/fl}$ line.

3.1. Validation of the $Stim1^{fl/fl}Stim2^{fl/fl}\times Snap25^{cre}$ mouse line

The specificity and efficiency of *Stim1* and *Stim2* deletion was validated on the mRNA level by qPCR. In $Stim1^{fl/fl}Stim2^{fl/fl}\times Snap25^{cre}$ mice, a reduced mRNA level of *Stim1* and *Stim2* was detected in spinal cord and cortex samples in comparison to $Stim1^{fl/fl}Stim2^{fl/fl}$ control (**Figure 18 B** and **C**, respectively). Nevertheless, *Stim1* reduction in spinal cord samples was merely a trend. mRNA expression levels of the *Orai* gene family, as well as *Stim* expression in spleen samples, were unchanged (**Figure 18 A**). Thus, the data suggested that $Stim1^{fl/fl}Stim2^{fl/fl}\times Snap25^{cre}$ mouse line has an efficient CNS-specific deletion of *Stim1* and *Stim2* without a deletion in the immune system and no effect on other SOCE-related genes in neural tissues.

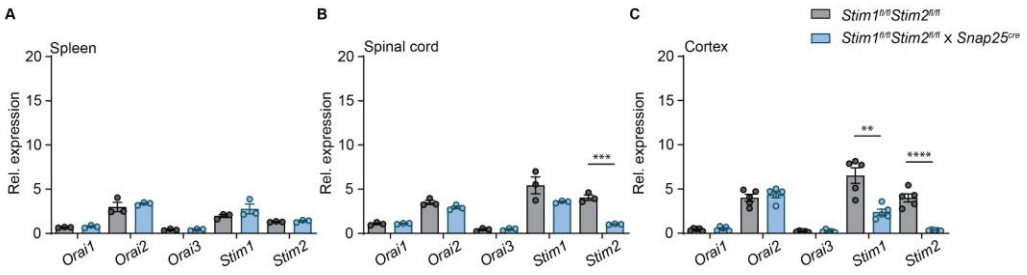

Figure 18 Validation of the $Stim1^{fl/fl}Stim2^{fl/fl}\times Snap25^{cre}$ mouse line

(**A-C**) qPCR mRNA expression of *Orai1*, *Orai2*, *Orai3*, *Stim1* and *Stim2* genes in the spleen, spinal cord, and cortex of $Stim1^{fl/fl}Stim2^{fl/fl}\times Snap25^{cre}$ and $Stim1^{fl/fl}Stim2^{fl/fl}$ mice. Healthy animals, 8-10 weeks of age (n=3) were used for the experiment. Data presented as a fold change to *Tbp* expression, and plotted as mean +/- s.e.m.. Statistical analysis was performed by unpaired, two-tailed Student's t-test, * $p< 0.05$; ** $p <0.01$

3.2. The effect of neuron-specific *Stim1* and *Stim2* deletions on CNS inflammation

In order to validate the role of nSOCE during CNS inflammation, which is postulated in Aim2 of the project, an EAE experiment was performed with $Stim1^{fl/fl}Stim2^{fl/fl}\times Snap25^{cre}$ mouse line.

3.2.1. Clinical and histological characterization of EAE progression in *Stim1*$^{fl/fl}$*Stim2*$^{fl/fl}$×*Snap25*^{cre} mice

A daily assessment of the animals during EAE progression showed a clear difference between the genotypes, as measured by AUC (**Figure 19 B**). Yet, no significant difference in the bodyweight of the animals at the day of immunization, the disease onset or the maximum clinical score (**Figure 19 C, D** and **E**, respectively) were observed. The change in the relative body weight during the disease course, which represents general inflammation was not different between the groups (Supplement 2). Of note, some animals exhibited an unusual general activity during the experiment, which did not resemble the common signs of sickness in the pre-clinical phase of the EAE (Day after immunization (DAI) 6-15). Since the experiment was performed blinded regarding the genotype additional comments were recorded in the daily assessment sheet. At the end of the experiment, the animals were separated according to the genotype and the activity notes were

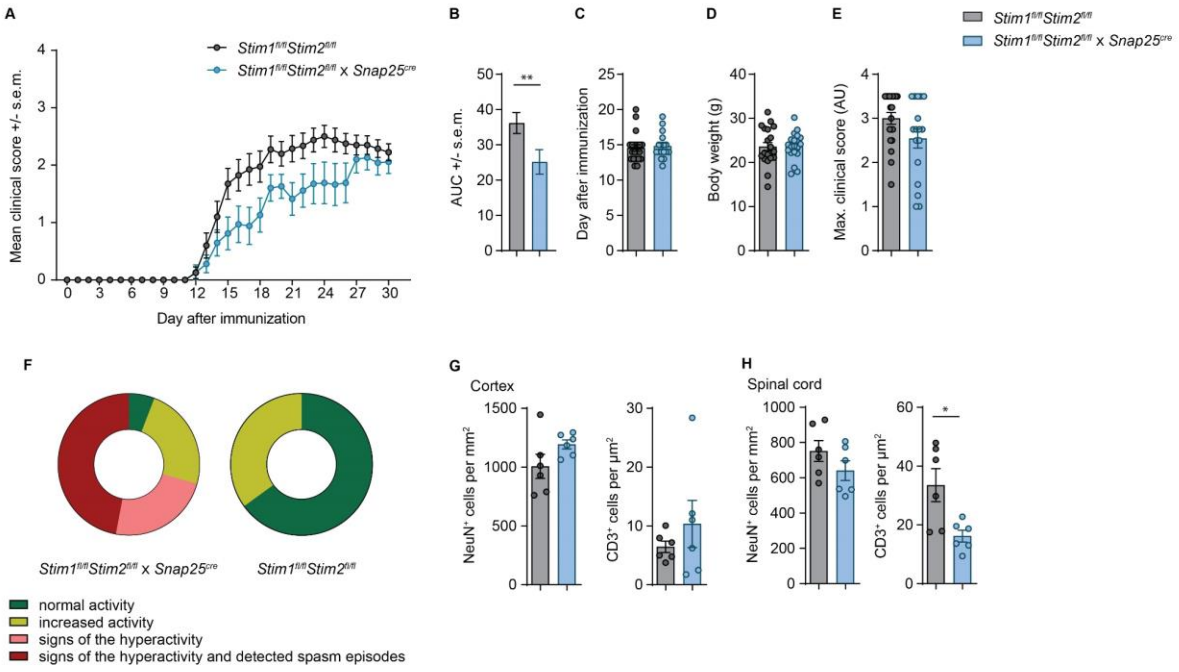

Figure 19 Characterization of the *Stim1*$^{fl/fl}$*Stim2*$^{fl/fl}$×*Snap25*^{cre} line during CNS inflammation

(**A**) Mean clinical scores of *Stim1*$^{fl/fl}$*Stim2*$^{fl/fl}$×*Snap25*^{cre} (n = 17) and *Stim1*$^{fl/fl}$*Stim2*$^{fl/fl}$ (n = 20) mice undergoing EAE. Curves show mean ± s.e.m; (**B-E**) Comparison of the AUC (B); day of the disease onset (C), body weight at the day of immunization (D); and maximum clinical score (E). (**F**) Analysis of animal activity during the EAE presented as a proportion. Color code: green – usual activity, yellow – increased activity (running, jumping), pink – unusual behavior (hyperactivity, paws tremor) and red – "epilepsy like" signs. (**G-H**) Quantification of neuronal density and immune cell infiltration in the cortex (**G**) and in the cervical spinal cord (**H**) at 30 DAI of *Stim1*$^{fl/fl}$*Stim2*$^{fl/fl}$ (n=6) and *Stim1*$^{fl/fl}$*Stim2*$^{fl/fl}$×*Snap25*^{cre} (n=6) mice. Neuronal density and the extent of immune cell infiltration into the CNS analyses were performed in the framework of the bachelor thesis of Lukas C. Reuter. Data plotted as mean +/- s.e.m; Statistical analysis was performed by unpaired, two-tailed Student's t-test. * p< 0.05, ** p< 0.01

summarized (**Figure 19 F**). The results of the activity assessment revealed a systemic effect of *Stim1* and *Stim2* deletions on CNS activity. Thus, additional experiments were planned to further validate this effect.

For histological assessment of the EAE, brain and spinal cord from six (per genotype) gender-matched animals with representative scores at the end of the EAE were taken for an additional validation of neuronal density and immune cell infiltration (**Figure 19 G** and **H**). There is no detectable difference in the neuronal density, but significantly fewer immune cells were counted in the spinal cord of the *Stim1/Stim2*-deficient mice in comparison to *Stim1*$^{fl/fl}$*Stim2*$^{fl/fl}$ animals (**Figure 19 H**). No difference was observed in the cortex for the neuronal density nor immune cell infiltration (**Figure 19 G**). To avoid improper allocation of the genotype, an additional validation of spleen samples from the corresponding animals was performed using qPCR (**Supplement 3**). The observed reduction of infiltrating immune cells without an effect on neuronal density during EAE in *Stim1*$^{fl/fl}$*Stim2*$^{fl/fl}$×*Snap25*^{cre} mice is an unusual observation for the neuron-mediated amelioration of EAE. Thus, additional validation of the immune system response to immunization is required for the final conclusions.

3.2.2. Validation of the immune response after EAE induction

To validate the immune response to EAE induction, analysis of the CNS infiltrating immune cell subsets at day 30 after immunization was performed by flow cytometry. Moreover, based on the observed atypical behavior at the pre-clinical phase, histopathological assessment of the brain and the spinal cord, as well as flow cytometry analysis of the immune cell subsets in the blood and spleen, were performed at day 11 post-immunization.

CNS infiltrating immune cell composition not altered at the chronic stage of the EAE in *Stim1*$^{fl/fl}$*Stim2*$^{fl/fl}$×*Snap25*^{cre} mice

To reveal CNS infiltrating immune cell subsets composition, immune cells were isolated from brain and spinal cord tissues at the chronic stage of the EAE and were analyzed by flow cytometry. The relative proportion of the analyzed immune subsets did not differ between the genotypes in the spinal cord samples (**Figure 20 C**). Nevertheless, the absolute number of immune cells infiltrating into the spinal cord of animals with *Stim1* and *Stim2* deletions was remarkably lower in comparison to *Stim1*$^{fl/fl}$*Stim2*$^{fl/fl}$ (**Figure 20 D**), but only CD8$^+$ T cells had significantly lower counts in the spinal cord (**Supplement 4**). The current analysis confirmed a significant reduction in CD3$^+$ cells (which can be estimated as the sum of CD4$^+$ and CD8$^+$ T cells) infiltration into the spinal cord at the chronic stage of the EAE (**Supplement 4**). No significant difference in the relative and absolute count of immune cell subsets in the brains of *Stim1*$^{fl/fl}$*Stim2*$^{fl/fl}$×*Snap25*^{cre} mice was observed (**Figure 20 A** and **B**). Yet, the absolute number of neutrophils was significantly higher in the *Stim1/Stim2* deficient animals in comparison to the *Stim1*$^{fl/fl}$*Stim2*$^{fl/fl}$ animals (**Supplement 4**).

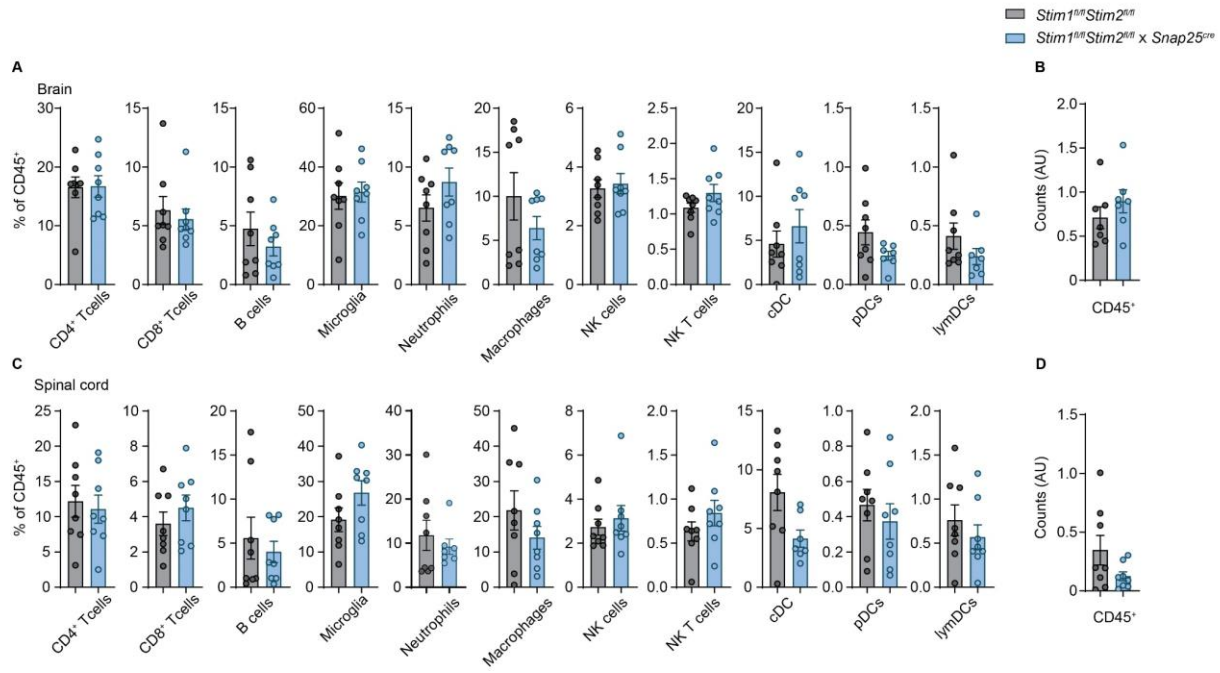

Figure 20 Immune cells composition at the chronic EAE of *Stim1*$^{fl/fl}$*Stim2*$^{fl/fl}$×*Snap25*^{cre} mice

(A-D) Relative proportion of CD4 T cells, CD8 T cells, B cells, microglia, neutrophils, macrophages, NK cells, NK T cells, cDC, pDC, and lymDC among CD45 positive cells and absolute counts of CD45 positive cells in the brain, and the spinal cord of *Stim1*$^{fl/fl}$*Stim2*$^{fl/fl}$×*Snap25*^{cre} (n=8) and *Stim1*$^{fl/fl}$*Stim2*$^{fl/fl}$ (n=8) mice at the chronic stage of EAE (DAI 30) analyzed by flow cytometry. Data plotted as mean +/- s.e.m. Statistical analysis was performed by unpaired, two-tailed Student's t-test.

Overall immune system response not altered at the pre-symptomatic stage of the EAE in *Stim1*$^{fl/fl}$*Stim2*$^{fl/fl}$×*Snap25*^{cre} mice

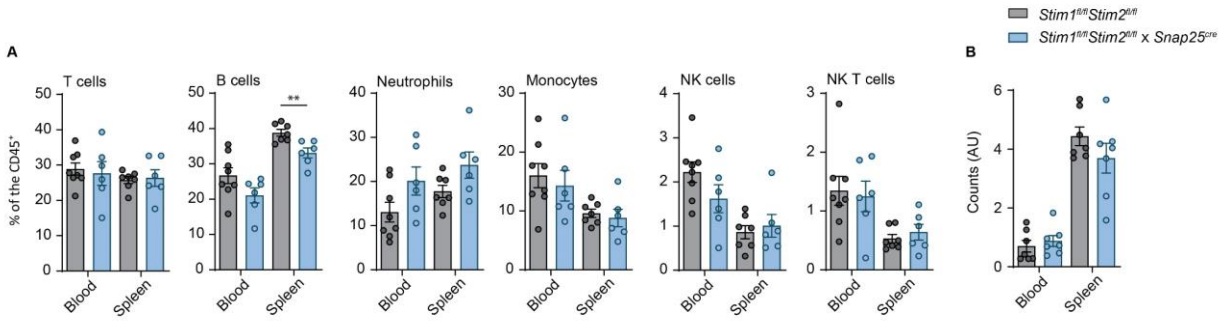

Figure 21 Immune cell composition at the pre-acute EAE of *Stim1*$^{fl/fl}$*Stim2*$^{fl/fl}$×*Snap25*^{cre} mice

(**A**) Relative proportion of T cells, B cells, neutrophils, monocytes, NK cells, and NK T cells among CD45 positive cells and (**B**) absolute counts of CD45 positive cells for the blood and spleen samples from *Stim1*$^{fl/fl}$*Stim2*$^{fl/fl}$×*Snap25*^{cre} (n=6) and *Stim1*$^{fl/fl}$*Stim2*$^{fl/fl}$ (n=6) mice at the pre-acute stage of EAE (DAI 11) analyzed by flow cytometry.

Blood and spleen samples were taken for flow cytometry analysis at day 11 after the immunization to validate immune system response to EAE induction. The overall amount of CD45$^+$ immune cells was not altered by the genotype neither in blood nor in spleen samples (**Figure 21 B**). No difference in the relative distribution of the immune cell subsets was detected, except for a

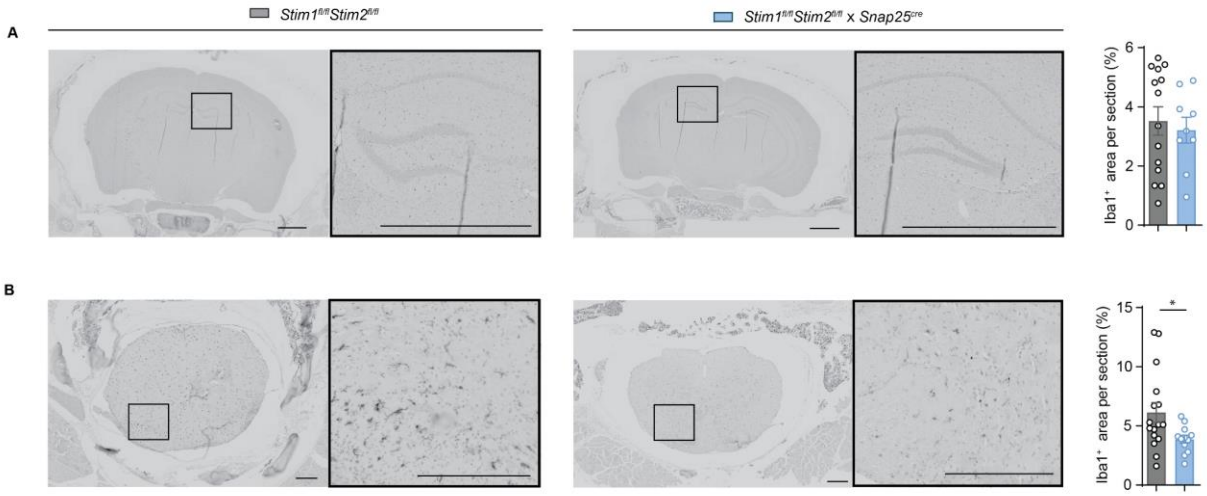

Figure 22 Histological validation of the pre-acute EAE in *Stim1*$^{fl/fl}$*Stim2*$^{fl/fl}$×*Snap25*^{cre} mice

(**A**) A representative image and the corresponding quantification of microglia (Iba1) staining in brain sections of *Stim1*$^{fl/fl}$*Stim2*$^{fl/fl}$×*Snap25*^{cre} (n=5) and *Stim1*$^{fl/fl}$*Stim2*$^{fl/fl}$ (n=8) mice at the pre-acute phase of EAE (DAI 11). Scale bar is 500 µm. (**B**) A representative image and the corresponding quantification of microglia (Iba1) staining in cervical spinal cord sections of *Stim1*$^{fl/fl}$*Stim2*$^{fl/fl}$×*Snap25*^{cre} (n=6) and *Stim1*$^{fl/fl}$*Stim2*$^{fl/fl}$ (n=8) mice at the pre-acute phase of EAE (DAI 11). Scale bar is 250µm. 2 sections were analyzed per animals. Some sections were excluded due to significant damage of the tissue. Data plotted as mean +/- s.e.m. Statistical analysis was performed by unpaired, two-tailed Student's t-test. * p< 0.05.

reduced relative presentation of B cells in the spleen samples from *Stim1*$^{fl/fl}$*Stim2*$^{fl/fl}$×*Snap25*^{cre} mice (**Figure 21 A**).

CNS has reduced signs of inflammation at the pre-symptomatic stage of the EAE in *Stim1*$^{fl/fl}$*Stim2*$^{fl/fl}$×*Snap25*^{cre} mice

Histological validation of the immune response during the pre-symptomatic stage of the EAE in *Stim1*$^{fl/fl}$*Stim2*$^{fl/fl}$×*Snap25*^{cre} mice was performed on brain and spinal cord samples. The samples were stained for CD3, B cells and Iba1 markers. There were no CD3 or B cells detected in the stained sections (data not shown), nevertheless significantly higher amount of Iba1-positive cells (activated microglia cells) were observed in the spinal cord samples from the *Stim1*$^{fl/fl}$*Stim2*$^{fl/fl}$ animals in comparison to the *Stim1*$^{fl/fl}$*Stim2*$^{fl/fl}$×*Snap25*^{cre} animals (**Figure 22**).

3.3. *Stim1*$^{fl/fl}$*Stim2*$^{fl/fl}$×*Snap25*^{cre} line has a distinguished phenotype

Signs of hyperactivity and an atypical clinical picture during the pre-symptomatic EAE course suggest a systemic effect of neuronal *Stim1* and *Stim2* deletions on CNS function. Additionally, the reduced immune cell infiltration at the chronic stage of the EAE and the reduced signs of inflammation at the early EAE disease course point to an indirect effect on immune system. Furthermore, in the small cohort of animals used for flow cytometry analysis of the CNS infiltrating immune cells, an episode of a generalized seizure was recorded in one *Stim1*$^{fl/fl}$*Stim2*$^{fl/fl}$×*Snap25*^{cre} mouse (movie sup). In the C57BL/6 mouse line, which is used as a background strain, epilepsy was not reported to be present during EAE, thus this observation was highly unexpected. Therefore, the analysis of the *Stim1*$^{fl/fl}$*Stim2*$^{fl/fl}$×*Snap25*^{cre} mouse line at the healthy state was performed.

The animal caretakes from the UKE mouse core facility did not report any abnormalities in the *Stim1*$^{fl/fl}$*Stim2*$^{fl/fl}$×*Snap25*^{cre} mouse line. Instead, typical breeding behavior, body weight and nest formation were observed. In addition, any fundamental changes were not expected based on the reported experiments with the mouse line containing the global deletion of *Stim2* and the reported experiments that meant to elucidate the role of *Stim1* in neurons. However, in order to decipher whether physiological changes in the *Stim1*$^{fl/fl}$*Stim2*$^{fl/fl}$×*Snap25*^{cre} mouse line appear only after EAE induction or is it a basic phenotype of the line, further behavioral and statistical analysis of the colony were performed. Statistical analysis of the long-term survival, offspring counts and body weight at the mature adult age were performed using the transgenic animal database and an evaluation of the animals utilized for experiments (**Figure 23**). As can be seen in **Figure 23 B**, **C**, no differences in the counts of offspring nor body weight of the animals (combined data for all animals entering the experiments) were observed. By contrast, the Kaplan–Meier curve showed

a significant difference in the long-term survival of the animals. This difference reached a significant level after 20 weeks and became even more pronounced with the prolonged observation time (**Figure 23 A**).

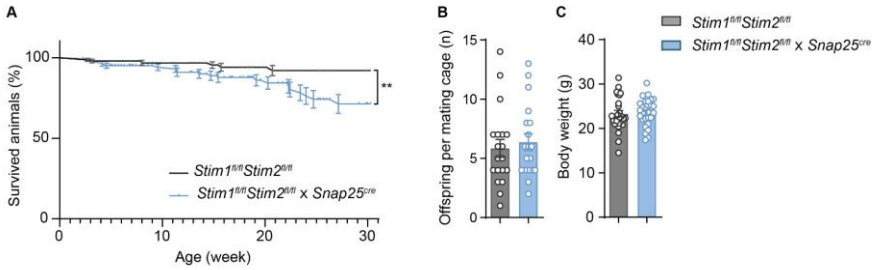

Figure 23 Characterization of the *Stim1*$^{fl/fl}$*Stim2*$^{fl/fl}$×*Snap25*^{cre} mouse line

(A) A Kaplan–Meier curve for 163 *Stim1*$^{fl/fl}$*Stim2*$^{fl/fl}$×*Snap25*^{cre} and 150 *Stim1*$^{fl/fl}$*Stim2*$^{fl/fl}$ mice. The animals were censored at different ages in a similar proportion for both genotypes. **p<0.01 (Long-rank test). **(B)**18 mating cages with 1 or 2 females per cage with at least 4 born litters per cage are presented. **(C)** Body weight comparison (n=28 animals per genotype) of mature adult age- (8-10 weeks) and gender matched mice. Statistical analysis was performed by unpaired, two-tailed Student's t-test

3.3.1. Histological validation of healthy animals with a neuron-specific *Stim1/Stim2* deletion

Reduced long-term survival and the phenotype observed during the EAE course could be a result of changes present in *Stim1*$^{fl/fl}$*Stim2*$^{fl/fl}$×*Snap25*^{cre} mice regardless of aging or EAE induction.

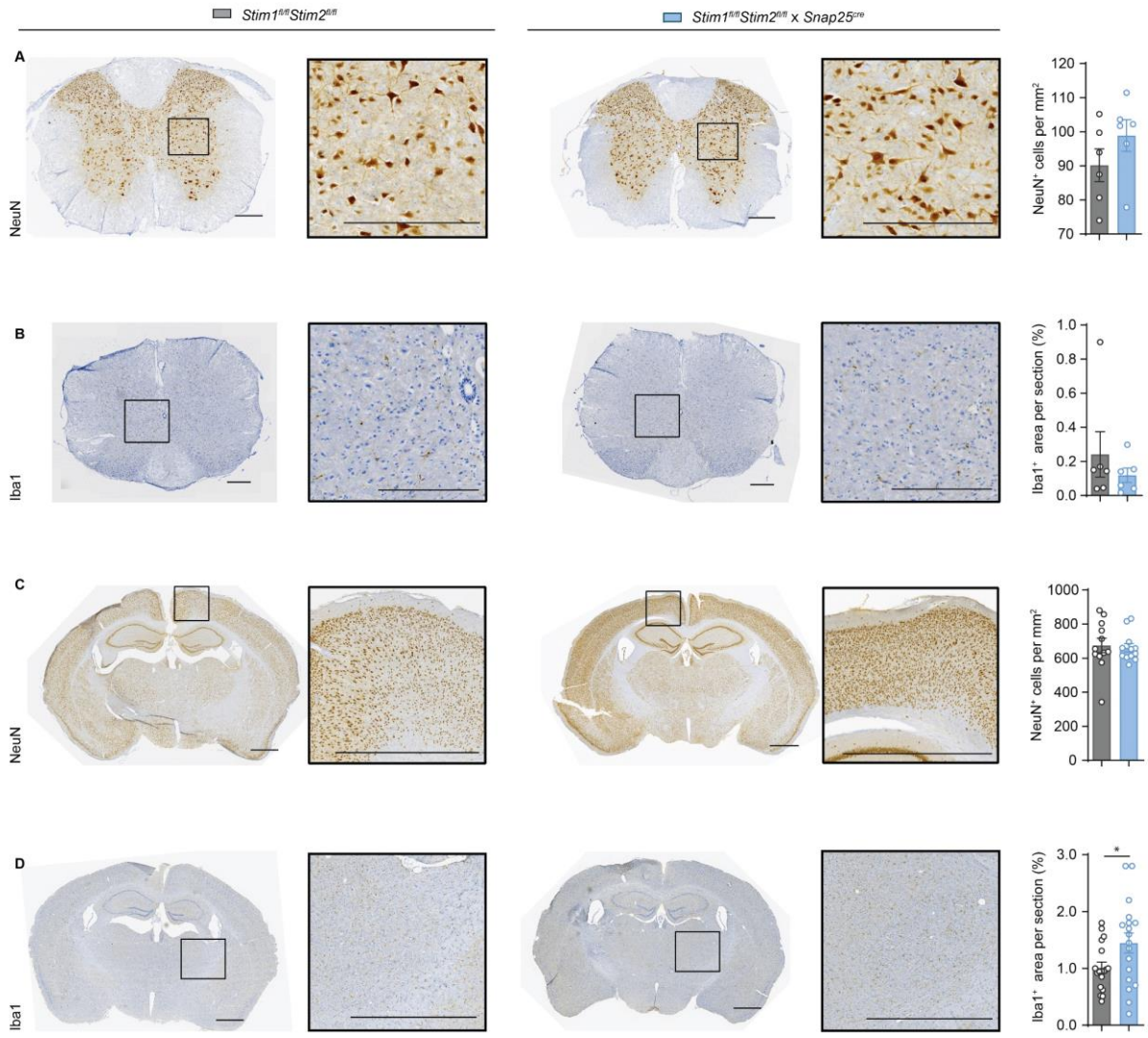

Figure 24 Histological characterization of the CNS of *Stim1*$^{fl/fl}$*Stim2*$^{fl/fl}$×*Snap25*^{cre} mice

(A-B) Representative images and the corresponding quantification of neuronal density (**A,** NeuN) and microglia (**B**, Iba1) staining in the spinal cord of healthy *Stim1*$^{fl/fl}$*Stim2*$^{fl/fl}$×*Snap25*^{cre} (n=6) and *Stim1*$^{fl/fl}$*Stim2*$^{fl/fl}$ (n=6) mice. Scale bar is 250µm. (**C-D**) Representative images and the corresponding quantification of neuronal density (**C**, NeuN) and microglia (**D**, Iba1) staining in the brain of healthy *Stim1*$^{fl/fl}$*Stim2*$^{fl/fl}$×*Snap25*^{cre} (n=18, 3 regions from 6 mice) and *Stim1*$^{fl/fl}$*Stim2*$^{fl/fl}$ (n=18, 3 regions from 6 mice) mice. Scale bar is 250µm. 2 cervical spinal cord sections and 1 brain section (per anterior; middle and posterior region) were analyzed per animal. Data plotted as mean +/- s.e.m. Statistical analysis was performed by unpaired, two-tailed Student's t-test. * p< 0.05

Thus, histological validation of the *Stim1*$^{fl/fl}$*Stim2*$^{fl/fl}$×*Snap25*^{cre} mouse line was performed by analysis of 6 brains (anterior; middle and posterior regions) and cervical spinal cords per genotype of healthy gender- and age- matched animals (**Figure 24**). No general abnormalities were observed in the brain nor the spinal cord. As can be seen in **Figure 24 A**, neuronal density in the spinal cord was not affected by the *Stim1/Stim*2 deletion. A trend of increased neuronal count in the spinal cord of the *Stim1*$^{fl/fl}$*Stim2*$^{fl/fl}$×*Snap25*^{cre} animals can be noted. There was no increase in microglia activation (Iba1^{+}) in spinal cord samples (**Figure 24 B**). In the brain section no difference in the cortical neuronal density was observed but a significant increase in active microglia was detected in the samples from *Stim1*$^{fl/fl}$*Stim2*$^{fl/fl}$×*Snap25*^{cre} mice (**Figure 24 C** and **D**). These obtained findings about the neuronal density further support the data generated by Lukas C. Reuter in his bachelor thesis with an alternative staining method and a manual quantification of cortical and spinal cord neuronal density.

3.3.2. *Stim1*$^{fl/fl}$*Stim2*$^{fl/fl}$×*Snap25*^{cre} mouse show abnormal hyperactivity behavior

In cooperation with the behavioral biology unit of the ZMNH (UKE), an experimental proposal for basic behavioral investigation of the *Stim1*$^{fl/fl}$*Stim2*$^{fl/fl}$×*Snap25*^{cre} line was designed. It included an open field, Y-maze. water-maze, elevated plus-maze and rotarod experiments to test the general behavior and the cognitive function of the mouse line. Animals were litter- and gender- matched, and not more than two matched couple were used from a single litter.

Open field

The analysis of the open field experiment suggests a significant difference between the genotypes in both males and females. Both genders from the *Stim1*$^{fl/fl}$*Stim2*$^{fl/fl}$×*Snap25*^{cre} line show an increased overall moved distance and a reduced distance to the cage walls (**Figure 25 A, B** and **D, E** respectively). This indicates hyperactivity and fear-like phenotype. Nevertheless, the total recorded distance was significantly different only for the males (**Figure 25 A**). The female mice reached significance only at the end of the experiment. The data (distance) is significantly influenced by time, in the way that animals with the *Stim1* and *Stim2* deletions increase their activity throughout the experiment.

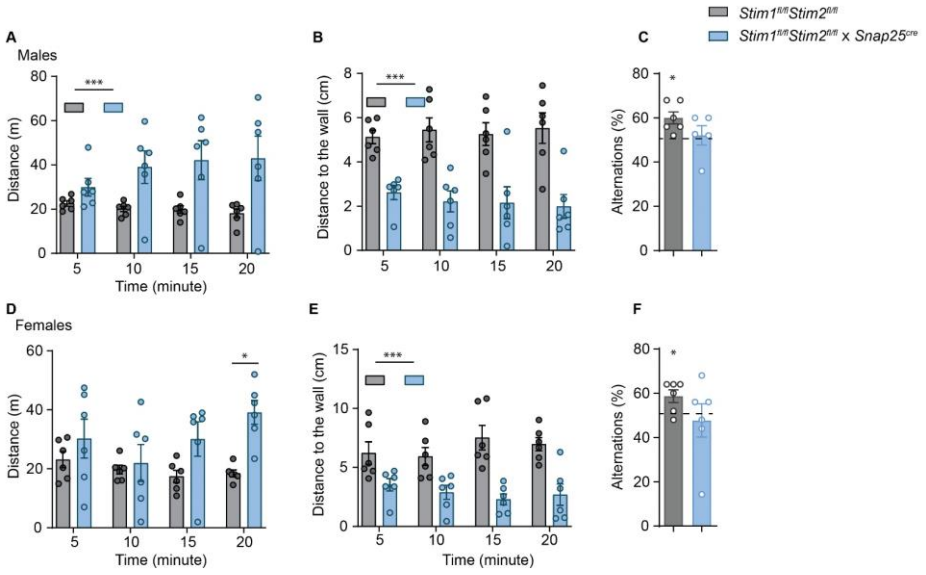

Figure 25 Behavioral analysis of *Stim1*$^{fl/fl}$*Stim2*$^{fl/fl}$×*Snap25*^{cre} mice

Quantification of the results from Open field and Y maze tests for males (A, B, C) and females (D, E, F). (**A, D**) Total distance recorded during the open field test in defined time frame (0 to 5 minutes; 5 to 10 minutes; 10 to 15 minutes, 15 to 20 minutes from the beginning of the experiment). (**B, E**) Average distance to the wall of experimental box during the open field test in defined time frame. (**C, F**) Y maze alternations (% of transitions to the new arm among all transitions recorder during the experiment). 6 animals per gender from the *Stim1*$^{fl/fl}$*Stim2*$^{fl/fl}$×*Snap25*^{cre} line and litter- gender- matched *Stim1*$^{fl/fl}$*Stim2*$^{fl/fl}$ mice were used in the open field test. Same cohort was used for the Y maze test, but 1 male from the *Stim1*$^{fl/fl}$*Stim2*$^{fl/fl}$×*Snap25*^{cre} line died prior the experiment. Statistical analysis was performed by two-way ANOVA for A,B,D,E; unpaired, two-tailed Student's t-test for D; unpaired, one-tailed Student's t-test for C and F. *p <0.05, **p <0.01 , ***p <0.001.

Y maze

Y-maze experiment was performed after the completion of the open field. Mice with *Stim1* and *Stim2* deletions from both genders show significantly reduced alternation during the experiment (**Figure 25 C, F**).

Additional remarks

Based on the already observed results from the open field and the Y maze tests, further planned experiments were canceled due to ethical reasons. Animals showed obvious signs of hyperactivity and anxiety during the handling. In addition, knock out animals show signs of emotional suffering and stress; a few episodes of epileptic seizures were observed in *Stim1*$^{fl/fl}$*Stim2*$^{fl/fl}$×*Snap25*^{cre} mice, and one animal died.

3.4. *Stim1* and *Stim2* deletion alters neuronal Ca^{2+} homeostasis *in vitro*

Effect of *Stim1* and *Stim2* neuron-specific deletion was further explored on cellular level *in vitro* using primary neuronal cultures. Ca^{2+} live cell imaging was performed for the intracellular Ca^{2+} levels and spontaneous Ca^{2+} transients characterization. Primary neurons with *Stim1* and *Stim2* or *Stim2* only deletions were compared with cultured *Stim1*$^{fl/fl}$*Stim2*$^{fl/fl}$ or *Stim2*$^{fl/fl}$ neurons. Cultures were kept under the same condition and preparation of the cultures was performed in 1:1 matching. Deletion was achieved by endogenous (or AAV induced) expression of the cre protein in the *Stim1*$^{fl/fl}$*Stim2*$^{fl/fl}$ or *Stim2*$^{fl/fl}$ neurons. Control of the cre expression was performed by using AAV7 vector with a mCherry-cre reporter. Only mCherry positive neurons were taken for the analysis. Genetically encoded fluorescent Ca^{2+} indicator expression was induced by transduction with AAV7 vector. Since, animals with *Stim1* and *Stim2* deletion show hyperactive phenotype and signs of an epilepsy predisposition, Ca^{2+} live cell imaging experiments include stimulation with bicuculline[k] as an *in vitro* model for epilepsy (**Figure 26 A**).

[k] Bicuculline - a competitive antagonist of the neurotransmitter γ-aminobutyric acid at the GABAA receptor, and used in model systems for epilepsy.[182]

3.4.1. *Stim1* and *Stim2* deficient neurons

Primary neuronal cultures derived from *Stim1*$^{fl/fl}$*Stim2*$^{fl/fl}$×*Snap25*^{cre} and *Stim1*$^{fl/fl}$*Stim2*$^{fl/fl}$ mouse lines were used for *in vitro* experiments. Significant differences between cultures were observed in the mean Ca^{2+} level already at the resting state. Neurons with the *Stim1* and *Stim2* deletion had a reduced effective Ca^{2+} level at the resting state and the difference increased further after the bicuculine stimulation (**Figure 26 B**). This result is accomplished by an analysis of the activity of the cultures (frequency of spontaneous Ca^{2+} transients). *Stim1* and *Stim2* deficient neurons had a significant increase in the frequency at the resting state, but after the bicuculline stimulation no differences could be detected between the genotypes (**Figure 26 C**). Analysis of the amplitude of the Ca^{2+} transients show that at the resting state neurons with *Stim1* and *Stim2* deletion have a trend to a higher amplitude of transients in comparison to the *Stim1*$^{fl/fl}$*Stim2*$^{fl/fl}$ neurons. The effect of bicuculine application on the amplitude change for the *Stim1* and *Stim2*-deficient neurons is significant but mild (+19% rise). On the other side bicuculine drives a massive rise in the amplitude of the transients in the *Stim1*$^{fl/fl}$*Stim2*$^{fl/fl}$ neurons (+63% rise) (**Figure 26 D**).

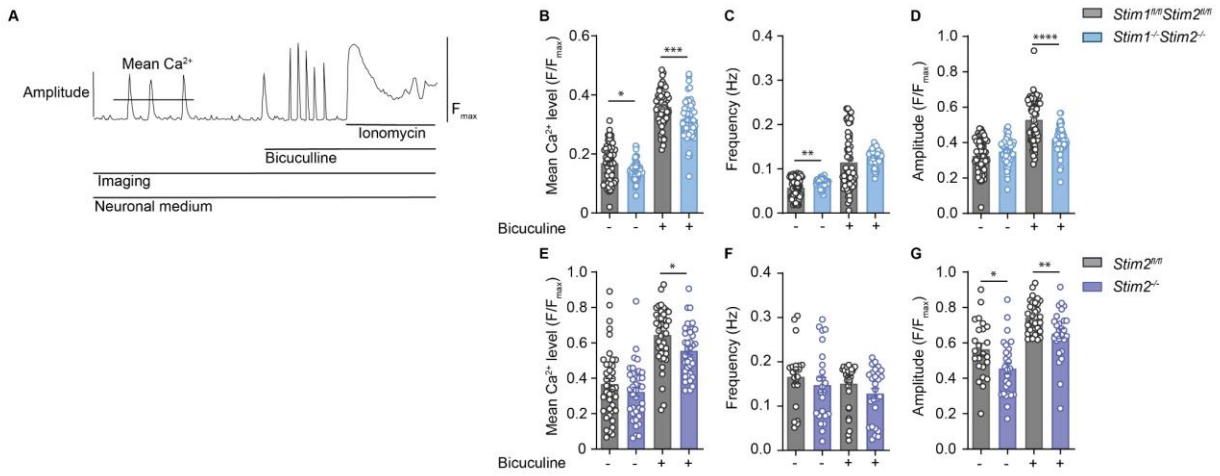

Figure 26 Neuronal Ca^{2+} activity in *Stim1, Stim2* deficient neurons

(**A**) Schematic overview of the experimental procedure and analyzed parameters of the Ca^{2+} transients. (**B-D**) Quantification of the mean Ca^{2+} level, the frequency and the amplitude of the Ca^{2+} transients from *Stim1*$^{-/-}$*Stim2*$^{-/-}$ (n=57) and *Stim1*$^{fl/fl}$*Stim2*$^{fl/fl}$ (n=60) neurons from 2 independent preparations. For the analysis, neurons without Ca^{2+} rise after the ionomycin application were excluded. For the frequency and the amplitude analysis neurons without the presence of spontaneous Ca^{2+} transients were excluded. (**E-G**) Quantification of the mean Ca^{2+} level, the frequency and the amplitude of the Ca^{2+} transients from *Stim2*$^{-/-}$ (n=37) and *Stim2*$^{fl/fl}$ (n=41) neurons from 3 independent preparations. For the analysis, neurons without Ca^{2+} rise after the ionomycin application were excluded. For the frequency and the amplitude analysis neurons without the presence of spontaneous Ca^{2+} transients were excluded. Statistical analysis was performed by unpaired, two-tailed Student's t-test. *p <0.05, **p <0.01 , ***p <0.001, ****p <0.0001.

3.4.2. *Stim2*-deficient neurons

Additional experiments with primary neuronal cultures derived from the *Stim2*$^{fl/fl}$ mouse line were performed in a similar manner. *Stim2* deletion was achived by transduction with AAV7 vector with a *cre* insertion. At the resting state, there was no difference in the mean Ca^{2+} level, even though the amplitude of the Ca^{2+} transients in the acive cell was significantly lower in the *Stim2*-deficient neurons in comparison to the *Stim2*$^{fl/fl}$ control. After the bicuculine application, the mean Ca^{2+} and the amplitude of the transients were significantly lower in the neurons with *Stim2* deletion (**Figure 26 E, G**). No difference was observed in the frequency of the Ca^{2+} transients between the genotypes (**Figure 26 F**).

IV. Discussion

1. Composition of neuronal CRAC

1.1. Murine neuronal CRAC profile

The first aim of the project was to validate the profile of SOCE-related gene expression in murine neurons and neuronal tissue. Among the tested neural tissues, *Orai2* to *Orai1* and *Orai2* to *Orai3* ratios show the highest value in the hippocampal samples. *Orai2* expression was 69 and 52 times higher in the hippocampus in comparison to the *Orai1* and *Orai3* respectively. Since the hippocampal samples have the highest neuronal density among other tissues, the obtained results suggest that *Orai2* is the dominant expressed *Orai2* form in neurons. Further validation of the neuronal expression profile using cultured neurons show that *Orai2* to *Orai1* ratio is rising with the maturation of theculture from 7 (DIV 0 and DIV7) to 11 (DIV14), and further on to 38 (DIV21). *Orai3* expression was close to the detection limit at day 0 and day 7, and demonstrated a high variability. Nevertheless, *Orai2* to *Orai3* ratios in cultures grown for 14 and 21 days were 28 and 51, respectively. Published sequencing data from primary cortical neurons that were cultured for 7 days showed a similar value to the *Orai2* to *Orai1* ratio, which is approximately 5.[144] The dominance of the *Orai2* gene in the brain is further supported by an analysis of the *Orai* gene family expression data from the Bgee animal gene database.[145]

Enhanced expression of *Orai2* in mature primary neuronal culture suggests an important role of *Orai2* as part of the collective neuronal network activity, which is represented in the mature neuronal culture as spontaneous Ca^{2+} activity. Additionally, overexpression of the ORAI2 protein shows that the localization of ORAI2 in dendritic synapses and in axons is possible. Nevertheless, the lack of specific and effective antibodies limits the validation of the natural distribution of the ORAI2 protein within the neuron. The problem can be solved by genetic labeling of endogenous proteins at a single-cell resolution using the SLENDR[l] technique.[146] Analysis of the distribution of ORAI2 in neurons is of scientific interest in the field of nSOCE. It would help to better understand nSOCE function and its impact on neuronal Ca^{2+} homeostasis.

The expression profile of *Stim1* and *Stim2* shows an equal expression level for cultured neurons and all neural tissues tested, except for the hippocampus, where *Stim2* has a higher level in comparison to *Stim1.* Nevertheless, *Stim2/Stim1* ratio differs from the analyzed immune cell subsets with an increased abundance of *Stim2* gene expression. This indicates of distinguished

[l] SLENDR - single-cell labeling of endogenous proteins by clustered regularly interspaced short palindromic repeats (CRISPR)-Cas9-mediated homology-directed repair.

properties of neuronal SOCE in comparison to non-excitable cells. Based on studies about SOCE in non-excitable cells, shift to the higher *Stim2* expression would point to changes of SOCE function from ER Ca^{2+} refiling to Ca^{2+} level stabilization. This hypothesis based on the biophysical properties of STIM2. STIM2 requires mild reduction of ER Ca^{2+} level for its activation, but CRAC channels formed by STIM2 have a lower Ca^{2+} conductance. Published data demonstrate controversial results about the physiological role of *Stim1* or *Stim2* in the CNS. On the one hand, *Stim2* global deletion in mice leads to significant behavior changes and reduced SOCE in neurons.[129] On the other hand, forebrain specific deletion of *Stim1* or *Stim1/Stim2,* but not *Stim2* alone*,* leads to behavioral and physiological changes in mice, such as memory impairment and enhanced LTP.[147] Therefore, for the analysis of the role of SOCE in CNS inflammation, neither *Stim1* nor *Stim2* can be prioritized. Thus, *Orai2, Stim1* and *Stim2* genes have the highest potential to be involved in nSOCE functionality and were prioritized in the current work.

1.2. Murine neuronal CRAC profile during EAE

mRNA expression profile of CRAC components was analyzed in cortical, hippocampal, and spinal cord tissues from wild-type healthy controls, as well as animals at the acute and chronic stages of EAE. The most striking downregulation was detected for *Orai2* gene in the hippocampus at the acute stage. Since EAE induction does not result in a high immune cell infiltration into the hippocampus in the C57BL/6 mouse line, the detected downregulation of *Orai2* can possibly be explained by the neuronal feedback to the general immune response. The partial recovery of *Orai2* during the chronic phase of the disease supports this assumption. Similar *Orai2* profile was observed in the samples from cortical tissues. On the cellular level the reduction of the *Orai2* expression in cortical and hippocampal tissue during the acute EAE may be linked to synaptic loss and further recovery which was shown to be present in the EAE model with enhanced cortical inflammation.[148,149] This explanation is further supported by experiments with the mouse model of HD where *Orai2* downregulation contributes to the reduced spine loss.[150] The data presented in the current work also show a localization of ORAI2 in the dendritic spines *in vitro.* In contrast to the cortex and the hippocampus, mRNA expression of *Orai1* but not *Orai2* in spinal cord samples was affected by EAE. Upregulation of *Orai1* may reflect cell composition changes during the acute EAE. The spinal cord has relatively low neuronal density (in comparison to the cortex or the hippocampus) and the most prominent infiltration of the immune cells during EAE in C57BL/6 mice. Since the *Orai2* mRNA expression levels of the main immune subsets infiltrating the CNS during EAE (T and B cells) are comparable to *Orai2* expression level in the spinal cord, a possible reduction of *Orai2* expression in neurons could be masked. Nevertheless, insufficient knowledge about endogenous ORAI2 localization in neurons does not allow to make a more detailed

conclusion. Knowledge about the distribution of ORAI2 at healthy condition and during the acute and chronic phases of the EAE would help to localize ORAI2-mediated Ca^{2+} signaling, which is affected by CNS inflammation, in neurons on a structural level (axon, soma, dendrites or synapse). This would also allow to confirm or to reject the hypothesis about ORAI2 downregulation during acute EAE in the spinal cord.

EAE induction had a diverse effect on *Stim1* and *Stim2* expression levels. The mRNA expression of *Stim2* was affected to a greater extent in comparison to *Stim1*. If the biophysical properties of the neuronal *Stim1* and *Stim2* are similar to their properties in other cell types, downregulation of *Stim2* should shape the SOCE activation after a mild or moderate ER Ca^{2+} pool depletion, and thus reduce Ca^{2+} influx via SOCE during the base line activity. Like for *Orai2,* the highest changes of *Stim1* and *Stim2* mRNA expression levels were observed in the cortex and the hippocampus during the acute stage of EAE. There was no significant difference in the mRNA expression in the spinal cord samples during EAE. Based on the obtained data and literature analysis, it is not possible to make a solid conclusion about the privilege of *Stim1* or *Stim2* in neurons during CNS inflammation in mice. Nevertheless, deletion of both *Stim1* and *Stim2* could be used to investigate the contribution of nSOCE, which is the second aim of this dissertation.

2. *Orai2* deletion in CNS inflammation

Orai2 is the most expressed gene from the *Orai* gene family in neural tissue in mature C57BL/6 mice. Furthermore, it was the mainly expressed gene in the mature primary neuronal culture*.* Significant dysregulation of *Orai2* expression in neural tissue samples during acute EAE and a mild effect of ORAI2 on the SOCE function in non-excitable cells[109] led to the prioritization of *Orai2* for further analysis of nSOCE. ORAI2 could represent an attractive target for a potential neuroprotective therapeutic approach during CNS inflammation.

2.1. Global deletion of Orai2

2.1.1. The effect of global deletion of *Orai2* on SOCE-related genes

First, analysis of SOCE-related gene expression was performed for neural tissue from *Orai2*$^{-/-}$ mice in order to assess potential compensatory changes among SOCE genes. SOCE-related gene expression was not altered in *Orai2*-deficient animals, except for *Orai3* mRNA level in the spinal cord. *Orai3* mRNA level was significantly reduced in the spinal cord of *Orai2*$^{-/-}$ in comparison to wild-type mice and should be considered for the results interpretation. However, two points should be taken into account regarding the observed *Orai3* downregulation. First, since the reduction was observed only in spinal cord samples, spinal cord-specific neurons or non-neuronal cells are more likely to be the affected cells. Second, the absolute expression level was close to

the technical detection limit and the difference could be a technical artifact. Furthermore, role of *Orai3* was not reported in neurons except for a single publication, where *Orai3* downregulation was shown to lead to the reduction of SOCE influx in dorsal root ganglion neurons.[151] Since *Orai2* deletion is linked to the reduction of SOCE in neurons, the published result for *Orai3* would rather indicate a further “supportive” reduction of SOCE in the mouse line with the global *Orai2* deletion than a compensation effect on SOCE functionality. Under these conditions, the influence on *Orai3* can be considered as having no or a minimal impact on SOCE pathway in the *Orai2*$^{-/-}$ mouse model.

2.1.2. Global deletion of *Orai2* ameliorates EAE

The impact of SOCE under genetic ablation of *Orai2* was analyzed in the mouse model of CNS inflammation using the *Orai2*$^{-/-}$ mouse line. For the first time, a protective effect of global *Orai2* deletion was shown in the model of CNS inflammation in mice. Nevertheless, the results were difficult to interpret. On the one hand, amelioration of the clinical score at the recovery and the chronic phase of the EAE and trend to the reduced axonal damage were pointed to the enhance resistance of the neurons to the neurodegenerative processes during CNS inflammation. No difference in the onset of disease and body weight change provide an additional support toward hypothesis of CNS-mediated protection. On the other hand, a significant reduction of the immune cells infiltrating into spinal cord and a reduced amount of activated microglia at the chronic stage of the EAE raise the question about the cell type contributing to the observed phenotype. Analysis of the immune cells infiltrating into the CNS at the acute stage of the EAE, does not show a significant effect of the *Orai2* deletion on the overall immune response.

One possible explanation for the observed phenotype is that a reduced number of damaged axons in the acute phase leads to a reduced re-infiltration of immune cells in the later phase of the EAE. In this case, the observed protective phenotype would be mediated by neurons. To validate this hypothesis, a mouse model with neuronal-specific deletion of *Orai2* is required. Amelioration of the clinical symptoms of the EAE would clearly prove a neuronal origin of the phenotype observed in the *Orai2*$^{-/-}$ mouse line.

On the other hand, since the global deletion affects the immune system as well, the immune cells could also mediate the observed difference between *Orai2*$^{-/-}$ and wild-type mice. The most promising explanation, towards an immune system modulation, lays in the effect of *Orai2* deletion on dendritic cells. The overall picture of the immune cell composition during the acute EAE shows that dendritic cells are overrepresented among CNS infiltrating lymphocytes in. *Orai2*$^{-/-}$ in comparison to wild-type mice. Dendritic cells are antigen presenting cells of the immune system

which modulate the activity of T cells.[152] This can potentially explain the reduced numbers of $CD3^+$ at the chronic stage of the EAE in *Orai2* deficient mice even with relatively mild changes in the DCs amount. The role of *Orai2* in dendritic cells remains unknown for now, but experiments with pharmacological inhibition of SOCE using bone marrow dendritic cells (BMDCs) pointed to a significant impact of *Orai2* on the SOCE pathway in BMDCs.[153] Taking into account the role of the SOCE pathway, which is accepted to be the main source of Ca^{2+} for non-excitable cells and is critical for many immune cell functions including immune cell activation and immunological synapse formation, the effect of *Orai2* on dendritic cell function is of scientific interest. Nevertheless, further validation of the immunological effect of *Orai2* deletion is out of the scope of the current work.

2.2. Neuronal *Orai2* deletion does not influence clinical outcome of the EAE

In order to overcome the influence of non-neuronal cell types on the EAE disease score and in order to characterize the contribution of neuronal *Orai2* on neurodegeneration during CNS inflammation, neuron-specific knock out mouse lines were used.

2.2.1. *Orai2*$^{fl/fl}$*Eno2*^{cre} in CNS inflammation

Genetic deletion of a gene of interest in *Eno2* positive cells is a widely used neuron-specific mouse model. It was used for the generation of neuron-specific mouse models for the investigation of various neuronal disorders including spinal muscular atrophy[154], autism[155] , or MS[156] .

Significant reduction of *Orai2* mRNA expression was detected in all neural tissues. Nevertheless, a milder change of *Orai2* expression in the hippocampus in comparison to the cortex in *Orai2*$^{fl/fl}$*Eno2*^{cre} line indicates that the deletion is only in a subpopulation of neurons or that the deletion has a mosaic pattern. Additional validation of the *Orai2* deletion in immune cells showed that part of the T and B cell populations have a cre-mediated deletion of *Orai2* in the *Orai2*$^{fl/fl}$*Eno2*^{cre} mouse line. Therefore, the *Orai2*$^{fl/fl}$*Eno2*^{cre} mouse line could be considered to contain an immune-neuronal *Orai2* deletion.

No difference in the EAE disease course between *Orai2*$^{fl/fl}$*Eno2*^{cre} and *Orai2*$^{fl/fl}$ animals was observed. The results obtained from the EAE experiment and the mouse line validation have a few limitations which could mask a potential neuronal impact. Firstly, the amount of neurons with an *Orai2* deletion could be insufficient. This can lead to a mild protective effect, which cannot be observed in the EAE experiment with the current sample size. As a possible solution, experiments could be repeated with a significantly larger cohort, which is questionable from the ethical point of view. Secondly, in the *Orai2*$^{fl/fl}$*Eno2*^{cre} mouse line, the immune system modulation by *Orai2*

could not be excluded. Even though it was reported that the *Orai2* deletion has a mild or no effect on B and T cells proliferation, activity, and pathogenic potential in the inflammatory bowel disease (IBD) mouse model.[109] The limited knowledge about the influence of *Orai2* on the immune system does not allow to derive a conclusion about the role of *Orai2*-deficient T and B cells in the CNS inflammation mouse model based on the obtained results.

The focus of the dissertation is on the role of nSOCE. Therefore, motoneuron-specific deletion and more efficient pan-neuronal deletion of *Orai2* were further analyzed in an *in vivo* model of CNS inflammation.

2.2.2. Motor neuron-specific deletion of *Orai2* does not affect EAE progression

Motor neurons were chosen as a targeted neuronal population to characterize the impact of *Orai2* deletion on neurodegeneration during ongoing CNS inflammation due to two points. First, the availability of the highly specific mouse line with a *ChAT* positive motor neuron-specific *cre* expression profile. Second, in the EAE mouse model induced in C57BL/6 mouse line, which was used a background strain in this dissertation, the major readout of the clinical outcome is motor disability that correlates with the dysfunction and the damage of motor neurons.[157,158]

The mouse line with motor neuronal-specific deletion of *Orai2* was obtained by crossing *ChAT*^{cre} and *Orai2*$^{fl/fl}$ animals. EAE disease course was not differ between *Orai2*$^{fl/fl}$×*ChAT*^{cre} and *Orai2*$^{fl/fl}$ animals. This suggests that the *Orai2* deletion has no or only a minimal impact on the survival of motor neurons and their functionality during CNS inflammation in mice. The most critical problem in the design of the current experiment is the small population containing the *Orai2* deletion. Therefore, the current experiment does not provide sufficient data for the rejection of the hypothesis of whether the amelioration of the EAE clinical score, which was observed in the *Orai2*$^{-/-}$ mouse line, relies upon neurons.

2.2.3. Pan-neuronal deletion of *Orai2* does not affect EAE progression

Pan-neuronal *Orai2* deletion was obtained by crossing the *Orai2*$^{fl/fl}$ and the *Snap25*^{cre} lines. Validation of the resulting *Orai2*$^{fl/fl}$×*Snap25*^{cre} animals provides solid data about the specific and efficient deletion of *Orai2* in a wide range of neurons. Nevertheless, no difference in the EAE disease course was observed between *Orai2*$^{fl/fl}$×*Snap25*^{cre} and *Orai2*$^{fl/fl}$ mice. The obtained results provide solid evidence that amelioration of the EAE disease is not mediated by an increased neuronal survival during CNS inflammation.

2.3. Deletion of *Orai2 in vitro* does not affect the resting Ca^{2+} level in neurons

The complexity of the *in vivo* model does not provide sufficiently controlled conditions to address the third aim of the project about the effect of *Orai2* deletion on Ca^{2+} regulation in neurons. Thus, to address this question, *in vitro* experiments were performed using cultured primary neurons. The analysis of basic properties of Ca^{2+} homeostasis in cortical primary neurons does not indicate a significant effect of *Orai2* deletion *in vitro*. The amplitude of spontaneous Ca^{2+} transients and the mean Ca^{2+} levels were not different in *Orai2*-deficient neurons in comparison to wild-type control neurons. A recently published paper demonstrates that *Orai2* deletion contributes to Ca^{2+} influx into hippocampal neurons only after IP3-mediated ER Ca^{2+} depletion and not in RyR-mediated ER Ca^{2+} depletion.[159] Another publication demonstrated a protective effect of *Orai2* deletion during acute ischemic stroke in mice[160]. Furthermore, cultured *Orai2*-deficient cortical and hippocampal primary neurons showed a reduced baseline Ca^{2+} level. Nevertheless, in this experiment only young cortical neurons (DIV 6-7) displayed a reduced SOCE-mediated Ca^{2+} influx and a reduced base line Ca^{2+} level. Experiments with mature neuronal cortical culture (DIV19), presented in the same publication, showed no effect in the baseline and glutamate-induced Ca^{2+} influx level, which is in line with the results obtained in the current work. In addition, the protective phenotype during hypoxic conditions was shown only with mature hippocampal primary neurons.[160] Therefore, the protective potential of neuronal ORAI2 modulation could depend on the neuronal cell type, maturation state and the trigger of neuronal damage.

2.4. Summary

The results presented in the current work demonstrate for the first time that a global *Orai2* deletion leads to a protective phenotype in a mouse model of CNS inflammation, but the origin of the disease amelioration remains uncertain. In the mouse line with motor neuron-specific (*Orai2*$^{fl/fl}$×*ChAT*^{cre}), pan-neuron (*Orai2*$^{fl/fl}$×*Snap25*^{cre}), and partial neuronal/immune (*Orai2*$^{fl/fl}$×*Eno2*^{cre}) deletion of *Orai2* a protective phenotype could not be confirmed. Thus, the origin of the amelioration is probably derived from a non-neuronal cell population. In addition, the results from the *Orai2*$^{fl/fl}$*Eno2*^{cre} line point out that T and B cells, which are the major immune cell subtype infiltrating into the CNS during EAE, are not critically affected by *Orai2* deletion. The most promising direction for further investigation constitutes of dendritic cells, since they are overrepresented in spinal cord samples from *Orai2*$^{-/-}$ mice at acute EAE in comparison to wild-type controls. Another possible explanation for the observed phenotype is that *Orai2* affects epithelial or glial cells. Currently, there are no data regarding the role of *Orai2* in the epithelial cells, blood brain barrier function, or glia cells. Thus, further research is needed to characterize

the role of ORAI2 and its protective function during various neurodegenerative disorders, including MS.

3. *Stim1* and *Stim2* neuron-specific double deletion mouse model

In the first part of the dissertation, it was shown that neuronal *Orai2* deletion is irrelevant for the neurodegenerative processes during EAE and for resting Ca^{2+} levels in mature cortical neurons *in vitro*. To fulfil the second aim of the dissertation, which addresses the contribution of nSOCE to neurodegeneration during CNS inflammation, a mouse line with a double neuron-specific deletion of *Stim1* and *Stim2* was generated and analyzed. The specificity and the efficiency of the line were confirmed by qPCR analysis. According to the published literature the generated mouse line is the first line with a genetic deletion of critical components of SOCE in neurons, by which the classical mechanism of SOCE cannot be functional.

3.1. Neuron-specific knock out of *Stim1* and *Stim2* ameliorates EAE

A significant contribution of *Stim1* and *Stim2* deletion to the clinical outcome of CNS inflammation was observed at acute and chronic EAE. The overall picture at the chronic stage of the EAE, including histological validation of the neuronal and immune cell density in the cortex and the spinal cord, the onset of disease, bodyweight change and the maximum clinical score, implies to the modification of the immune response rather than an enhanced neuronal survival. On the other hand, the animals showed an unpredictable behavior including hyperactivity and spontaneous epileptic seizures. These were most obvious in the pre-clinical phase of the EAE, indicating a systemic effect of *Stim1* and *Stim2* deletion on CNS activity. Additional investigation does not show a difference in the immune cell subset composition infiltrating into the brain or the spinal cord at the chronic stage of the EAE. Moreover, no immune cells were observed in the spinal cord or brain samples in the pre-clinical phase of the EAE in $Stim1^{fl/fl}Stim2^{fl/fl}\times Snap25^{cre}$ which could enhance behavioral changes.

Hyperactivity and spontaneous epileptic seizures were observed in $Stim1^{fl/fl}Stim2^{fl/fl}\times Snap25^{cre}$ mice shortly after immunization. These phenotypes may be a result of the overlap of changes induced by *Stim1* and *Stim2* deletion and the increased synaptic activity and spine density, which are shown to be present in early stages of EAE.[161] On the other hand, similar neuronal density and amelioration of the clinical symptoms of the EAE in $Stim1^{fl/fl}Stim2^{fl/fl}\times Snap25^{cre}$ animals are conflicting results since the clinical outcome of the EAE usually correlates with decreased neuronal density in the spinal cord.[162] The possible explanation includes a higher basal neuronal density prior to immunization, or a modified immune response by an unknown mechanism of neuro-immune interaction. Aside from EAE, the observed unexpected behavioral changes in the

Stim1$^{fl/fl}$*Stim2*$^{fl/fl}$×*Snap25*^{cre} mouse line required a deeper investigation since the systemic changes induced by *Stim1* and *Stim2* deletion may influence mouse physiology and EAE disease progression.

3.2. *Stim1* and *Stim2* contribute to Ca^{2+} homeostasis *in vitro*

To gain knowledge about changes induced by *Stim1* and/or *Stim2* deletion on cellular level, experiments were performed on primary neuronal cultures. *In vitro* live-cell Ca^{2+} imaging of *Stim1*$^{-/-}$*Stim2*$^{-/-}$ mature primary neuronal culture supports the systemic effect of SOCE on neuronal activity, which was deduced from the previous *in vivo* experiments. Reduced mean Ca^{2+} level at the resting state and following stimulation may prevent neurons from neuronal damage that is caused by Ca^{2+} overload, which would suggest neuroprotective effect of *Stim1* and *Stim2* deletion. An increased frequency of Ca^{2+} transients reflects an increased electrical activity of the neuronal network. This correlates with the hyperactive behavior of *Stim1* and *Stim2* deficient mice.

While reduction in the effective Ca^{2+} levels can trivially be explained by the reduction of intracellular Ca^{2+} stores refiling in the absence of SOCE, an increased neuronal activity probably is a result of more complex changes in neurons. It was reported that downregulation of *Stim1* and *Stim2* in cortical neurons enhances NMDA-induced Ca^{2+} signals.[163] Enhanced NMDA-induced Ca^{2+} influx would be a reasonable explanation for the *in vitro* phenotype. Nevertheless, this would contradict the EAE results, since enhanced NMDA-induced Ca^{2} influx would exacerbates the EAE clinical score.[164]

Analysis of Ca^{2+} transients in *Stim2* deficient neurons *in vitro* shows milder but similar effects on effective neuronal Ca^{2+} levels after stimulation and an average amplitude of Ca^{2+} transients in comparison to the neurons with *Stim1* and *Stim2* double deletion. Reduction of the effective Ca^{2+} level remains in line with the protective phenotype observed in primary neuronal culture under hypoxic condition, and reduced base line Ca^{2+} level in young primary cortical culture (DIV 5 to 9).[129] Nevertheless, *Stim2* deletion did not have an effect on the firing rate of primary neuronal cultures. This suggests that the observed behavioral phenotype requires *Stim1* and *Stim2* double deletion or depends on *Stim1*.

3.3. Neuron-specific *Stim1* and *Stim2* deletion influences long-term survival, behavior and epileptic predisposition in mice

Characterization of healthy *Stim1*$^{fl/fl}$*Stim2*$^{fl/fl}$×*Snap25*^{cre} animals confirms the hypothesis about a systemic effect of neuronal *Stim1* and *Stim2* deletion on mouse physiology. *Stim1*$^{fl/fl}$*Stim2*$^{fl/fl}$×*Snap25*^{cre} mice showed an enhanced anxiety and reduced exploratory behavior in the open field and the Y maze tests. Some animals had a spontaneous epileptic seizure, which

was the reason for the interruption of the behavioral tests. In addition, *Stim1*$^{fl/fl}$*Stim2*$^{fl/fl}$×*Snap25*^{cre} mice showed a significantly reduced long-term survival. These prominent behavioral changes were unpredictable, since no difference in the offspring quantity, breeding behavior or routine handling were reported by the animal caretaker nor were observed during the handling of the animals prior to the experiments. Pronounced hyperactivity and seizure episodes were observed only after the EAE induction or during behavioral experiments. Daily assessment of the small cohort of *Stim1*$^{fl/fl}$*Stim2*$^{fl/fl}$×*Snap25*^{cre} animals at a normal night/day cycle for an 1 hour per day over the course of 4 weeks could not confirm spontaneous epileptic seizures but only pronounced hyperactivity. For behavioral experiments, the animals were placed in the reverse night/day circle 4 weeks prior to the start of the experiment. At this time frame, seizure-like episodes were detected during the handling and behavioral tests. This is could be linked to the high activity of the animals during the night.

Since the *Stim1*$^{fl/fl}$*Stim2*$^{fl/fl}$×*Snap25*^{cre} line is the first mammalian reported with a pan-neuronal *Stim1* and *Stim2* deletion, the mechanism resulting in this phenotype is difficult to decipher without a deeper molecular characterization. Nevertheless, a few phenotypes in the animal models with a genetic deletion of *Stim1* or *Stim2* were reported. Genetic deletion of the *stim2a* or *stim2b* was shown to result in hyperactivity and susceptibility to seizures in zebrafish larvae.[165,166] Mice with a global *Stim2* deletion exhibited behavioral changes in the Morris water maze task and spontaneous death after the age of 8 weeks.[129] In addition, neuron-specific *Stim1* or *Orai1* deletion enhanced chemoconvulsant-induced seizures in mice.[167] In contrast to this, aged female mice with *Orai1* neuron-specific overexpression exhibit spontaneous seizure-like events in addition to the downregulation of genes related to epilepsy and an enhanced chemoconvulsant-induced activity in hippocampal slice culture.[167,168] Unfortunately, in the published studies, potential compensatory expression of other SOCE-related genes was not reported in mice.

One speculative hypothesis derived from the results of the dissertation and the published data suggest that nSOCE activity depends on ORAI1, STIM1 and STIM2 proteins. A proper function of nSOCE requires a complicated CRAC channel formation by ORAI1-STIM2 with further recruitment of STIM1 in the optimal ratio. The picture is trivial for the *Stim1* and *Stim2* double deletion, where CRAC channel cannot be formed. In the case of *Orai1* overexpression, insufficient quantity of STIM1 and STIM2 proteins could probably prevent a formation of the heteromeric channel with an optimal STIM to ORAI ratio, which is reported to be 2 to 1, and by this would mimic the absence of SOCE to some extent.[169] The *Stim2* deletion in zebrafish larvae results in a comparable phenotype to the one presented in this dissertation, which would point towards the

important role of *Stim2* in the hyperactive phenotype. The most controversial points for the current speculation are the reduced life expectancy reported for *Stim2* only deletion in comparison to the results for neuron specific *Stim1* and *Stim2* double knock out mice, and the lack of enhanced neuronal network activity in the *Stim2*-deficient neurons. An additional observation that could not be explained is the reduced number of $CD3^+$ immune cells infiltrating into the CNS at the chronic EAE in *Stim1*$^{fl/fl}$*Stim2*$^{fl/fl}$×*Snap25*^{cre} animals.

Another speculative hypothesis would explain the obtained EAE results and the phenotype observed in healthy animals with neuron-specific *Stim1* and *Stim2* deletion. The explanation is based on an activity reported for STIM1. It was shown that *Stim1* deficiency induces spontaneous activation of stimulator of interferon genes (STING) protein and enhanced expression of type I interferons in murine embryonic fibroblasts.[170] A similar mechanism of action could be present in neurons in *Stim1*$^{fl/fl}$*Stim2*$^{fl/fl}$×*Snap25*^{cre} animals.[171] Enhanced production of type I interferons would explain the modulation of the clinical outcome of the EAE and could induce epileptic seizures. [172–175] Furthermore, reported seizures in different genetically modified mice could be explained by this theory. Nevertheless, the reported epileptic phenotype in *Stim2* deficient zebrafish, which highly overlaps with the phenotype observed in *Stim1*$^{fl/fl}$*Stim2*$^{fl/fl}$×*Snap25*^{cre} mice, can only be explained using remarkable assumptions. For example, the diversity in STING protein structure, which rather has a shift towards the modulation of NF-kB response and not interferon in zebrafish[176], would be sufficient for the exchange of a quenching protein from STIM1 to STIM2.

4. Outlook

The presented work shed new light on the SOCE pathway and its relevance to neuronal function and CNS response during pathological conditions. Nonetheless, many aspects remain open and require further investigation in order to comprehend the exact role of nSOCE in neurodegeneration and its relevance to CNS inflammation.

First of all, in the context of nSOCE regulation, *in vitro* characterization of Ca^{2+} homeostasis in *Stim1* deficient neurons is required. Analysis of the mean Ca^{2+} and the Ca^{2+} transient frequency in *Stim1*$^{-/-}$ neuronal cultures can provide significant information regarding the predisposition to epileptic seizures and the EAE phenotype observed in *Stim1*$^{fl/fl}$*Stim2*$^{fl/fl}$×*Snap25*^{cre} mice. Secondly, evaluation of interferon expression levels in *Stim1*$^{fl/fl}$*Stim2*$^{fl/fl}$×*Snap25*^{cre} animals should be performed in order to corroborate potential role of STING in the observed phenotype. *In vitro* evaluation of interferon levels with and without stimulation would complement the results obtained *in vivo*. This would provide important information about the possible mechanism of action of nSOCE component during EAE and could reduce further *in vivo* experiments. As a next step,

EAE experiment should be performed in *Stim1*-only and *Stim2*-only neuron-specific knock out mouse lines with an analysis of the immune cell subset composition infiltrating into the CNS at the acute stage of the disease. As a control experiment, neuron-specific deletion of *Stim1* and *Stim2* are needed to be combined with the mouse line carrying a mutation in *Sting* leading to a non-functional and an unstable STING protein e.g. $Sting^{Gt}$.[177] The EAE experiments and behavioral characterization of the mouse line would provide proof (or disproof) for the hypothesis about the protective mechanism observed in $Stim1^{fl/fl}Stim2^{fl/fl}\times Snap25^{cre}$ mice during EAE and important information about novel epileptogenic mechanisms mediated by SOCE.

Identification of the origin of *Orai2*-mediated protective EAE phenotype is of great scientific and practical interest. In order to validate whether the phenotype observed in *Orai2*-deficient mice depends on an immunological source assessment of cytokine production after MOG re-stimulation of immune cells is required (a re-call assay). An EAE experiment with a bone marrow chimera mouse model would be appropriate as the control. In case that the immune origin hypothesis would be rejected, single-cell sequencing analysis of CNS from $Orai2^{-/-}$ and wild-type animals can be performed to determine which cell types mediate an enhanced axonal resistance and reduce immune cell infiltration during EAE. Generation of a new tissue-specific knock out mouse line, based on the sequencing results, and utilizing it to re-validate the EAE phenotype could be the following up step. Based on the obtained results, inhibition of SOCE in the identified cell types can be used for the development of a novel neuroprotective therapy during CNS inflammation.

V. Summary

Multiple sclerosis (MS) is the most common inflammatory disorder of the central nervous system (CNS) with limited treatment options. Currently available therapy aims to reduce inflammation and to prevent immune cells infiltration into the CNS. Unfortunately, progressive neurodegeneration during MS has no approved treatment possibilities yet. Furthermore, the exact mechanism of neurodegeneration during MS is not fully understood. The pathogenesis of MS and other neurological disorders includes many processes that either influence Ca^{2+} or affected by Ca^{2+} homeostasis in neurons. Thus, modulation of neuronal Ca^{2+} homeostasis is an attractive neuroprotective and therapeutic strategy against neurodegenerative disorders.

Ca^{2+} release-activated Ca^{2+} channels (CRAC), which mediate a store operated calcium entry (SOCE), are the most recently identified Ca^{2+} channel family. Their specific roles in Ca^{2+} homeostasis and in cell function are not completely described, especially in neurons. SOCE contributes to neuronal damage under hypoxia and can influence mitochondria function and synaptic stability. However, the role of neuronal SOCE (nSOCE) during CNS inflammation was not investigated before.

In this work it was shown for the first time that nSOCE contributes to the pathological processes during CNS inflammation using the animal model of MS, experimental autoimmune encephalomyelitis (EAE). mRNA level analysis of SOCE-related genes has demonstrated domination of *Orai2* expression in healthy neural tissues and its dysregulation during the inflamed condition. Indeed, a global deletion of *Orai2* leads to amelioration of EAE in mice. Nevertheless, this work suggests that the observed protective phenotype is independent of the neuronal *Orai2*. However, experiments with a neuron-specific deletion of the critical components of SOCE (*Stim1* and *Stim2*) showed a protective role of SOCE genetic deletion during EAE with an influence on the immune system. Unexpectedly, this genetic modification leads to behavioral changes as well. Hyperactivity, exploratory deficits and reduced long-term life expectancy were validated in the current work. In fact, episodes of spontaneous epileptic seizures were detected as well and thus further behavioral tests were terminated due to ethical reasons. *In vitro* experiments showed that *Stim1* and *Stim2* deletion leads to enhanced activity of the neuronal network and reduced cytosolic Ca^{2+} level. Thus, the *in vitro* results stay in line with the behavioral and EAE phenotype observed *in vivo.*

Altogether, this work reveals that nSOCE plays an essential role in neuronal network excitability. Furthermore, nSOCE has a systemic effect on mice and it influences life expectancy. EAE

experiments indicate that critical components of SOCE participate in a yet undiscovered pathway involving the immune system and modulated by neurons. The data generated withing the scope of this work is of great scientific interest in the context of inflammatory neurodegenerative disorders like MS and could be used to further develop novel treatment strategies against neurodegeneration.

VI. Supplement

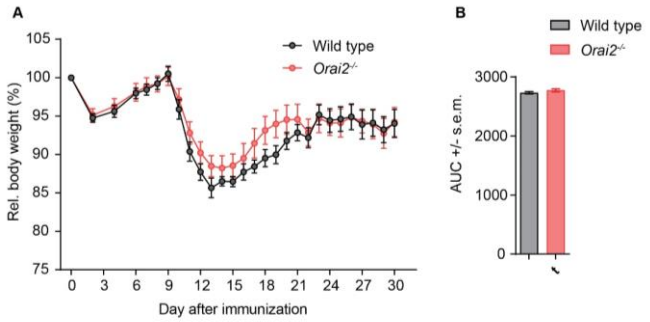

Supplement 1 Relative body weight change in *Orai2*$^{-/-}$ mice during EAE

(A-B) Mean relative body weight of *Orai2*$^{-/-}$ (n = 10) and wild-type (n = 10) mice undergoing EAE and AUC comparison. Data plotted as mean +/- s.e.m; Statistical analysis was performed by unpaired, two-tailed Student's t-test.

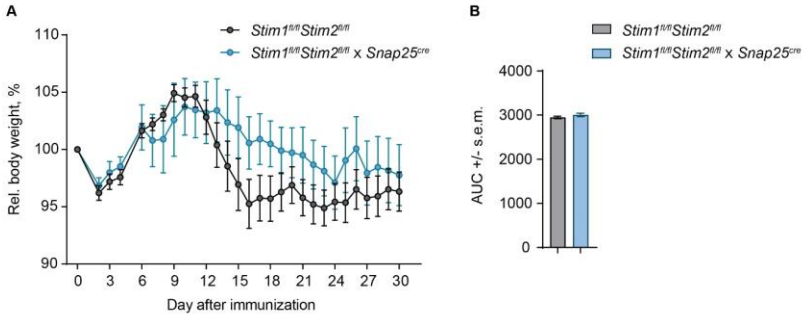

Supplement 2 Relative body weight change in *Stim1*$^{fl/fl}$*Stim2*$^{fl/fl}$×*Snap25*^{cre} mice during EAE

(**A-B**) Mean relative body weight of *Stim1*$^{fl/fl}$*Stim2*$^{fl/fl}$×*Snap25*^{cre} (n = 17) and *Stim1*$^{fl/fl}$*Stim2*$^{fl/fl}$ (n = 20) mice undergoing EAE and AUC comparison. Data plotted as mean +/- s.e.m; Statistical analysis was performed by unpaired, two-tailed Student's t-test.

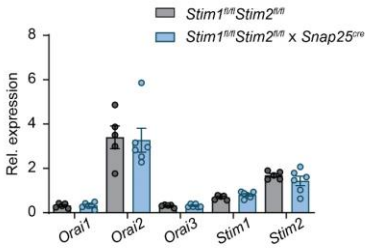

Supplement 3 Control qPCR of the *Stim1*$^{fl/fl}$*Stim2*$^{fl/fl}$×*Snap25*^{cre} mouse line

Analysis of *Orai1, Orai2, Orai3, Stim1* and Stim2 expression levels in the spleen of the animals used for the histological assays. Six animals from the *Stim1*$^{fl/fl}$*Stim2*$^{fl/fl}$×*Snap25*^{cre} mouse line and five animals from the *Stim1*$^{fl/fl}$*Stim2*$^{fl/fl}$ line were evaluated. Data presented as a fold change compared with *Tbp* expression, and plotted as mean +/- s.e.m. Statistical analysis was performed by unpaired, two-tailed Student's t-test.

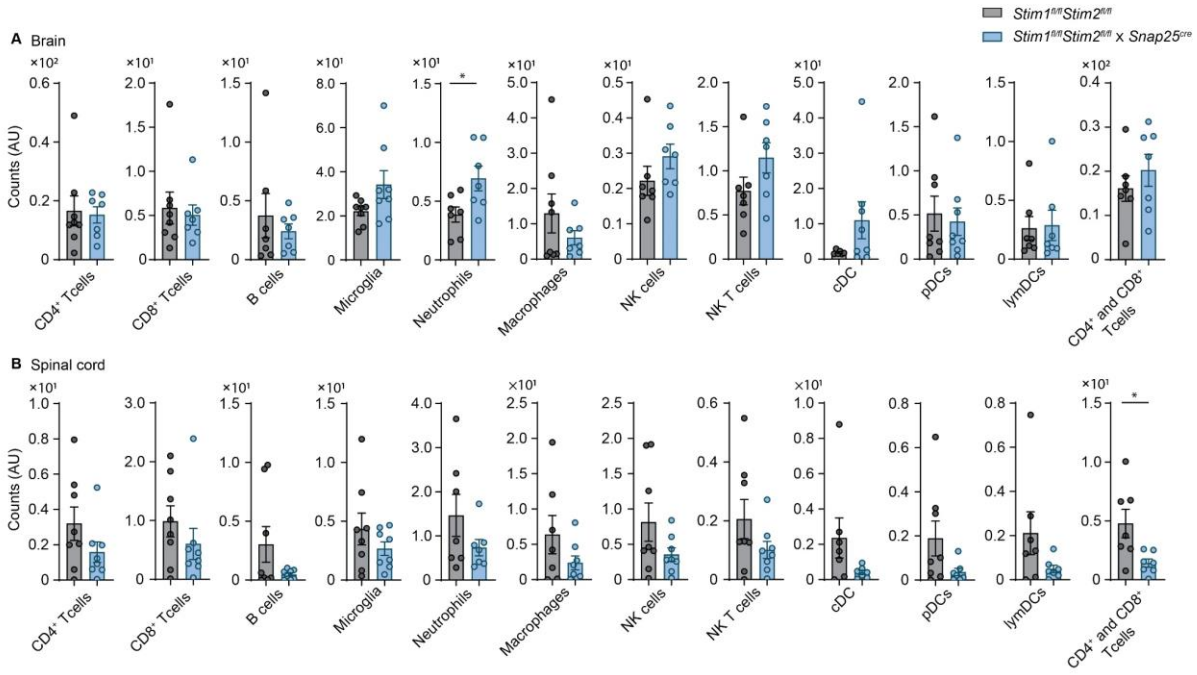

Supplement 4 Absolute quantification of the immune cell infiltration at chronic EAE in *Stim1*$^{fl/fl}$*Stim2*$^{fl/fl}$×*Snap25*^{cre} mice

(A-B) Absolute counts of CD4 T cells, CD8 T cells, B cells, microglia, neutrophils, macrophages, NK cells, NK T cells, cDC, pDC, lymDC, and CD4+CD8 T cells in the brain (A), and the spinal cord (B) of *Stim1*$^{fl/fl}$*Stim2*$^{fl/fl}$×*Snap25*^{cre} (n=8) and *Stim1*$^{fl/fl}$*Stim2*$^{fl/fl}$ (n=8) mice at chronic EAE analyzed by flow cytometry. Data plotted as mean +/- s.e.m. Statistical analysis was performed by unpaired, two-tailed Student's t-test, * p< 0.05.

VII. Bibliography

1. Conradsson, D., Ytterberg, C., von Koch, L. & Johansson, S. Changes in disability in people with multiple sclerosis: a 10-year prospective study. *J. Neurol.* **265**, 119–126 (2018).
2. The Multiple Sclerosis International Federation (MSIF), S. 2020. Atlas of MS 3 rd edition. *Mult. Scler. Int. Fed. (MSIF), Sept. 2020* 1–37 (2020).
3. Wingerchuk, D. M. Smoking: effects on multiple sclerosis susceptibility and disease progression. *Ther. Adv. Neurol. Disord.* **5**, 13–22 (2012).
4. Dyment, D. A., Ebers, G. C. & Dessa Sadovnick, A. Genetics of multiple sclerosis. *Lancet Neurol.* **3**, 104–110 (2004).
5. Muller, M., Terry, R., D., S. & R., D. Current Theories for Multiple Sclerosis Pathogenesis and Treatment. in *Autoimmune Diseases - Contributing Factors, Specific Cases of Autoimmune Diseases, and Stem Cell and Other Therapies* 3–24 (InTech, 2012). doi:10.5772/50005.
6. Stadelmann, C., Timmler, S., Barrantes-Freer, A. & Simons, M. Myelin in the central nervous system: Structure, function, and pathology. *Physiol. Rev.* **99**, 1381–1431 (2019).
7. Lucas, K. The 'all or none' contraction of the amphibian skeletal muscle fibre. *J. Physiol.* **38**, 113–133 (1909).
8. Kearney, H. *et al.* Cervical cord lesion load is associated with disability independently from atrophy in MS. *Neurology* **84**, 367–373 (2015).
9. Compston, A. & Coles, A. Multiple sclerosis. *Lancet* **372**, 1502–1517 (2008).
10. Carassiti, D. *et al.* Neuronal loss, demyelination and volume change in the multiple sclerosis neocortex. *Neuropathol. Appl. Neurobiol.* **44**, 377–390 (2018).
11. Trapp, B. D. *et al.* Cortical neuronal densities and cerebral white matter demyelination in multiple sclerosis: a retrospective study. *Lancet Neurol.* **17**, 870–884 (2018).
12. Lumsden, C. E. Consideration of Multiple Sclerosis in Relation to the Auto-Immunity Process. *Proc. R. Soc. Med.* **54**, 11–15 (1961).
13. Frischer, J. M. *et al.* The relation between inflammation and neurodegeneration in multiple sclerosis brains. *Brain* **132**, 1175–1189 (2009).
14. Stys, P. K., Zamponi, G. W., van Minnen, J. & Geurts, J. J. G. Will the real multiple sclerosis

please stand up? *Nat. Rev. Neurosci.* **13**, 507–514 (2012).

15. Myers, L. W. Immunologic therapy for secondary and primary progressive multiple sclerosis. *Curr. Neurol. Neurosci. Rep.* **1**, 286–293 (2001).

16. Rivers, T. M. & Schwentker, F. F. ENCEPHALOMYELITIS ACCOMPANIED BY MYELIN DESTRUCTION EXPERIMENTALLY PRODUCED IN MONKEYS. *J. Exp. Med.* **61**, 689–702 (1935).

17. Constantinescu, C. S., Farooqi, N., O'Brien, K. & Gran, B. Experimental autoimmune encephalomyelitis (EAE) as a model for multiple sclerosis (MS). *Br. J. Pharmacol.* **164**, 1079–1106 (2011).

18. Terry, R. L., Ifergan, I. & Miller, S. D. Experimental Autoimmune Encephalomyelitis in Mice. in *Methods in Molecular Biology* vol. 1304 145–160 (2014).

19. Mcdonald, W. I. The effects of experimental demyelination on conduction in peripheral nerve: A histological and electrophysiological study: I. Clinical and histological observations. *Brain* **86**, 481–500 (1963).

20. Smith, K. J., Blakemore, W. F. & McDonald, W. I. The restoration of conduction by central remyelination. *Brain* **104**, 383–404 (1981).

21. Levin, M. *et al.* Neurodegeneration in multiple sclerosis involves multiple pathogenic mechanisms. *Degener. Neurol. Neuromuscul. Dis.* 49 (2014) doi:10.2147/DNND.S54391.

22. Haines, J. L. *et al.* A complete genomic screen for multiple sclerosis underscores a role for the major histocompatability complex. *Nat. Genet.* **13**, 469–471 (1996).

23. Ebers, G. C. *et al.* A full genome search in multiple sclerosis. *Nat. Genet.* **13**, 472–476 (1996).

24. Kawachi, I. & Lassmann, H. Neurodegeneration in multiple sclerosis and neuromyelitis optica. *J. Neurol. Neurosurg. Psychiatry* **88**, 137–145 (2017).

25. Stys, P. White Matter Injury Mechanisms. *Curr. Mol. Med.* **4**, 113–130 (2004).

26. Trapp, B. D. & Stys, P. K. Virtual hypoxia and chronic necrosis of demyelinated axons in multiple sclerosis. *Lancet Neurol.* **8**, 280–291 (2009).

27. Fern, R., Davis, P., Waxman, S. G. & Ransom, B. R. Axon Conduction and Survival in CNS White Matter During Energy Deprivation: A Developmental Study. *J. Neurophysiol.* **79**, 95–105 (1998).

28. Yu, S. P. & Choi, D. W. Na + -Ca 2+ Exchange Currents in Cortical Neurons: Concomitant Forward and Reverse Operation and Effect of Glutamate. *Eur. J. Neurosci.* **9**, 1273–1281 (1997).

29. Craner, M. J. *et al.* Molecular changes in neurons in multiple sclerosis: Altered axonal expression of Nav1.2 and Nav1.6 sodium channels and Na+/Ca2+ exchanger. *Proc. Natl. Acad. Sci.* **101**, 8168–8173 (2004).

30. Rosenkranz, S. C. *et al.* Enhancing mitochondrial activity in neurons protects against neurodegeneration in a mouse model of multiple sclerosis. *Elife* **10**, (2021).

31. Friese, M. A. *et al.* Acid-sensing ion channel-1 contributes to axonal degeneration in autoimmune inflammation of the central nervous system. *Nat. Med.* **13**, 1483–1489 (2007).

32. Schattling, B. *et al.* TRPM4 cation channel mediates axonal and neuronal degeneration in experimental autoimmune encephalomyelitis and multiple sclerosis. *Nat. Med.* **18**, 1805–1811 (2012).

33. Danbolt, N. C. Glutamate uptake. *Prog. Neurobiol.* **65**, 1–105 (2001).

34. Olney, J. W. & Sharpe, L. G. Brain Lesions in an Infant Rhesus Monkey Treated with Monosodium Glutamate. *Science (80-.).* **166**, 386–388 (1969).

35. Olney, J. W. Brain Lesions, Obesity, and Other Disturbances in Mice Treated with Monosodium Glutamate. *Science (80-.).* **164**, 719–721 (1969).

36. Stover, J. F. *et al.* Neurotransmitters in cerebrospinal fluid reflect pathological activity. *Eur. J. Clin. Invest.* **27**, 1038–1043 (1997).

37. Rothman, S. Synaptic release of excitatory amino acid neurotransmitter mediates anoxic neuronal death. *J. Neurosci.* **4**, 1884–1891 (1984).

38. Lewerenz, J. & Maher, P. Chronic Glutamate Toxicity in Neurodegenerative Diseases—What is the Evidence? *Front. Neurosci.* **9**, 1–20 (2015).

39. Lau, A. & Tymianski, M. Glutamate receptors, neurotoxicity and neurodegeneration. *Pflugers Arch.* **460**, 525–42 (2010).

40. Bonfoco, E., Krainc, D., Ankarcrona, M., Nicotera, P. & Lipton, S. A. Apoptosis and necrosis: two distinct events induced, respectively, by mild and intense insults with N-methyl-D-aspartate or nitric oxide/superoxide in cortical cell cultures. *Proc. Natl. Acad. Sci.* **92**, 7162–7166 (1995).

41. Sendrowski, K. *et al.* Study of the protective effect of calcium channel blockers against neuronal damage induced by glutamate in cultured hippocampal neurons. *Pharmacol. Reports* **65**, 730–736 (2013).

42. Lee, B. K. *et al.* Effects of KR-33028, a novel Na+/H+ exchanger-1 inhibitor, on glutamate-induced neuronal cell death and ischemia-induced cerebral infarct. *Brain Res.* **1248**, 22–30 (2009).

43. Hofer, A. M. & Brown, E. M. Extracellular calcium sensing and signalling. *Nat. Rev. Mol. Cell Biol.* **4**, 530–538 (2003).

44. Brown, E. M. *et al.* Cloning and characterization of an extracellular Ca2+-sensing receptor from bovine parathyroid. *Nature* **366**, 575–580 (1993).

45. Mellström, B., Savignac, M., Gomez-Villafuertes, R. & Naranjo, J. R. Ca2+-operated transcriptional networks: Molecular mechanisms and in vivo models. *Physiol. Rev.* **88**, 421–449 (2008).

46. Brini, M., Calì, T., Ottolini, D. & Carafoli, E. Intracellular Calcium Homeostasis and Signaling. in *Metal Ions in Life Sciences* vol. 12 119–168 (2013).

47. Smith, S. J., Buchanan, J., Osses, L. R., Charlton, M. P. & Augustine, G. J. The spatial distribution of calcium signals in squid presynaptic terminals. *J. Physiol.* **472**, 573–593 (1993).

48. Lipscombe, D. *et al.* Spatial distribution of calcium channels and cytosolic calcium transients in growth cones and cell bodies of sympathetic neurons. *Proc. Natl. Acad. Sci.* **85**, 2398–2402 (1988).

49. Grienberger, C. & Konnerth, A. Imaging Calcium in Neurons. *Neuron* **73**, 862–885 (2012).

50. Bronner, F. Extracellular and Intracellular Regulation of Calcium Homeostasis. *Sci. World J.* **1**, 919–925 (2001).

51. Li, G. Y., Fan, B. & Zheng, Y. C. Calcium overload is a critical step in programmed necrosis of ARPE-19 cells induced by high-concentration H2O2. *Biomed. Environ. Sci.* **23**, 371–377 (2010).

52. Orrenius, S., Zhivotovsky, B. & Nicotera, P. Regulation of cell death: The calcium-apoptosis link. *Nat. Rev. Mol. Cell Biol.* **4**, 552–565 (2003).

53. Katz, B. & Miledi, R. Ionic requirements of synaptic transmitter release. *Nature* **215**, 651

(1967).

54. Evans, R. C. & Blackwell, K. T. Calcium: Amplitude, Duration, or Location? *Biol. Bull.* **228**, 75–83 (2015).

55. Patterson, M., Sneyd, J. & Friel, D. D. Depolarization-induced calcium responses in sympathetic neurons: Relative contributions from Ca2+ entry, extrusion, ER/mitochondrial Ca 2+ uptake and release, and Ca2+ buffering. *J. Gen. Physiol.* **129**, 29–56 (2007).

56. Südhof, T. C. Calcium control of neurotransmitter release. *Cold Spring Harb. Perspect. Biol.* **4**, (2012).

57. Brini, M., Calì, T., Ottolini, D. & Carafoli, E. Neuronal calcium signaling: function and dysfunction. *Cell. Mol. Life Sci.* **71**, 2787–814 (2014).

58. Dolphin, A. C. A short history of voltage-gated calcium channels. *Br. J. Pharmacol.* **147**, S56–S62 (2006).

59. Dolphin, A. C. Voltage-gated calcium channels: Their discovery, function and importance as drug targets. *Brain Neurosci. Adv.* **2**, 239821281879480 (2018).

60. Catterall, W. A. Voltage-Gated Calcium Channels. *Cold Spring Harb. Perspect. Biol.* **3**, a003947–a003947 (2011).

61. Shen, J. & Yakel, J. L. Nicotinic acetylcholine receptor-mediated calcium signaling in the nervous system. *Acta Pharmacol. Sin.* **30**, 673–680 (2009).

62. Engelman, H. S. & MacDermott, A. B. Presynaptic ionotropic receptors and control of transmitter release. *Nat. Rev. Neurosci.* **5**, 135–145 (2004).

63. Hiruma, H. & Bourque, C. W. P2 purinoceptor-mediated depolarization of rat supraoptic neurosecretory cells in vitro. *J. Physiol.* **489**, 805–811 (1995).

64. Egan, T. M. Contribution of Calcium Ions to P2X Channel Responses. *J. Neurosci.* **24**, 3413–3420 (2004).

65. Sharp, A. J. *et al.* P2x7 deficiency suppresses development of experimental autoimmune encephalomyelitis. *J. Neuroinflammation* **5**, 33 (2008).

66. Brini, M. & Carafoli, E. The Plasma Membrane Ca2+ ATPase and the Plasma Membrane Sodium Calcium Exchanger Cooperate in the Regulation of Cell Calcium. *Cold Spring Harb. Perspect. Biol.* **3**, a004168–a004168 (2011).

67. Strehler, E. E. & Zacharias, D. A. Role of Alternative Splicing in Generating Isoform

Diversity Among Plasma Membrane Calcium Pumps. *Physiol. Rev.* **81**, 21–50 (2001).

68. Stauffer, T. P., Guerini, D. & Carafoli, E. Tissue Distribution of the Four Gene Products of the Plasma Membrane Ca2+ Pump. *Journal of Biological Chemistry* vol. 270 12184–12190 (1995).

69. Raza, M. *et al.* Aging is associated with elevated intracellular calcium levels and altered calcium homeostatic mechanisms in hippocampal neurons. *Neurosci. Lett.* **418**, 77–81 (2007).

70. Mata, A. M., Berrocal, M. & Sepúlveda, M. R. Impairment of the activity of the plasma membrane Ca2+-ATPase in Alzheimer's disease. *Biochem. Soc. Trans.* **39**, 819–822 (2011).

71. Kurnellas, M. P., Nicot, A., Shull, G. E. & Elkabes, S. Plasma membrane calcium ATPase deficiency causes neuronal pathology in the spinal cord: a potential mechanism for neurodegeneration in multiple sclerosis and spinal cord injury. *FASEB J.* **19**, 1–19 (2005).

72. Nicot, A., Kurnellas, M. & Elkabes, S. Temporal pattern of plasma membrane calcium ATPase 2 expression in the spinal cord correlates with the course of clinical symptoms in two rodent models of autoimmune encephalomyelitis. *Eur. J. Neurosci.* **21**, 2660–2670 (2005).

73. Wanaverbecq, N., Marsh, S. J., Al-Qatari, M. & Brown, D. A. The Plasma Membrane Calcium-ATPase as a Major Mechanism for Intracellular Calcium Regulation in Neurones from the Rat Superior Cervical Ganglion. *J. Physiol.* **550**, 83–101 (2003).

74. Taylor, C. W. & Tovey, S. C. IP3 Receptors: Toward Understanding Their Activation. *Cold Spring Harb. Perspect. Biol.* **2**, a004010–a004010 (2010).

75. Verkhratsky, A. Physiology and Pathophysiology of the Calcium Store in the Endoplasmic Reticulum of Neurons. *Physiol. Rev.* **85**, 201–279 (2005).

76. Santulli, G. & Marks, A. Essential Roles of Intracellular Calcium Release Channels in Muscle, Brain, Metabolism, and Aging. *Curr. Mol. Pharmacol.* **8**, 206–222 (2015).

77. Higashida, H. *et al.* Cyclic ADP-ribose as a universal calcium signal molecule in the nervous system. *Neurochem. Int.* **51**, 192–199 (2007).

78. Brini, M. & Carafoli, E. Calcium Pumps in Health and Disease. *Physiol. Rev.* **89**, 1341–1378 (2009).

79. Fan, M. *et al.* Structure and mechanism of the mitochondrial Ca2+ uniporter holocomplex. *Nature* **582**, 129–133 (2020).

80. Maack, C. *et al.* Elevated cytosolic Na+ decreases mitochondrial Ca2+ uptake during excitation-contraction coupling and impairs energetic adaptation in cardiac myocytes. *Circ. Res.* **99**, 172–182 (2006).

81. Drago, I., De Stefani, D., Rizzuto, R. & Pozzan, T. Mitochondrial Ca2+ uptake contributes to buffering cytoplasmic Ca2+ peaks in cardiomyocytes. *Proc. Natl. Acad. Sci.* **109**, 12986–12991 (2012).

82. Qi, H., Li, L. & Shuai, J. Optimal microdomain crosstalk between endoplasmic reticulum and mitochondria for Ca2+ oscillations. *Sci. Rep.* **5**, 7984 (2015).

83. Griffiths, E. J. & Rutter, G. A. Mitochondrial calcium as a key regulator of mitochondrial ATP production in mammalian cells. *Biochim. Biophys. Acta - Bioenerg.* **1787**, 1324–1333 (2009).

84. Xia, Z. & Storm, D. R. The role of calmodulin as a signal integrator for synaptic plasticity. *Nat. Rev. Neurosci.* **6**, 267–276 (2005).

85. Wacquier, B., Combettes, L. & Dupont, G. Dual dynamics of mitochondrial permeability transition pore opening. *Sci. Rep.* **10**, 1–10 (2020).

86. Lipstein, N. *et al.* Dynamic Control of Synaptic Vesicle Replenishment and Short-Term Plasticity by Ca2+-Calmodulin-Munc13-1 Signaling. *Neuron* **79**, 82–96 (2013).

87. Sun, T. *et al.* The role of calcium/calmodulin-activated calcineurin in rapid and slow endocytosis at central synapses. *J. Neurosci.* **30**, 11838–47 (2010).

88. Ben-Johny, M. & Yue, D. T. Calmodulin regulation (calmodulation) of voltage-gated calcium channels. *J. Gen. Physiol.* **143**, 679–692 (2014).

89. Cimler, B. M., Andreasen, T. J., Andreasen, K. I. & Storm, D. R. P-57 is a neural specific calmodulin-binding protein. *J. Biol. Chem.* **260**, 10784–10788 (1985).

90. Timofeeva, Y. & Volynski, K. E. Calmodulin as a major calcium buffer shaping vesicular release and short-term synaptic plasticity: facilitation through buffer dislocation. *Front. Cell. Neurosci.* **9**, 1–13 (2015).

91. Witte, M. E. *et al.* Calcium Influx through Plasma-Membrane Nanoruptures Drives Axon Degeneration in a Model of Multiple Sclerosis. *Neuron* **101**, 615-624.e5 (2019).

92. Jousset, H., Frieden, M. & Demaurex, N. STIM1 Knockdown Reveals That Store-operated Ca2+ Channels Located Close to Sarco/Endoplasmic Ca2+ ATPases (SERCA) Pumps Silently Refill the Endoplasmic Reticulum. *J. Biol. Chem.* **282**, 11456–11464 (2007).

93. Prakriya, M. & Lewis, R. S. Store-Operated Calcium Channels. *Physiol. Rev.* **95**, 1383–1436 (2015).

94. Lin, A. H. Y., Sun, H., Paudel, O., Lin, M.-J. & Sham, J. S. K. Conformation of ryanodine receptor-2 gates store-operated calcium entry in rat pulmonary arterial myocytes. *Cardiovasc. Res.* **111**, 94–104 (2016).

95. Glitsch, M. D. Store-operated Ca2+ entry depends on mitochondrial Ca2+ uptake. *EMBO J.* **21**, 6744–6754 (2002).

96. Ben-Kasus Nissim, T. *et al.* Mitochondria control store-operated Ca 2+ entry through Na + and redox signals. *EMBO J.* **36**, 797–815 (2017).

97. Singh, B. B., Liu, X., Tang, J., Zhu, M. X. & Ambudkar, I. S. Calmodulin Regulates Ca2+-Dependent Feedback Inhibition of Store-Operated Ca2+ Influx by Interaction with a Site in the C Terminus of TrpC1. *Mol. Cell* **9**, 739–750 (2002).

98. López, J. J. *et al.* Two-pore channel 2 (TPC2) modulates store-operated Ca2+ entry. *Biochim. Biophys. Acta - Mol. Cell Res.* **1823**, 1976–1983 (2012).

99. Ong, H. L., de Souza, L. B. & Ambudkar, I. S. Role of TRPC Channels in Store-Operated Calcium Entry. in *Advances in Experimental Medicine and Biology* vol. 898 87–109 (2016).

100. Putney, J. W. A model for receptor-regulated calcium entry. *Cell Calcium* **7**, 1–12 (1986).

101. Liou, J. *et al.* STIM Is a Ca2+ Sensor Essential for Ca2+-Store-Depletion-Triggered Ca2+ Influx. *Curr. Biol.* **15**, 1235–1241 (2005).

102. Feske, S. *et al.* A mutation in Orai1 causes immune deficiency by abrogating CRAC channel function. *Nature* **441**, 179–185 (2006).

103. Soboloff, J., Rothberg, B. S., Madesh, M. & Gill, D. L. STIM proteins: dynamic calcium signal transducers. *Nat. Rev. Mol. Cell Biol.* **13**, 549–565 (2012).

104. https://blast.ncbi.nlm.nih.gov/.

105. Trebak, M. & Putney, J. W. ORAI calcium channels. *Physiology* **32**, 332–342 (2017).

106. Guzman, R. *et al.* Expression of ORAI1, a Plasma Membrane Resident Subunit of the CRAC Channel, in Rodent and Non-rodent Species. *J. Histochem. Cytochem.* **62**, 864–

878 (2014).

107. Hou, X., Pedi, L., Diver, M. M. & Long, S. B. Crystal structure of the calcium release-activated calcium channel orai. *Science (80-.).* **338**, 1308–1313 (2012).

108. Liu, X. *et al.* Molecular understanding of calcium permeation through the open Orai channel. *PLOS Biol.* **17**, e3000096 (2019).

109. Vaeth, M. *et al.* ORAI2 modulates store-operated calcium entry and T cell-mediated immunity. *Nat. Commun.* **8**, 14714 (2017).

110. Alansary, D., Bogeski, I. & Niemeyer, B. A. Facilitation of Orai3 targeting and store-operated function by Orai1. *Biochim. Biophys. Acta - Mol. Cell Res.* **1853**, 1541–1550 (2015).

111. Roos, J. *et al.* STIM1, an essential and conserved component of store-operated Ca 2+ channel function. *J. Cell Biol.* **169**, 435–445 (2005).

112. WILLIAMS, R. T. *et al.* Identification and characterization of the STIM (stromal interaction molecule) gene family: coding for a novel class of transmembrane proteins. *Biochem. J.* **357**, 673 (2001).

113. Graham, S. J. L., Dziadek, M. A. & Johnstone, L. S. A cytosolic STIM2 preprotein created by signal peptide inefficiency activates ORAI1 in a store-independent manner. *J. Biol. Chem.* **286**, 16174–16185 (2011).

114. Manji, S. S. M. *et al.* STIM1: A novel phosphoprotein located at the cell surface. *Biochim. Biophys. Acta - Protein Struct. Mol. Enzymol.* **1481**, 147–155 (2000).

115. Zbidi, H. *et al.* STIM1 and STIM2 are located in the acidic Ca2+ stores and associates with Orai1 upon depletion of the acidic stores in human platelets. *J. Biol. Chem.* **286**, 12257–12270 (2011).

116. Zheng, L., Stathopulos, P. B., Li, G. Y. & Ikura, M. Biophysical characterization of the EF-hand and SAM domain containing Ca2+ sensory region of STIM1 and STIM2. *Biochem. Biophys. Res. Commun.* **369**, 240–246 (2008).

117. Demaurex, N. & Frieden, M. Measurements of the free luminal ER Ca 2+ concentration with targeted “cameleon” fluorescent proteins. *Cell Calcium* **34**, 109–119 (2003).

118. Brandman, O., Liou, J., Park, W. S. & Meyer, T. STIM2 Is a Feedback Regulator that Stabilizes Basal Cytosolic and Endoplasmic Reticulum Ca2+ Levels. *Cell* **131**, 1327–1339

(2007).

119. Deng, X., Wang, Y., Zhou, Y., Soboloff, J. & Gill, D. L. STIM and Orai: Dynamic Intermembrane Coupling to Control Cellular Calcium Signals. *J. Biol. Chem.* **284**, 22501–22505 (2009).

120. Covington, E. D., Wu, M. M. & Lewis, R. S. Essential role for the CRAC activation domain in store-dependent oligomerization of STIM1. *Mol. Biol. Cell* **21**, 1897–1907 (2010).

121. Yuan, J. P. *et al.* SOAR and the polybasic STIM1 domains gate and regulate Orai channels. *Nat. Cell Biol.* **11**, 337–343 (2009).

122. Hirve, N., Rajanikanth, V., Hogan, P. G. & Gudlur, A. Coiled-Coil Formation Conveys a STIM1 Signal from ER Lumen to Cytoplasm. *Cell Rep.* **22**, 72–83 (2018).

123. Yen, M. & Lewis, R. S. Numbers count: How STIM and Orai stoichiometry affect store-operated calcium entry. *Cell Calcium* **79**, 35–43 (2019).

124. Gruszczynska-Biegala, J., Pomorski, P., Wisniewska, M. B. & Kuznicki, J. Differential Roles for STIM1 and STIM2 in Store-Operated Calcium Entry in Rat Neurons. *PLoS One* **6**, e19285 (2011).

125. Lis, A. *et al.* CRACM1, CRACM2, and CRACM3 Are Store-Operated Ca2+ Channels with Distinct Functional Properties. *Curr. Biol.* **17**, 794–800 (2007).

126. Lopez, E. *et al.* STIM1 phosphorylation at Y 316 modulates its interaction with SARAF and the activation of SOCE and I CRAC. *J. Cell Sci.* **132**, jcs226019 (2019).

127. Kimura, M. *et al.* High pH-sensitive store-operated Ca2+ entry mediated by Ca2+ release-activated Ca2+ channels in rat odontoblasts. *Front. Physiol.* **9**, 1–10 (2018).

128. Lu, B. & Fivaz, M. Neuronal SOCE: Myth or Reality? *Trends Cell Biol.* **26**, 890–893 (2016).

129. Berna-Erro, A. *et al.* STIM2 regulates capacitive Ca2+ entry in neurons and plays a key role in hypoxic neuronal cell death. *Sci. Signal.* **2**, 1–11 (2009).

130. Steinbeck, J. A. *et al.* Store-operated calcium entry modulates neuronal network activity in a model of chronic epilepsy. *Exp. Neurol.* **232**, 185–194 (2011).

131. Baba, A. *et al.* Activity-Evoked Capacitative Ca 2+ Entry: Implications in Synaptic Plasticity. *J. Neurosci.* **23**, 7737–7741 (2003).

132. Korkotian, E., Oni-Biton, E. & Segal, M. The role of the store-operated calcium entry channel Orai1 in cultured rat hippocampal synapse formation and plasticity. *J. Physiol.* **595**,

125–140 (2017).

133. Yap, K. A. F. *et al.* STIM2 regulates AMPA receptor trafficking and plasticity at hippocampal synapses. *Neurobiol. Learn. Mem.* **138**, 54–61 (2017).

134. Sun, S. *et al.* Reduced Synaptic STIM2 Expression and Impaired Store-Operated Calcium Entry Cause Destabilization of Mature Spines in Mutant Presenilin Mice. *Neuron* **82**, 79–93 (2014).

135. Wu, J. *et al.* Enhanced Store-Operated Calcium Entry Leads to Striatal Synaptic Loss in a Huntington's Disease Mouse Model. *J. Neurosci.* **36**, 125–141 (2016).

136. Gross, S. A. *et al.* Murine ORAI2 Splice Variants Form Functional Ca2+ Release-activated Ca2+ (CRAC) Channels*. *J. Biol. Chem.* **282**, 19375–19384 (2007).

137. Wallace, T. L. & Johnson, E. M. Cytosine arabinoside kills postmitotic neurons: Evidence that deoxycytidine may have a role in neuronal survival that is independent of DNA synthesis. *J. Neurosci.* **9**, 115–124 (1989).

138. Tsvilovskyy, V. *et al.* Deletion of Orai2 augments endogenous CRAC currents and degranulation in mast cells leading to enhanced anaphylaxis. *Cell Calcium* **71**, 24–33 (2018).

139. Oh-hora, M. *et al.* Dual functions for the endoplasmic reticulum calcium sensors STIM1 and STIM2 in T cell activation and tolerance. *Nat. Immunol.* **9**, 432–443 (2008).

140. Song, A. J. & Palmiter, R. D. Detecting and Avoiding Problems When Using the Cre–lox System. *Trends Genet.* **34**, 333–340 (2018).

141. Brewer, G. J., Torricelli, J. R., Evege, E. K. & Price, P. J. Optimized survival of hippocampal neurons in B27-supplemented neurobasal?, a new serum-free medium combination. *J. Neurosci. Res.* **35**, 567–576 (1993).

142. Oh-hora, M. *et al.* Dual functions for the endoplasmic reticulum calcium sensors STIM1 and STIM2 in T cell activation and tolerance. *Nat. Immunol.* **9**, 432–443 (2008).

143. Berna-Erro, A. *et al.* STIM2 Regulates Capacitive Ca2+ Entry in Neurons and Plays a Key Role in Hypoxic Neuronal Cell Death. *Sci. Signal.* **2**, ra67–ra67 (2009).

144. Sun, Z., Williams, D. J., Xu, B. & Gogos, J. A. Altered function and maturation of primary cortical neurons from a 22q11.2 deletion mouse model of schizophrenia. *Transl. Psychiatry* **8**, 85 (2018).

145. Bastian, F. *et al.* Bgee: Integrating and Comparing Heterogeneous Transcriptome Data Among Species. in *Data Integration in the Life Sciences* 124–131 (Springer Berlin Heidelberg, 2008). doi:10.1007/978-3-540-69828-9_12.

146. Mikuni, T., Nishiyama, J., Sun, Y., Kamasawa, N. & Yasuda, R. High-Throughput, High-Resolution Mapping of Protein Localization in Mammalian Brain by In Vivo Genome Editing. *Cell* **165**, 1803–1817 (2016).

147. Garcia-Alvarez, G. *et al.* Impaired spatial memory and enhanced long-term potentiation in mice with forebrain-specific ablation of the Stim genes. *Front. Behav. Neurosci.* **9**, 1–12 (2015).

148. Merkler, D., Ernsting, T., Kerschensteiner, M., Brück, W. & Stadelmann, C. A new focal EAE model of cortical demyelination: multiple sclerosis-like lesions with rapid resolution of inflammation and extensive remyelination. *Brain* **129**, 1972–83 (2006).

149. Jafari, M. *et al.* Phagocyte-mediated synapse removal in cortical neuroinflammation is promoted by local calcium accumulation. *Nat. Neurosci.* **24**, 355–367 (2021).

150. Wu, J., Ryskamp, D., Birnbaumer, L. & Bezprozvanny, I. Inhibition of TRPC1-Dependent Store-Operated Calcium Entry Improves Synaptic Stability and Motor Performance in a Mouse Model of Huntington's Disease. *J. Huntingtons. Dis.* **7**, 35–50 (2018).

151. Wei, D., Mei, Y., Xia, J. & Hu, H. Orai1 and Orai3 Mediate Store-Operated Calcium Entry Contributing to Neuronal Excitability in Dorsal Root Ganglion Neurons. *Front. Cell. Neurosci.* **11**, 1–15 (2017).

152. Fu, Y. *et al.* NLRC3 expression in dendritic cells attenuates CD4+ T cell response and autoimmunity. *EMBO J.* **38**, e101397 (2019).

153. Bandyopadhyay, B. C., Pingle, S. C. & Ahern, G. P. Store-operated Ca 2+ signaling in dendritic cells occurs independently of STIM1. *J. Leukoc. Biol.* **89**, 57–62 (2011).

154. Frugier, T. Nuclear targeting defect of SMN lacking the C-terminus in a mouse model of spinal muscular atrophy. *Hum. Mol. Genet.* **9**, 849–858 (2000).

155. Kazdoba, T. M., Leach, P. T. & Crawley, J. N. Behavioral phenotypes of genetic mouse models of autism. *Genes, Brain Behav.* **15**, 7–26 (2016).

156. Kang, Z. *et al.* Act1 mediates IL-17–induced EAE pathogenesis selectively in NG2+ glial cells. *Nat. Neurosci.* **16**, 1401–1408 (2013).

157. Vogt, J. *et al.* Lower motor neuron loss in multiple sclerosis and experimental autoimmune encephalomyelitis. *Ann. Neurol.* **66**, 310–322 (2009).

158. Bannerman, P. G. *et al.* Motor neuron pathology in experimental autoimmune encephalomyelitis: studies in THY1-YFP transgenic mice. *Brain* **128**, 1877–1886 (2005).

159. Chen-Engerer, H.-J. *et al.* Two types of functionally distinct Ca2+ stores in hippocampal neurons. *Nat. Commun.* **10**, 3223 (2019).

160. Stegner, D. *et al.* Loss of Orai2-Mediated Capacitative Ca 2+ Entry Is Neuroprotective in Acute Ischemic Stroke. *Stroke* **50**, 3238–3245 (2019).

161. Acharjee, S. *et al.* Reduced Microglial Activity and Enhanced Glutamate Transmission in the Basolateral Amygdala in Early CNS Autoimmunity. *J. Neurosci.* **38**, 9019–9033 (2018).

162. Smith, T., Groom, A., Zhu, B. & Turski, L. Autoimmune encephalomyelitis ameliorated by AMPA antagonists. *Nat. Med.* **6**, 62–66 (2000).

163. Gruszczynska-Biegala, J. *et al.* STIM Protein-NMDA2 Receptor Interaction Decreases NMDA-Dependent Calcium Levels in Cortical Neurons. *Cells* **9**, 160 (2020).

164. Grasselli, G. *et al.* Abnormal NMDA receptor function exacerbates experimental autoimmune encephalomyelitis. *Br. J. Pharmacol.* **168**, 502–517 (2013).

165. Gupta, R. K., Wasilewska, I., Palchevska, O. & Kuźnicki, J. Knockout of stim2a Increases Calcium Oscillations in Neurons and Induces Hyperactive-Like Phenotype in Zebrafish Larvae. *Int. J. Mol. Sci.* **21**, 6198 (2020).

166. Wasilewska, I., Gupta, R. K., Wojtaś, B., Palchevska, O. & Kuźnicki, J. stim2b Knockout Induces Hyperactivity and Susceptibility to Seizures in Zebrafish Larvae. *Cells* **9**, (2020).

167. Hori, K., Tsujikawa, S., Novakovic, M. M., Yamashita, M. & Prakriya, M. Regulation of chemoconvulsant-induced seizures by store-operated Orai1 channels. *J. Physiol.* **598**, 5391–5409 (2020).

168. Majewski, Wojtas, Maciąg & Kuznicki. Changes in Calcium Homeostasis and Gene Expression Implicated in Epilepsy in Hippocampi of Mice Overexpressing ORAI1. *Int. J. Mol. Sci.* **20**, 5539 (2019).

169. Hoover, P. J. & Lewis, R. S. Stoichiometric requirements for trapping and gating of Ca 2+ release-activated Ca 2+ (CRAC) channels by stromal interaction molecule 1 (STIM1). *Proc. Natl. Acad. Sci.* **108**, 13299–13304 (2011).

170. Srikanth, S. *et al.* The Ca2+ sensor STIM1 regulates the type I interferon response by retaining the signaling adaptor STING at the endoplasmic reticulum. *Nat. Immunol.* **20**, 152–162 (2019).

171. Delhaye, S. *et al.* Neurons produce type I interferon during viral encephalitis. *Proc. Natl. Acad. Sci.* **103**, 7835–7840 (2006).

172. Mathur, V. *et al.* Activation of the STING-Dependent Type I Interferon Response Reduces Microglial Reactivity and Neuroinflammation. *Neuron* **96**, 1290-1302.e6 (2017).

173. Getts, D. R. *et al.* Role of IFN-γ in an experimental murine model of West Nile virus-induced seizures. *J. Neurochem.* **103**, 1019–1030 (2007).

174. Borham, L. E. *et al.* The effect of some immunomodulatory and anti-inflammatory drugs on Li-pilocarpine-induced epileptic disorders in Wistar rats. *Brain Res.* **1648**, 418–424 (2016).

175. Kundap, U. P., Paudel, Y. N., Kumari, Y., Othman, I. & Shaikh, M. F. Embelin Prevents Seizure and Associated Cognitive Impairments in a Pentylenetetrazole-Induced Kindling Zebrafish Model. *Front. Pharmacol.* **10**, (2019).

176. de Oliveira Mann, C. C. *et al.* Modular Architecture of the STING C-Terminal Tail Allows Interferon and NF-κB Signaling Adaptation. *Cell Rep.* **27**, 1165-1175.e5 (2019).

177. Sauer, J.-D. *et al.* The N -Ethyl- N -Nitrosourea-Induced Goldenticket Mouse Mutant Reveals an Essential Function of Sting in the In Vivo Interferon Response to Listeria monocytogenes and Cyclic Dinucleotides. *Infect. Immun.* **79**, 688–694 (2011).

178. myelin. (n.d.) Miller-Keane Encyclopedia and Dictionary of Medicine, Nursing, and Allied Health, Seventh Edition. (2003). Retrieved May 25 2021 from https://medical-dictionary.thefreedictionary.com/myelin.

179. saltatory conduction. (n.d.) Collins Dictionary of Biology, 3rd ed.. (2005). Retrieved May 3 2021 from https://medical-dictionary.thefreedictionary.com/saltatory+conduction.

180. Guo, J. *et al.* Structures of the calcium-activated, non-selective cation channel TRPM4. *Nature* **552**, 205–209 (2017).

181. Kretsinger, R. H. & Nockolds, C. E. Carp Muscle Calcium-binding Protein. *J. Biol. Chem.* **248**, 3313–3326 (1973).

182. bicuculline. (n.d.) Segen's Medical Dictionary. (2011). Retrieved May 4 2021 from https://medical-dictionary.thefreedictionary.com/bicuculline.

ACKNOWLEDGEMENTS

I would like to thank Prof. Dr. Manuel A. Friese for giving me the opportunity to work on this exciting project, for his supervision, scientific discussions and advice. I am thankful for the opportunity to improve my scientific and soft skills by visiting scientific conferences and by being a part of the DFG *Forschungsgruppe* FOR2289.

I thank Prof. Dr. Robert Blick for the supervision and advice during my work to build my interdisciplinary vision of the project.

Many thanks to Dr. Sina Rosenkranz for the excellent supervision, motivational and scientific support, deep scientific and private discussions. I utterly enjoyed our work on developing and discussing new ideas together.

I would like to thank all ZMNH mentor program members, namely Dr. Gaia Pigino, Prof. Dr. Simon Wiegert and Dr. Anne Willing, for sharing their scientific experience and providing excellent advice for the project development.

I thank Dr. Inbal Ipenberg for motivational support and detailed unbiased proofreading of this thesis and scientific discussions.

I am very grateful to head of Behavioral Unit UKE ZMNH Dr. Fabio Morellini and Dr. Kristin Hartmann from mouse neuropathology department at UKE for providing their expertise for important experiments presented in this dissertation.

I would like to thank all members of INIMS for the great working atmosphere, support, scientific and non-scientific discussions. Special thanks to Simone Träger, Vanessa Vieira and Nina Kursave for the technical help and support.

In the end, I am very thankful for everybody who supported and motivated me in the last years. I am especially thankful to my friends and my family for the unconditional support.

AFFIDAVIT

I hereby confirm that this dissertation is my own written work and that I have used no sources and aids other than indicated.

Artem Shaposhnykov Place, Date